

VILNIUS UNIVERSITY  
CENTER FOR PHYSICAL SCIENCES AND TECHNOLOGY

Karolis  
RATAUTAS

# Laser-assisted formation of electro- conductive circuit traces on dielectric materials by electroless metal plating technique

**DOCTORAL DISSERTATION**

Technological Sciences, Materials Engineering 08T

---

VILNIUS 2019

The research was performed in 2014 - 2018 in the Department of Laser Technologies of the Center for Physical Sciences and Technology.

**Scientific supervisor:**

Dr. Gediminas Račiukaitis (Center for Physical Sciences and Technology, Technological Sciences, Material Engineering – 08T).

## TABLE OF CONTENTS

ACKNOWLEDGEMENTS .....	6
LIST OF ABBREVIATIONS .....	7
1. INTRODUCTION.....	9
1.1 The aim of the research .....	11
1.2 Practical value and novelty.....	11
1.2.1 The novelty of the research results .....	11
1.2.2 Practical value of the thesis .....	11
1.3 Statements to be defended.....	12
1.4 Approbation.....	12
1.4.1 Scientific papers .....	12
1.4.2 Patents .....	14
1.4.3 International Conference presentations .....	14
1.4.4 Author contribution .....	19
1.4.5 Co-author contribution .....	19
2. LITERATURE REVIEW .....	20
2.1 Fields of MID applications.....	20
2.1.1 Moulded interconnect devices.....	21
2.1.2 MID application sectors .....	23
2.1.3 Research areas in MID technology.....	26
2.1.4 Flexible electronics.....	27
2.2 Polymers.....	29
2.3 Laser interaction with polymers .....	32
2.3.1 Absorption.....	32
2.3.2 Ablation.....	33
2.4 Electroless autocatalytic plating.....	36
2.4.1 Autocatalytic copper deposition.....	37
2.5 Techniques of circuit formation on dielectrics .....	37
2.5.1 Photolithography .....	38

2.5.2 MIPTEC .....	38
2.5.3. Inject and aerosol printing .....	39
2.5.4 LIFT .....	40
2.5.5 Laser sintering of ink paste.....	41
2.5.6 Laser-induced selective activation .....	42
2.5.7 Laser-assisted metal deposition from the liquid phase.....	43
2.5.8 Laser direct structuring.....	44
2.5.9 Comparison of the methods.....	46
3. EXPERIMENTAL SETUP .....	48
3.1 Samples preparation for LDS .....	48
3.2 Samples preparation for SSAIL .....	48
3.3 Laser experimental setup for LDS.....	49
3.4 Laser experimental setup for SSAIL .....	50
3.5 Metal plating for LDS .....	51
3.6 Chemical activation and plating procedures for SSAIL process.....	51
3.7 Sheet resistance measurements for quality evaluation .....	51
3.8 Morphology analysis with SEM and optical microscopes .....	52
3.9 XPS analysis.....	52
3.10 Surface wetting of water measurements.....	53
3.11 Raman spectroscopy.....	53
3.12 Adhesion measurements.....	53
3.13 Profile measurements .....	54
4. LDS EXPERIMENTS WITH PP DOPED MWCNT .....	55
4.1 Analysis of plated surfaces for different parameters of laser activation .....	55
4.2 Raman spectroscopy for analysis of laser-activated surfaces.....	61
4.3 Test of the plating spatial selectivity .....	64
4.4. Discussion of the activation mechanism .....	65
4.5 Results and conclusions.....	66

5. SELECTIVE SURFACE ACTIVATION INDUCED BY LASER (SSAIL) METHOD FOR SELECTIVE PLATING OF POLYMERS.....	67
5.1 Surface activation with pico- and nanosecond laser pulses.....	68
5.2 XPS analysis of samples.....	74
5.3 Wetting dynamics analysis of processed surface .....	76
5.4 Results and conclusions.....	79
6. EVALUATION OF SELECTIVELY-PLATED SURFACE QUALITY, RELIABILITY AND OPTIMISATION OF THE SSAIL PROCESS .....	80
6.1 Sheet resistance .....	80
6.2 Selectivity.....	91
6.3 Adhesion.....	95
6.4 Evaluation of optimal laser processing parameters .....	97
6.5 Alternative method for plating quality evaluation.....	99
6.5.1 Percolation model of the sheet resistance.....	100
6.5.2 Area fraction of copper dependence on the colour difference...	100
6.5.3 Sheet resistance dependence on the colour difference .....	102
6.6 Influence of parameters in activation and plating .....	103
6.6.1 Concentration of regents and temperature of the bath.....	104
6.6.2 Double activation procedure.....	107
6.7 Spatial resolution of SSAIL .....	110
6.8 Demonstrators .....	112
6.9 Results and conclusions.....	114
LIST OF CONCLUSIONS .....	115
SUMMARY .....	116
REFERENCES .....	117

## ACKNOWLEDGEMENTS

I am very grateful to my scientific supervisor Dr. G. Račiukaitis for his great support, for his patience, motivation and useful advices.

Thanks to Dr. A. Jagminienė, Dr. I Stankevičienė, and Prof. E. Norkus from the Catalysis Department for collaboration work developing new technology and friendly atmosphere.

Thanks to my colleagues Dr. Paulius Gečys and especially to Dr. Mindaugas Gedvilas for advices and valuable discussions.

Thanks to Dr. N. Li Pira from Fiat Research Centre for collaboration in samples preparation of PP with MWCNT.

Thanks to Dr. S. Sinopoli from BioAge srl for fabrication of Fiat 500 glove box cover demonstrator.

Thanks to M. Vyšniauskas for the collaboration work with 3D laser processing and also to my students: M. Sadauskas and I. Andriulionytė.

I also express my thanks to, Dr. R. Trusovas, Dr. S. Indrišiūnas, Dr. E Stankevičius, E. Markauskas, J. Dudutis, A. Žemaitis, and other colleagues from the Department of Laser Technologies for a friendly atmosphere in the laboratory.

Special thanks to my wife Irma and daughter Elena for supporting me during never-ending studies.

Part of this work was supported by project APPOLO funded by the European Union FP7 Program under the grant agreement No 609355 and project LAPOME funded by Lithuanian Research Council (grant No 01.2.2-LMT-K-718-01-0004).

## LIST OF ABBREVIATIONS

### List of acronyms

a. u.	Arbitrary units;
ABS	Acrylonitrile butadiene styrene;
CAD	Computer-aid design
CAGR	Compound annual growth rate;
EDTA	Ethylenediaminetetraacetic acid;
FPC	Flexible printed circuit;
FS	Fused silica glass;
I H	First harmonic;
II H	Second harmonic;
III H	Third harmonic.
LCP	Liquid crystals polymer;
LDS	Laser direct structuring;
MIPTEC	Microscopic integrated device technology
MID	Moulded interconnect device;
MWCNT	Multiwall carbon nanotubes;
PA	Polyamide;
PC	Polycarbonate;
PEEK	Poly ether-ether-ketone;
PET	Polyethylene terephthalate;
PP	Polypropylene;
PPA	Polyphthalamide;
SEM	Scanning Electron Microscope;
SSAIL	Selective surface activation induced by a laser;

XPS X-ray photoelectron spectroscopy;

### List of symbols

B average normalised blue colour component;  
G average normalised green colour component;  
M Molar concentration;  
 $P_{\max}$  maximum power;  
R average normalised red colour component;  
sq square;  
T temperature;  
t time;  
 $\Omega$  Ohms;

### List of Greek symbols

$\Delta E$  average normalised difference of colour components;  
 $\alpha$  absorption coefficient;  
 $\sigma$  electrical conductivity;  
 $\Phi_{\text{crit}}$  percolation threshold;  
 $\Phi_{\text{frac}}$  areal fraction

# 1. INTRODUCTION

Our modern world requires thousands of functional devices for assistance in daily life. The number of these devices significantly increases due to growing human's needs and accelerated the pace of life. Therefore, the large quantities of these appliances in our surrounding demand the miniaturisation of a single device. At the same time, the reduction of the processing cost and material consumption should be taken into account. First, the geometrical shape takes a crucial role here for space saving issues. Specially designed 3D part can miniaturise the device significantly. Second, the structural material is essential in order to produce a mechanically robust and light-weighting device. The moulding technology can solve these problems with freedom in geometry and offering a variety of engineering polymers, which can be light, strong and cost-effective materials. However, an only a mechanical function containing device does not satisfy our modern world requirements. Many appliances must be smart. Therefore, it should include functional integration with electronics.

Consequently, the contradiction between miniaturisation and functionality appears. PCB (Printed Circuit Board) does not offer the solution being flat, rigid and requiring a lot of additional parts: housing, connectors, interfaces – cables [1]. Therefore, the three-dimensional integration of electronics in a single free-shaped moulded part could be a solution. Such devices are called Moulded Interconnect Devices (MID).

MID is an injection-moulded thermoplastic part with electronic circuits directly integrated into a polymeric component – it offers material, weight and cost savings, by the elimination of connectors between separate PCBs, shortening process chain and integration of contact surfaces, e.g. for switches, sensors and antennas [1]. MID has a great potential in automotive, aviation, lighting, computing or even medicine sectors where emerging innovation demands to increase the number of the electronic component into a device. The MID approach requires a combination of various technologies to fabricate a product from different materials. A final product integrates various mechanical and electrical functionalities.

The main technological problem of MID is to produce electrical circuit traces on a plastic part. A standard known technique such as photolithography could not be applied in a conventional way since the parts generally have complex 3D geometrical shapes. There are several well-known methods of the laser-induced local metal deposition on polymers which might fit for circuit traces fabrication: metal nano-ink printing [2, 3] ink paste layer sintering [4, 5], laser-

induced selective activation [6] and laser direct structuring (LDS) [7]. The last two methods utilise chemical metal deposition in addition to laser treatment. All of them except LDS face difficulties when they are applied for three-dimensional parts.

LDS is the method using precursors mixed in a polymer matrix [7]. These precursor additives are activated during the laser writing process in order to convert them into a catalyst for electroless deposition of the metal, and thus the laser-scanned area can be selectively plated [7]. LDS is state of the art and the most commercialised process for MID production. There are a few commercial materials for LDS available on the market. However, most of the LDS polymers are based on expensive metal-organic fillers, such as palladium-based metalorganic compounds or copper oxide spinel crystal microparticles [7], thus increasing the price of the raw material several times (for example, a cost ratio is 1:4 in the case of raw PC/ABS and with LDS additives) [8]. Therefore, the cost of the material stops further expansion of the technology to automotive and consumer goods sectors. In addition, a high amount of metalorganic additives reduces the mechanical properties of a moulded part — moreover, metal-based additives in the polymer matrix shield electromagnetic radiation and limits MID application in the gigahertz frequency range [9, 10].

One of the tasks of this research was related with a search of the technology which is capable of avoiding the use of expensive additives to the polymer body and in this way to reduce the costs of MID fabrication.

In the first part of the experimental work, a new composite material – polypropylene (PP) with multiwall carbon nanotubes (MWCNT) as additives for the LDS approach was investigated. Processing parameters for plating quality were deeply analysed. The work included not only tests of the material, but the physical-chemical mechanisms of laser-induced selective metal deposition were also investigated.

The second part of the work presents a new method for laser-assisted local metal deposition. The process includes laser modification of the polymer surface with a pulsed laser, chemical activation of laser-modified areas and electroless metal deposition on the locally activated surface. The new method was invented during the doctoral studies period and was called “selective surface activation induced by a laser (SSAIL)”. The main advantages of the SSAIL process comparing with the state of the art method – LDS is that SSAIL does not require special additives in the polymer matrix, unlike LDS does not use metalorganic additives [8] or multiwall carbon nanotubes [11].

Therefore, SSAIL could open a broad area of application where current methods of electronics integration are still too expensive. Experimental studies have shown the potential application abilities for a broad range of polymeric materials and glass. In addition, the SSAIL process was deeply analysed using advanced research methods. Therefore, the mechanism of activation of the laser-modified surface was suggested, and optimal processing regimes for several polymers and glasses were found.

### 1.1 The aim of the research

The aim of the research was to investigate the laser-induced selective metal deposition using electroless plating technique for the electrical circuit formation on dielectric materials. Two tasks were set in order to achieve the goal:

1. Research of the Laser Direct Structuring method, using new cost-effective additive – multiwall carbon nanotubes in low concentration.
2. Investigation of newly invented technology – SSAIL - for electro-conductive circuit traces formation on polymers, optimising processing speed, quality and analysing the mechanism of selective metallisation.

### 1.2 Practical value and novelty

#### 1.2.1 The novelty of the research results

1. New additive material – multiwall carbon nanotubes for conductive tracks formation on polymers utilising the laser direct structuring technique has been investigated, and the mechanism of selective metal deposition was proposed.
2. The new method – SSAIL (selective surface activation induced by laser) for electro-conductive circuit fabrication was discovered, and mechanism of activation of the laser-modified surface has been suggested.
3. The SSAIL method was validated on a broad range of polymers and glass.

#### 1.2.2 Practical value of the thesis

1. The results of the investigation for new additives – multiwall carbon nanotubes in the laser direct structuring approach can be applied for moulded interconnect device production and, therefore, to reduce the production cost by using the material with a lower cost.

2. The new method for circuit formation on dielectrics – SSAIL can be applied for moulded interconnect devices production, flexible electronics and electronics on glass materials as a lower-cost technology comparing with state-of the art methods (LDS or MIPTEC) used in industry.
3. Developed electroless plating bath and technique can be applied over industrial activities where the plating on dielectrics is necessary.

### 1.3 Statements to be defended

1. Interconnected and electrically conductive structure of carbon nanotubes within a polymer matrix induced by laser re-melting surface of polypropylene doped with carbon nanotubes could work as a catalyst for electroless metal deposition in the electroless plating process and can be applied for the Laser Direct Structuring technology.
2. Selective electroless metal deposition can be achieved by picosecond laser modification of polymers or glass surface, followed by treatment in the catalyst silver nitrate bath and electroless plating.
3. Laser processing parameters strongly influence the quality of the copper-plated surface, and optimal processing regime could be found by evaluating electrical conductance of the metal layer, its adhesion to the substrate and spatial selectivity of plating.

### 1.4 Approbation

Results of the research presented in this thesis were published in 4 peer-reviewed scientific papers [A1-A4]. Together with co-authors, one international patent application [P1] was prepared, and two national patents [P2-P3] were issued. Moreover, results were presented in 12 contributions to conferences [C1-C12]. In total, the publication list includes 15 scientific papers, 3 patents, and 27 presentations at the conference.

#### 1.4.1 Scientific papers

##### **Publication related to the topic of the thesis (CA WoS)**

A1. M. Gedvilas, K. Ratautas, E. Kacar, A. Jagminienė, I. Stankevičienė, E. Norkus, N. Li Pira, G. Račiukaitis, *Evaluation of Quality of Electrolessly Deposited Copper on Polymer after Laser-Induced Selective Activation*, Scientific Reports. **6**, 22963 (2016). DOI: 10.1038/srep22963

- A2. K. Ratautas, M. Gedvilas, A. Jagminienė, I Stankevičienė, E. Norkus, N. Li Pira, S. Sinopoli, G. Račiukaitis, *Laser-induced selective metallization of polypropylene doped with multiwall carbon nanotubes*, Appl. Surf. Sci., **412**, 319-326 (2017) DOI: 10.1016/j.apsusc.2017.03.238
- A3. M. Gedvilas, K. Ratautas, E. Kacar, A. Jagminienė, I. Stankevičienė, E. Norkus, N. Li Pira, G. Račiukaitis, *Percolation effect of a Cu layer on a MWCNT/PP nanocomposite substrate after laser direct structuring and autocatalytic plating*, RSC Advances. **8**, 30305 (2018). DOI: 10.1039/c8ra04813d
- A4. K. Ratautas, A. Jagminienė, I Stankevičienė, E. Norkus, G. Račiukaitis, *Laser-assisted selective copper deposition on commercial PA6 by catalytic electroless plating – process and activation mechanism*, Appl. Surf. Sci., **470**, 405-410, (2019) DOI: 10.1016/j.apsusc.2018.11.091

#### **Other publication related to the topic of the thesis**

- A5. K. Ratautas, M. Gedvilas, I. Stankevičienė, A. Jagminienė, E. Norkus, G. Račiukaitis, S. Sinopoli, U. Emanuele, N.L. Pira, *Laser-induced selective metal plating on PP and PC/ABS polymers surface* 12th International Congress Molded Interconnect Devices - Scientific Proceedings, MID 2016, art. No. 7738925 (2016).
- A6. K. Ratautas, M. Gedvilas, I. Stankevičienė, A. Jagminienė, E. Norkus, N. L. Pira, S. Sinopoli, U. Emanuele, G. Račiukaitis, *Laser-induced selective copper plating of polypropylene surface*, Proceedings of SPIE - The International Society for Optical Engineering 9735, art. No. 973507 (2016).
- A7. K. Ratautas, A. Jagminienė, I. Stankevičienė, E. Norkus, G. Račiukaitis, *Laser assisted fabrication of copper traces on dielectrics by electroless plating*, Procedia CIRP **74**, 367-370 (2018)
- A8. K. Ratautas, A. Jagminienė, I. Stankevičienė, E. Norkus, G. Račiukaitis, *Laser Assisted Selective Metallization of Polymers*, 13th International Congress Molded Interconnect Devices - Scientific Proceedings, MID 2018, pp. 30-32. (2018)

#### **Publication not directly related to the thesis (CA WoS)**

- A9. K. Ratautas, M. Gedvilas, G. Račiukaitis, A. Grigonis, *Nanoparticle formation after nanosecond-laser irradiation of thin gold films*, J. Appl. Phys. **212**, 01308-01314 (2012). DOI: 10.1063/1.4731253
- A10. K. Ratautas, M. Gedvilas, B. Voisiat, G. Račiukaitis, A. Grigonis, *Transformation of a Thin Gold Film to Nanoparticles after Nanosecond –*

*Laser Irradiation*, J. Laser Micro/Nanoeng. **3**, 355-361 (2012). DOI: 10.2961/jlmn.2012.03.0022

A11. K. Ratautas, G. Račiukaitis, M. Gedvilas, *Sphere-to-Plate Glass Welding using Picosecond-Laser Radiation*, J. Laser Micro/Nanoeng. **8**, 175-182 (2013). DOI: 10.2961/jlmn.2013.02.0011

A12. R. Trusovas, K. Ratautas, G. Račiukaitis, J. Barkauskas, I. Stankevičienė, G. Niaura, R. Mažeikienė, *Reduction of graphite oxide to graphene with laser irradiation*, Carbon **52**, 574-582 (2013). DOI: 10.1016/j.carbon.2012.10.017

A13. R. Trusovas, K. Ratautas, G. Račiukaitis, *Graphene layer formation in pinewood by nanosecond and picosecond laser irradiation*, Appl. Surf. Sci., **471**, 154-161, (2019) DOI: 10.1016/j.apsusc.2018.12.005

#### **Other publication not directly related to the thesis**

A14. M. Gedvilas, K. Ratautas, B. Voisiat, K. Regelskis, G. Raciukaitis *Plateau-Rayleigh instability triggered transformation in thin chromium film on glass substrate under nanosecond laser irradiation*. Proceedings of SPIE 5: 8612-86212 (2013).

A15. Ratautas K., Gedvilas M., Račiukaitis G. Picosecond laser welding of spherical glass bead to substrate, Physics Procedia 41, 620 – 622 (2013).

### 1.4.2 Patents

#### **International patents application related to the topic of the thesis**

P1. K. Ratautas, A. Jagminienė, I. Stankevičienė, E. Norkus, G. Račiukaitis, **Method for formation of electro-conductive traces on polymeric article surfaces**, EPO application, PTC/IB2017/055362, filing 2017 09 06, priority 2016 09 13.

#### **National patents related to the topic of the thesis**

P2. K. Ratautas, A. Jagminienė, I. Stankevičienė, E. Norkus, G. Račiukaitis, selective plating method of polymeric article, LT6517, issued 2018 06 11, Received 2016 09 13, app. no: 2016-513

P3. K. Ratautas, A. Jagminienė, I. Stankevičienė, E. Norkus, G. Račiukaitis, Method of conductive trace fabrication on polymeric article, LT6518, issued 2018 06 11, Received 2016 09 13, app. no: 2016-514

### 1.4.3 International Conference presentations

#### **Directly related to the topic of the thesis**

C1. E. Kacar, K. Ratautas, M. Gedvilas, I. Stankevičienė, A. Jagminienė, G. Račiukaitis, *Evaluation of the Surface Topographies of Different*

***Polymers Structured by Nd:YVO<sub>4</sub> Laser for Autocatalytic Copper Plating***, 15th International Symposium on Laser Precision Microfabrication 2014, Vilnius, 2014 Lithuania June 17-20. (poster)

C2. K. Ratautas, M. Gedvilas, I. Stankevičienė, A. Jagminienė, E. Norkus, N, Li Pira, S. Sinopoli, G. Račiukaitis, ***Laser Writing for Selective Copper Plating on Plastics for Electronics Application***, 7th International Congress on Laser Advanced Materials Processing 2015 (LAMP 2015), Kitakyushu, Japan, 2015 May 24-29. (oral)

C3. K. Ratautas, M. Gedvilas, I. Stankevičienė, A. Jagminienė, E. Norkus, N, Li Pira, S. Sinopoli, G. Račiukaitis, ***Selective Copper Plating on Polymers Induced by Laser Activated Fillers***, Lasers in Manufacturing 2015, Munich, Germany, 2015 June 22-25. (oral)

C4. K. Ratautas, M. Gedvilas, I. Stankevičienė, A. Jagminienė, E. Norkus, N, Li Pira, S. Sinopoli, G. Račiukaitis, ***Laser-induced selective copper plating of polypropylene surface***, SPIE Photonic West, LASE 2016, San Francisco, USA, 2016 February 8-11. (oral)

C5. K. Ratautas, M. Gedvilas, I. Stankevičienė, A. Jagminienė, E. Norkus, N, Li Pira, S. Sinopoli, G. Račiukaitis, ***Laser-induced selective copper plating on plastics***, 12th International Congress Molded Interconnect Devices (MID 2016), Wuerzburg, Germany, 2016 September 28-30. (oral)

C6. K. Ratautas, A. Jagminienė, I. Stankevičienė, E. Norkus, N, Li Pira, S. Sinopoli, G. Račiukaitis, ***Laser writing for selective copper seeding on polymers***, International Conference on Laser Ablation 2017 (COLA 2017), Marseille, France, 2017 September 3-8. (poster)

C7. K. Ratautas, A. Jagminienė, I. Stankevičienė, E. Norkus, N, Li Pira, S. Sinopoli, G. Račiukaitis, ***Laser Assisted Selective Copper Plating on Polymers***, 25th International Conference on Advanced Laser Technology (ALT 2017), Busan, South Korea, 2017 September 10-15. (poster)

C8. K. Ratautas, I. Stankevičienė, A. Jagminienė, E. Norkus, G. Račiukaitis, ***Local copper deposition on dielectrics using Selective Surface Activation Induced by Laser (SSAIL)***, 19th International Symposium on Laser Precision Microfabrication 2018, Edinburgh 2018 June 25 – 28. (oral)

C9. K. Ratautas, M. Vyšniauskas, I. Stankevičienė, A. Jagminienė, E. Norkus, G. Račiukaitis, ***Selective surface activation induced by laser***

*(SSAIL) method for electronic circuit traces formation of 3D moulded interconnect devices (MID)*, 19th International Symposium on Laser Precision Microfabrication 2018, Edinburgh 2018 June 25 – 28. (poster)

C10. K. Ratautas, A. Jagminienė, I. Stankevičienė, E. Norkus, G. Račiukaitis, *Laser assisted fabrication of copper traces on dielectrics by electroless plating*, LANE 2018 - 10<sup>th</sup> CIRP Conference on Photonic Technologies, Fuerth, Germany, 2018 September 3-6. (oral)

C11. K. Ratautas, A. Jagminienė, I. Stankevičienė, E. Norkus, G. Račiukaitis, *New laser-assisted method for copper circuit fabrication on dielectrics*, 11th International Conference on Photo-Excited Processes and Applications – ICPEPA 11, Vilnius, Lithuania, 2018 September 9-12. (poster)

C12. K. Ratautas, I. Stankevičienė, A. Jagminienė, E. Norkus, G. Račiukaitis, *Laser Assisted Selective Metallization of Polymers and Glass*, 13<sup>th</sup> International Congress Molded Interconnect Devices (MID 2018), Wuerzburg, Germany, 2018 September 25-26. (oral)

#### **Conference presentations (not directly related to the topic of the thesis)**

C13. G. Račiukaitis, M. Gedvilas, K. Ratautas, K. Regelskis: *Instability – Triggered Transformation in Thin Metal Films under Laser Irradiation*, EMRS 2012, May 14-18, Strasbourg, France. (oral)

C14. K. Ratautas, M. Gedvilas, G. Račiukaitis, A. Grigonis: *Self – Organization in Thin Gold Film to Nanoparticles after Nanosecond Laser Irradiation*, International conference on Radiation Interaction with materials and its use in technologies 2012, May 15-18, Kaunas, Lithuania. (poster)

C15. K. Ratautas, M. Gedvilas, G. Račiukaitis, A. Grigonis: *Welding of Glass Bead on a Glass Substrate using Picosecond Laser Radiation*, International conference on Radiation Interaction with materials and its use in technologies 2012, May 15-18, Kaunas, Lithuania. (poster)

C16. R. Trusovas, K. Ratautas, G. Račiukaitis, J. Barkauskas, I. Stankevičienė, R. Mažeikienė, *Formation of Graphene Domains in Graphite Oxide by Picosecond Laser Treatment*, 4-th Int. Conf. „Radiation interaction with material and its use in technologies”, 2012, May 15-18, Kaunas, Lithuania. (poster)

- C17. K. Ratautas, M. Gedvilas, B. Voisiat, G. Račiukaitis, A. Grigonis: ***Transformation of Thin Gold Film to Nanoparticles after Nanosecond – Laser Irradiation***, 13<sup>th</sup> International Symposium on Laser Precision Microfabrication, 2012 June 12-15, Washington DC, USA. (oral)
- C18. K. Ratautas, M. Gedvilas, G. Račiukaitis: ***Sphere-to-Plate Glass Welding using Picosecond-Laser Radiation***, 13<sup>th</sup> International Symposium on Laser Precision Microfabrication, 2012 June 12-15 Washington DC, USA. (oral)
- C19. R. Trusovas, K. Ratautas, G. Račiukaitis, J. Barkauskas, R. Mažeikienė, ***Fabrication of graphene channels in graphite oxide by applying picosecond lasers***, International conference on advance Laser Technologies 12, 2012 September 2-6, Tübingen, Switzerland. (oral)
- C20. A. Novikau, V. Shautsova, B. Voisiat, K. Ratautas, M. Gedvilas, G. Račiukaitis, ***Formation of periodic metal nanoparticles arrays using direct laser interference ablation and numerical simulation of their optical characteristics***, EMRS 2012, September 18-21, Warsaw, Poland. (oral)
- C21. K. Ratautas, M. Gedvilas, G. Račiukaitis, ***Picosecond laser welding of spherical glass bead to substrate***, International Conference on Lasers in Manufacturing 2013, June 21-25, Munich, Germany. (oral)
- C22. K. Ratautas, M. Gedvilas, G. Račiukaitis, ***Picosecond laser glass Welding in Vacuum Insulated Glazing (VIG) Technology***, International Symposium on Fundamentals in Laser Assisted Micro and Nano Technologies 2013, July 24-28, Saint Petersburg, Russia. (poster)
- C23. K. Ratautas, M. Gedvilas, G. Račiukaitis, ***Picosecond Laser Glass Welding in Vacuum Insulated Glazing (VIG) Technology***, International Lithuanian-Belarus seminar 2013, November 21-22, Vilnius, Lithuania. (poster)
- C24. M. Gedvilas, B. Voisiat, K. Ratautas, A. Vinčiūnas, S. Indrišiūnas, M. Brikas, G. Račiukaitis, ***Lazeriai nanotechnologijoms: nanodalelių generavimas skysčiuose ir ant funkcinių paviršių***, „Nanotechnologijos: Mokslas ir praktika“ 2014, May 15-16, Lithuania academy of science, Vilnius, Lithuania. (oral)

C25. K. Ratautas, G. Račiukaitis, ***Formation of Nanoparticles, after Irradiation of Thin Gold Film with Nanosecond Pulses and Its Application for SERS***, LPM 2014, June 17-20 Vilnius, Lithuania. (oral)

C26. R. Trusovas, K. Ratautas, G. Račiukaitis, G. Niaura, ***Graphene formation in wood by 1064 nm laser irradiation***, 11th International Conference on Photo-Excited Processes and Applications – ICPEPA 11, Vilnius, Lithuania, 2018 September 9-12. (poster)

C27. R. Trusovas K. Ratautas, G. Račiukaitis, G. Niaura, ***Formation of graphene structures in wood by laser irradiation***, 11<sup>th</sup> International Conference on Plasma Physics and Plasma Technology, Minsk, Belarus, 2018 September 17-21. (oral)

#### 1.4.4 Author contribution

Author of the thesis made the main theoretical and experimental work of this study, listed as follows:

- Development of experimental setup and research method;
- Design of experiment, planning, leadership in activities related to the topic;
- Laser structuring experiments;
- Part of chemical plating and activation experiments;
- Characterisation of fabricated samples with microscopic methods;
- Sheet resistance measurements;
- Wetting dynamics measurements and analysis;
- Raman spectra measurements and analysis;
- Analysis, interpretation and visualisation of the results, preparation of scientific articles and presentation of the conferences.

#### 1.4.5 Co-author contribution

- Dr. Aldona Jagminienė, dr. Ina Stankevičienė and Prof Eugenijus Norkus gave ideas for activation and plating techniques
- Part of chemical activation and plating experiments were made by Dr. Aldona Jagminienė, dr. Ina Stankevičienė.
- Part of Raman spectra analysis was done by prof. Gediminas Niaura.
- XPS analysis and measurements were done by dr. Mindaugas Andrulėvičius at the Kaunas University of Technology.
- The main part of the colour difference evaluation method for plating quality was developed by dr. Mindaugas Gedvilas.

## 2. LITERATURE REVIEW

### 2.1 Fields of MID applications

Research of this work was intended for circuit traces formation on free-shaped dielectrics. The most robust photolithography technology perfectly works on flat surfaces and there are attempts to transfer it to more complex geometries [7]. Moulded interconnect devices is an alternative approach which exhibits its benefits on three-dimensional substrates.

The idea was to improve one significant step of the in-mould integrated electronics processing.

MID is intended to provide economic goals through the reduction of parts, shorter process chains, minor material consumption, and higher reliability [1]. MID is perfectly designed to be suitable for keeping the energy and resource conservation [12]. The benefits of 3D design come from the ability to define orientation between components [1]. Moreover, stacking and precision placement of chips and the forming of cavities is possible. The versatility of the MID layout, therefore, enables the integration of contact surfaces for switches or sensors and passive electrical functions (including capacitances, inductances, or resistances) and antennas for transmission or reception of electromagnetic waves [1].

One of the main technological problem of MID is to produce electro-conducting circuit traces on the plastic part. A conventional (industrial) technique such as photolithography could not be applied since the parts generally have complex 3D geometrical shapes. The laser writing for selective plating of polymers can also be used on 3D surfaces since localised and selective activation of a polymer is feasible with a laser beam. Scanning of the laser beam on 3D surfaces can be simply achieved technologically [13]. There are several well-known methods for circuit formation (which are described in Section 2.4. Circuit formation on dielectrics techniques), but most of them face with difficulties for MID application due to limitation for complex geometrical shapes or high cost [14].

Flexible electronics is another modern technology capable of coping with miniaturisation issues [15]. Flexible electronics is an electronic device where the circuit with its components is mounted on flexible plastic substrates, allowing the circuit board to conform to the desired shape, or to bend during its use. This technology could be easily adaptable to complex shapes [16]. In

addition, the substrate is very thin, in the range of tens of microns, what helps to reduce weight and save more space.

One of the significant challenges of this technology is a cost-efficient fabrication of reliable electro-conductive circuit traces.

### 2.1.1 Moulded interconnect devices

MID is an injection-moulded thermoplastic part with fabricated electro-conductive circuit traces [1]. It was developed in 1980 by the companies located in the United States [17]. The USA has been a leader in the MID technology starting from the beginning - the 1980s to the 1990s. After 1990, Germany overtook the leadership in this field and kept it up to date [18]. In the beginning, the development was intended for various materials and metallisation processes.

The MID market is growing. From 2000 to 2014, it increased from 7 to 150 million euros. Since 2014, the MID market has grown by more than 183 million euros [1]. Such rapid growth of the market was influenced by increasing demand for new applications in automotive and healthcare areas. Therefore, it improved quality and all the processes of the MID chain.

The technology of 3D MIDs allows metal circuits to be formed on top of the arbitrary shaped plastic surface. The process chain for manufacturing of MID can be divided into three steps including moulding, fabrication of conductive circuit traces and the assembly of electronics which are represented in Figure 1.



Figure 1. The principle of MID technology [19].

Different from the traditional PCB electronics, the 3D-MID technology opens an opportunity to combine 3D space and functionality where the standard technologies fail. The advantages of MID could be classified as follows [1]:

### **Freedom of design:**

- MID offers excellent opportunity to make 3D shaped devices. Therefore, the miniaturisation can be achieved.
- MID allows integrating mechanics and electronics in one unit of the device.
- New functionalities of devices can be created.
- The versatility of the MID layout enables the integration of contact surfaces for switches or sensors and passive electrical functions (including capacitances, inductances, or resistances) and antennas for the transmission or reception of electromagnetic waves.
- The flexible and arbitrary shape is beneficial to engineers because they have more area for electronics assembling on 3D surfaces in comparison to the planar surface [19].

### **Economisation of production:**

- MID economisation process comes with the ability to reduce the number of parts, for example, no connection cables or rigid PCB boards are necessary.
- Miniaturisation also helps to save material consumptions.
- The process chain is shorter, as some assembling functions are eliminated.
- As a result, other expenses related to the reduced process steps, as logistics are also minimised [19].

**Environmental sustainability.** As a result of the shorter process chain, the material consumption can be reduced remarkably. Therefore, MID helps to preserve the resources, and due to this, it is more environmental-friendly comparing with current technologies. [20].

**Innovation.** MID technology is orientated to production-perfect and function-oriented product development. There are several processes to make a final MID product (device). Each process is followed by optimisation. Thus, from one side, MID technology fosters process innovation as shown in Figure 2. On the other hand, the MID technology opens new areas for the products with new technological capabilities; this leads to product innovations [20].

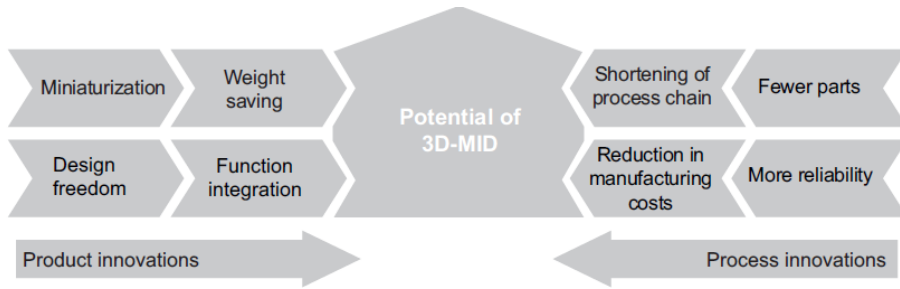


Figure 2. Potential of 3D-MID [20].

### 2.1.2 MID application sectors

Telecommunication application accounted for more than 60% of the global revenue of MID in 2015 with expected CAGR of 13.6% from 2016 to 2023. The growth can be primarily attributed to increased usage in antennas of mobile devices. Automotive is forecast to witness the fastest growth in the coming years at 14.8% CAGR, owing to increase product adoption in brake-light fixtures. Medical segment is forecasted to be over 20 million USD by 2023. Surging adoption in medical devices, it is expected to further boost demand over the next seven years [20].

A brief introduction to industrial sectors of MID applications [20]:

#### Automotive

Modern cars need a variety of sensors and electronic assistants that provide the comfort and increase the safety of vehicle passengers [1]. Therefore, a huge number of additional components has to be used, and that increases the manufacturing cost as well.

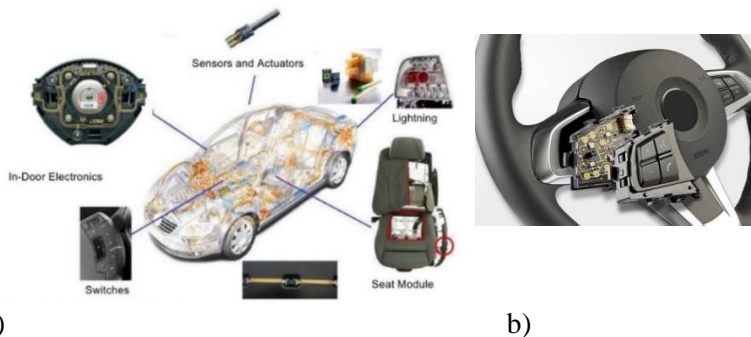


Figure 3. a) Automotive sectors of MID application [21] and b) steering wheel controls (Manufacturer: TRW Automotive for BMW [22]).

Miniaturisation is essential, and functional diversity continues to expand. Those factors have a positive effect on demand for MID integration.

At the same time, due to the too high pressure of costs in the car-making industry, MID parts have to be an economically viable alternative to conventional technologies. [20]. Potential MID applications in automotive are shown in Figure 3.

In automotive, MID is used in various areas. More than a half of the MID products are dedicated to sensors and connectors, because of the higher demand for miniaturisation, integration and weight saving. Also, MID is applied for switches and control modules of the vehicles [23, 1]. Another growing sector of MID applications is lighting, also applied in automotive. Many LED lighting modules for turn signals are already produced utilising MID by manufacturers such as BMW [17].

### **Medicine**

With increasing the interest in healthy lifestyle, medical sector demands of miniaturisation and cost efficiency in healthcare equipment production. One of the essential sectors of medical devices is a system of audiology, for example, hearing aids. Integrated microphones and speakers (specially orientated in the space) have to create a sense of surrounding sound and at the same time fit into the small housing. Single-use, disposable products are another possible application. Sterile sample carriers have to be used for bioanalysis. Type variety, design, miniaturisation and cost reduction characterise the development of portable electronic devices. The consumers expect in cutting-edge and compact devices which enclosure more and more functions. Due to the rapid development in the software and chip technology, new diagnostic procedures are continually opening up. Small diagnostic devices help to improve the lives of millions of patients. Small diagnostic and monitoring devices for the drug application carry along, such as blood glucose meters are on the disposition of patients today. [20],[24].

### **Computers, telecommunication**

IT and telecommunication is a specific sector of MID [25]. It covers more than 60% of the whole MID market. Since all portable IT and telecommunication devices are getting thinner, less space is left for electronic components. Asia is the leader in telecommunication and computing products manufacturing. The highest MID production volume in this sector is dedicated to antennas. Smartphones and portable IT products such as laptops have increasing demand

in MID products. Moreover, most of the wireless fidelity (Wi-Fi), Bluetooth and universal mobile telecommunications systems (UMTS) are fabricated using the MID technology.



*Figure 4. MID applications in IT and telecommunications. Laptop Wi-Fi antenna (left) and smartphone antenna (right) made using MID technologies [19].*

### **Automation**

Automation is also the sphere where MID technology can offer its benefits. As automation industry requires high flexibility and profitability, the MID can fit in this field very well. For example, intelligent sensors which are based on the arrangement of light emitting diodes (LED) or sensor chips and the radio-frequency identification devices can be offered by MID technology. Moreover for long-range RFID antennas enables not-contacting data transition, what is essential in a smart factory or logistics [1, 19].

### **Lighting**

LED lighting technology is expanding very rapidly and is changing conventional lighting technique in many areas – from automotive to the building interior. Since LED has very high efficiency, less heat is generated to the ambient and the substrate as well. Therefore, it enables to use MID production in lighting where the substrate is made from plastic and is sensitive to high heat flows. The leader in this area is the automotive industry. Moreover, it is expanding in the consumer goods sector as well [14].

### **Others**

The aerospace industry and the military sector are other essential fields for the MID application. These applications focus on the three-dimensional arrangement of sensors, but, to date, very little information has been put into the public domain [1]. The household goods sector can be assumed as a future up-and-coming sector. [20].

The most promising application areas of MID products can be mentioned as follows: sensors, antennas, 3D wiring, interconnect device/package (a new rising application area), plug connectors and optical devices, for example, lighting, reflecting or sensing [20].

### 2.1.3 Research areas in MID technology

3D-MID technology possesses various steps in the process chain. These investigation areas can be separated into four major sectors [26]:

- substrate materials;
- interconnect-device manufacture technologies;
- 3D assembly and interconnection technology;
- quality and reliability;

The most common structural material for MID is thermoplastic, because it is easily and fast producible to the desired shape, for example using injection moulding technique. The major problem with thermoplastics is concerned to their thermal properties: low heat conduction, low softening temperature. Therefore, high temperature-proofed polymers with high electrical resistance are objects of the research activities. Another area is biocompatible materials, which might extend the range of possible applications in the medical technology sector. Thermosets as a substrate material is also under research. The most research activities for the substrate is initiated by companies who are focused on technology-related to special substrate materials for example in LDS. Since LDS uses special additives in plastic for the selective plating procedure, it requires a lot of RTD work in polymer chemistry. Most of the additives are based on organic metal complex (like palladium complex). Recently, the most used in industry are copper oxide spinel crystal particles. The high amount of additives alter the mechanical and thermal properties of the plastic material. Moreover, a transparent and coloured plastic material is also hard to achieve, when black or grey colour additives are used [17].

Interconnect device manufacturing includes the formation of circuit traces on the moulded part. This research could be referred to the most important and complicated. 3D-MID's include a large variety of different technological methods and processes to manufacture circuit traces. They could be divided into selective plating and printing technologies. Most of the plating technologies are laser-assisted, such as microscopic integrated processing technology (MIPTEC)[27] or laser direct structuring (LDS) [7], laser-induced metallization (LIM), laser-induced selective activation (LISA). Printing – inkjet printing based processes, laser-induced forward transfer (LIFT)[3], laser restructuring print (LRP) [17]. Others are plasma spraying technologies. All

details about the technologies are presented in the chapter: 2.4 Circuit formation on dielectrics techniques.

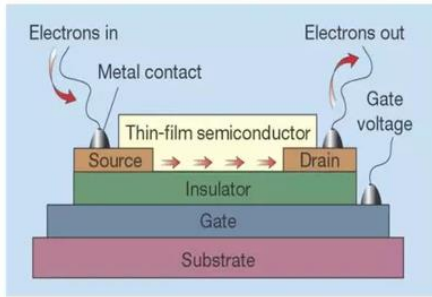
Another essential technological challenge in the MID process chain is assembling and soldering. All known technologies are created for assembly on a planar substrate. New methods and machines should be created for the MID process, which is capable of assembling on substrates with complicated 3D geometry. Soldering is another problem. Conventional solder paste working temperature is too high for many engineering polymers. Therefore, new methods and paste have to be developed [1].

#### 2.1.4 Flexible electronics

The definition of flexible electronics is the technology of mounting electronic devices on flexible substrates. History of flexible electronics reaches almost sixty years period. It started in 1960 for solar cells application [16]. The aim was to achieve high power/weight ratio for extra-terrestrial application in satellites. Therefore, the single-crystal silicon solar cells were thinned down to ~ 100 microns and assembled on a plastic substrate in order to provide support [16]. Currently, the applications of flexible electronics are countless: from personal devices (e.g., wearable health monitoring devices) to large-area sensors (e.g., an electronic skin, biomedical devices), and smart tagging of products with radio-frequency identification tags).

There are three levels of flexible electronics: bendable or rollable, permanently shaped, and elastically stretchable [28]. Depending on a type of use it can be classified as follows: flex to install, for bending only during the installation process in order to fit in the desired shape of housing (space saving); dynamic operation, where bending is required as a part of the operation of the device; or stacked flexible electronics in various configurations.

Recently, the most growing sector of application is flexible displays. Thin Film Transistors (TFT) technology enabled to produce flexible displays using LCD or OLED technologies. TFT is made from a flexible substrate, and metal contacts (circuit), amorphous silicon (or another type of semiconductor) is deposited on top and covered by an insulator layer. TFT scheme is shown in Figure 5. The last layer is a gate electrode which is usually transparent, produced from ITO [16].



a)

b)

Figure 5. TFT scheme a) [29] and LG flexible display b).[30]

Flexible electronics could be divided into two sectors: flexible electronics components (semiconductors) and flexible circuits [31]. As this work is related more to the circuit formation, we will focus more on flexible circuits.

The advantage of FPCs [16]

- thinner than PCB;
- can be used for dynamic application as flexing;
- freedom of FPC configuration.

Disadvantages of FPCs

- the price is higher than the PCB;
- high risk of damage;
- assembling is complicated;
- repairing is complicated or even impossible.

Application of flexible circuits is very wide from automotive or aircraft industries to consumer electronics [16]. Separately from flexible electronics components, flexible circuits are used as a connecting cable in electronics devices such as printers or automotive.

Fabrication techniques of flexible circuits can be divided into three approaches: additive printing, subtractive etching and additive plating processes. The most used is the subtractive etching process because many technological steps are overtaken from PCB manufacture process [32]. The process contains a flexible substrate adhered with copper foil, then follows the conventional lithographic process. However, the process is not sufficient for small quantities of production. Moreover, it is strictly limited with the substrate material and has very long process chain.

Additive printing is the technology which includes inject printing [33], aerosol printing [34] laser-induced forward transfer (LIFT) [3]. The additive printing

process is still under development, but there are several industrial applications as well.

Additive plating process chain is very similar to subtractive etching. The main difference is that metal is deposited using electroless plating on the dielectric substrate, instead of using metal foil [32].

The main technological problem of flexible circuit which limits its expansion to other fields is adhesion of metal to the substrate. Another critical issue is the cost of production. Standard conventional techniques have many processing steps which raise the price of production. Printing techniques usually use costly materials like silver ink what increases the price more [31]. The significant advantages of additive printing techniques are potentiality to use the roll to roll process [32].

## 2.2 Polymers

Polymers are a substance whose molecules consist of many repetitive structural units, called monomers, which are joined by covalent chemical bonds. Polymers can consist of hundreds or thousands of monomers. Classification by structure is as follows: linear – polymers which are joined together to long chain, for example, HDPE or PVC, branched polymers – these polymers contain linear chains having some branches, e.g., low-density polyethene, crosslinked polymers – synthesized from bifunctional or trifunctional monomers and has strong covalent bonds between linear polymers lines, like vulcanized rubber. Polymers can be classified by chemical families for example – polyurethanes, polyesters, polyamides. Sometimes it is necessary to divide polymers into groups by composition. If the polymer contains a single type of monomer – it is a homopolymer. Although when two different types of monomers are joined in the same polymer chain, the polymer is called a copolymer, for example, PC/ABS [35].

More convenient to classify polymers according to their mechanical and thermal properties. Polymers could be divided into two major classes: plastics and elastomers. The last one better known as rubber can be elongated to large scales under load at room temperature, because of its long polymer chains that have many cross-linkages structures. They are very elastic but return to their original shape once the load is removed [36]. Plastics are harder than elastomers and cannot be elastically deformed.

Plastics are important engineering material, because of its excellent mechanical, dielectric or chemical properties. They can be moulded to the

desired shape, have high mechanical strength, low weight, low thermal and electrical conduction, good toughness, excellent resistance to acids, bases and moisture. In addition, they are relatively low in cost.

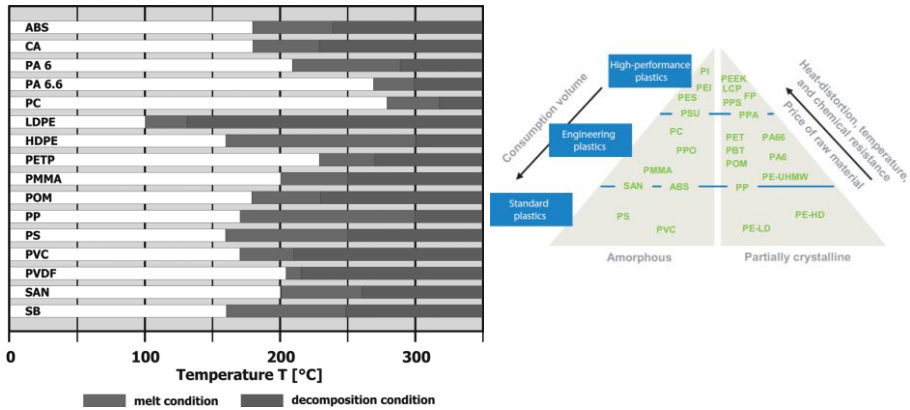
Plastics again are classified by their mechanical properties to thermoplastics and thermosets [37].

**Thermoplastics:** These plastics do not undergo any chemical change after being heated and can be moulded/welded afterwards. They usually are shaped very easily after applying high pressure and temperature. Therefore, such a process allows applying fast injection moulding procedure for fabrication of plastic parts. The process of heating, reshaping and retaining the same on cooling can be repeated several times. They usually have a linear or very slightly branched chain structure. Common thermoplastics are acrylics, polyvinyl chloride, nylons, polypropylene, polystyrene, polymethyl methacrylate, etc. [38]. Thermoplastics are more widely used than thermosets, because of its simple fabrication process.

Thermosets undergoes chemical changes during heating and formation process, such as extensive cross-linking and cannot be re-melted or reformed into another shape but decompose upon heating to high temperatures. Thermosets contains strongly crosslinked chain structure. Thermosets comparing with thermoplastics are stronger but brittle, has higher thermal and electrical resistance. There are two main methods for initiation of cross-linking reactions – heating upon certain temperature, or some resins can be shaped at low temperature by adding a cross-linking agent (for example epoxy resin). A compression moulding techniques are applied to thermosets which are quite slow due to complicated polymerisation process [36]. Use of thermosets is limited by difficult processing conditions [39].

Application of polymers is determined by their characteristics. However, there is also a demand to modify these properties. Therefore, other – foreign materials are introduced as an additive to enhance or modify their properties. Several types of additives are used: fillers, plasticisers, stabilisers, colourants, and flame retardants. Fillers like wood flour, sand, clay, talc are used to increase the tensile, compressive strength of specific polymer, abrasion resistance, and dimensional stability. Plasticiser is applied to improve the flexibility of plastics. Therefore, the liquid substance of low molecular weight is added. The stabiliser is needed to counteract deteriorative processes such as oxidation, radiation, and environmental deterioration. Colourants are used to achieve the desired colour of the polymer. For this purpose, dyes (dissolves)

or pigments (remains as a separate phase) are added. Flame retardants are used to enhance flammability resistance of combustible polymers [36], [38].



a) Melting and decomposition temperatures of thermoplastics [39];  
 b) Plastics pyramid including worldwide consumption figures [1].

Properties of the final moulded plastic can be classified to mechanical, thermal, electrical properties, workability and chemical resistance.

Depending on the application field, some properties are more important than others [40]. For an electronic application, the most relevant properties of the material are electrical, mechanical, thermal and thermomechanical properties. Since many thermoplastics has very high electrical insulation, the research is more focused on thermal and thermomechanical properties of thermoplastics, especially for MID applications [1].

The thermoplastic material has to have high-temperature resistance because of the soldering process during the electronics assembly. Figure 6 a) represents melting and decomposition temperatures of important industrial plastics. Since most of plastics cannot be heated above 200 °C temperature, specific soldering methods with specialised solder paste should be applied for MID. Another important issue is thermal conductivity. Although plastics have a very low thermal conductivity, local elongation can appear. This is very important for an application which has a thermocycling environment. High thermal expansion coefficient probably is the biggest challenge for thermoplastics in the MID application. MID contains different materials: polymers (as a substrate, carrier), metals (circuit traces) and assembled electronic components. The large difference in the thermal expansion coefficient for plastics and metal circuit traces can cause huge problems, resulting in trace

breaking. However, the polymer material should have attractive cost as well. Polymers with higher temperature resistance and lower thermal expansion are more expensive [1]. The compromise between price and material properties best illustrates the plastics pyramid in Figure 6 b).

## 2.3 Laser interaction with polymers

### 2.3.1 Absorption

Every material interaction with the laser usually starts with the absorption of radiation. The energy band gap of polymers is relatively wide [41]. Therefore, absorption by electrons can be achieved for the wavelengths in the ultraviolet range. Photon energy must exceed bonding energy of polymers which starts from several ( $\sim 3.6$  eV for C-C) eV [42]. At irradiation in Far IR  $\sim 2.5$ - $10$   $\mu\text{m}$ , the absorption is driven by vibrational energy level interaction - photon-phonon transfer [43]. Many finished plastic parts contain additives, as filler and colourants (like carbon black) which linearly absorb laser radiation in a very wide spectrum, even for the 1064 nm wavelength [42, 44]. In the case of ultrashort pulse lasers – picosecond and femtoseconds range, the nonlinear absorption can appear. This is very important for processing optically transparent materials like PMMA, PC or PET. Nonlinear absorption can be multiphoton and tunnelling process (see Figure 7) [45].

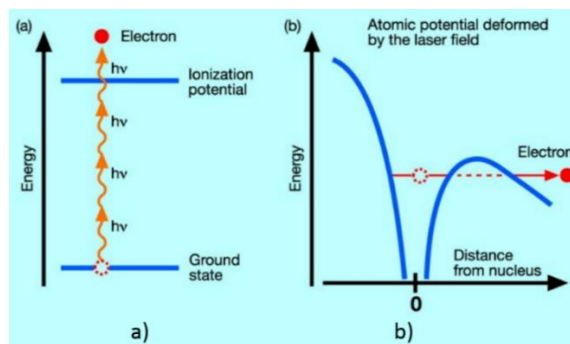


Figure 7. Nonlinear absorption mechanism of the laser beam for transparent materials: multiphoton absorption a) and tunnelling effect b) [45].

Multiphoton absorption appears then the concentration of photons is very high. Therefore, radiation intensity should be kept very high, at least  $\sim 10^{11}$   $\text{W}/\text{cm}^2$  for the 1064 nm wavelength. Energy band gap value must be equal to the sum of photon energies. Several photons are absorbed using virtual energy levels. Another nonlinear absorption process is tunnelling ionisation. This

process appears when the field of electromagnetic ionisation is very high and deforms atomic potential. Therefore, the electron has a finite barrier at one side and can tunnel through it as shown in Figure 7 b. Which process is the dominant determines Keldysh parameter  $K = \frac{\omega}{e} \sqrt{\frac{m c n \Delta E \epsilon_0}{I}}$ , here  $\omega$  is the reduced frequency of radiation,  $e$  and  $m$  are electron charge, and mass respectively,  $c$  and  $n$  are the speed of light and refraction index of the material,  $\Delta E$  is the energy band gap,  $\epsilon_0$  is the dielectric constant. L. Keldysh showed, that when  $K \gg 1$ , the tunnelling process is dominant. Multiphoton ionization dominates when ( $K \ll 1$ ). In some cases, both processes are important. For example if, the wavelength is 1064 nm and the material is glass,  $K \sim 1$  [46].

A bandgap of polymers (strength of covalent bonds) is much higher than the energy of photons in visible spectrum. Therefore, direct, linear absorption of light by polymers is feasible only in ultraviolet spectral range. The nonlinear absorption mechanism usually is a primary stage of absorption process, which is necessary for generation of free electrons. Utilising lasers with high intensity of radiation, multiphoton absorption is possible, when a few photons excite an electron from valance to conduction band. Free electrons which are in the conduction band can absorb the laser light, by interaction with atoms and gaining their kinetic energy. The phenomenon is called “inverse bremsstrahlung” [47]. When an electron has energy higher than the band gap in a polymer, it can excite a new one to the conduction band by collision with electrons of the valence band. The process is called impact ionisation. In the case, when one electron ionises more electrons and subsequent electrons ionises others – avalanche ionisation starts [13]. The impact and avalanche ionisation play a significant role in light energy absorption process in polymers.

### 2.3.2 Ablation

Two types of decomposition can occur in the polymers: photothermal and photochemical [43]. Photothermal mechanism of decomposition – the absorbed laser energy leads to heating of polymer and thermal decomposition can be induced due to increased temperature of material. Photochemical mechanism of decomposition – The photons in the polymer are absorbed directly by electrons in the polymer molecule and chemical (decomposition) reactions can be induced. A photo-mechanical mechanism of decomposition can be assumed as a particular case of the photo-thermal process. The photo-mechanical mechanism can occur when a high pressure or stress are created by rapid pulse heating due to fast energy input into material by ultra-short

pulse absorption. After the energy transfer, the material could be modified or removed. The removal process is called ablation [<sup>43</sup>, <sup>48</sup>].

The polymer consists of large macromolecules; which cannot simply evaporate. Therefore, a polymer removal process is different from other (non polymeric material) by making free atoms. After energy transfer, the polymer chain is decomposed by heating, or photo-chemically. Sufficient number of bonds must be broken in polymeric chain in order that ablation process could start. Decomposition can be classified into two groups [<sup>43</sup>]. First one is end-chain scission, sometimes also called "unzipping", when monomers are released at the borders of backbone structure. The second one is random chain scission when polymeric bonds are broken in the middle of the backbone. Random chain scission leads to the formation of both monomers and oligomers (short chains with ten or fewer monomers). Another competing process is "chain-stripping", i.e. cleaving reactions in the side chain and cross-linking reaction. The unzipping forms a monomer or other lower molecular weight products. The random chain scission leads to char formation. The eliminated parts of the polymer are typically lost through the gas phase components.

Usually, ablation and modification processes occur at the same time, because not removed, but heated material is modified. The modification can be chemical, and physical – by changing structure (morphology), crystallinity. Ablation mechanism of polymers is not fully understood yet, and there are still ongoing discussions about the processes during their ablation [<sup>43</sup>]. There are two main models of polymers ablation: photochemical ablation, when laser photon energy is high enough to break bonds of polymer molecules and thermochemical decomposition, when absorbed laser radiation increases the temperature of the polymer high enough to cut the bonds thermally [<sup>44</sup>].

Photochemical ablation allows to achieve high resolution of micro processing since all energy is applied to the material for bond breaking, and no thermal side effects appear. However, photochemical ablation is possible only with lasers working in the ultraviolet range, usually excimer lasers. Ultraviolet range laser processing must be performed in a vacuum environment because ambient air absorbs the radiation. In this research work, NIR or visible range wavelength were used. However, nonlinear absorption of short laser pulses can initiate the photochemical processes. Therefore both processes are important here [<sup>48</sup>].

Pulse duration is another important parameter in pulsed laser processing. Nanosecond laser ablation has several stages: absorption, heating, evaporation and plasma formation as a result of the pulse-vapour interaction. The nanosecond laser ablation process still contains thermal side effect. The surface contains more melted areas after processing with a nanosecond laser comparing to effect of a picosecond laser.

Picosecond laser interaction with polymer could be completely different. Much higher intensity of laser radiation facilitate increase of multiphoton absorption, and direct breaking of chemical bonds in polymer chains could be dominating. Rapid energy transfer to quite a small area can result in many new processes depending on radiation intensity: shock wave generation, Coulomb explosion, phase explosion [49]. Cold ablation in laser processing describes the mechanism of material removal when the thermal side effect is avoided. It could be achieved in particular cases by ultrashort laser pulses. Due to the very short time scales involved in the ablation with femtosecond laser pulses, the ablation process can be considered as a direct solid-vapour (or solid-plasma) transition. In this case, the lattice is heated on a picosecond timescale which results in the creation of vapour and plasma phases followed by a rapid expansion [50,51]. The heat affected zones are also minimised due to shorter Gaussian “tail” of the temporal envelope of the ultrashort pulse. Another way to create “cold” ablation is to use burst mode of laser pulses [52]. Kerse et al. describe the process when heat affected zones are removed by the next laser pulse in the burst at a very high-frequency scale  $\sim 10$  MHz. In the NIR range, significant differences in ablation of PMMA with nanosecond and picosecond pulses were observed by Wen et al [53]. Using the 1064 nm wavelength, ablation with picosecond pulses was influenced by multiphoton absorption.

Pinho et al. showed that Coulomb repulsion could also act as a part of the ablation process at higher fluencies  $\sim 10^{13}$  W/m<sup>2</sup> [49]. Differences for pico- and nanosecond pulse processing can be divided into two parts: difference in absorption behaviour and differences caused by rapid energy transfer.

Another essential property of pulse laser ablation is incubation of material modification and related defects after each laser pulse [54, 44] – the process when the ablation threshold is reduced by the influence of primary laser pulses.

## 2.4 Electroless autocatalytic plating

Definition of electroless (or chemical) plating describes the process of metal deposition on other metal or non-metal including dielectrics without an external electric current. An important feature of the process is that deposited metal itself is a catalyst for the ongoing plating reaction. Therefore, such a process is called autocatalysis [55]. The solution for electroless copper plating which contains formaldehyde as a reducer has been known since the middle of XX century. The solution includes an alkaline environment, hydrated formaldehyde (methanediol), Cu(II) complexes with various ligands, additives for solution and plating stability. There are many types of stabiliser (equilibrators) which are necessary for following processes: methanediol deprotonisation, complex formation and other interactions between components of the chemical solution. Each of these processes has specific influence for the plating[56].

Electroless plating solution contains metal (M) ions - a source of material to plate, ligands (L), which is necessary to keep metal in a complex and protect from undesired chemical reactions in a solution, reducer (Red) – source of electrons for metal reduction, buffer for formation of alkaline environment and additives for various purpose (Ox refers to oxidized form of reducer). General metal ions reduction equation is written in (1).

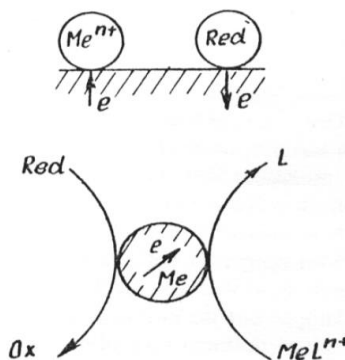
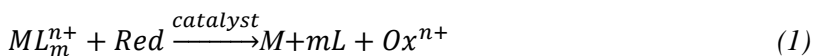


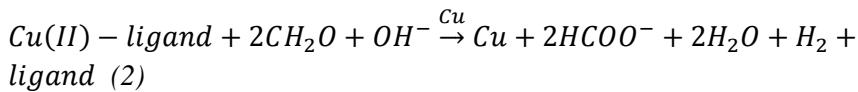
Figure 8. Reducer oxidation and metal ion reduction reactions [57].

The catalyst is necessary for the oxidation reaction of reducer – to transfer an electron to the metal ion. The complete process explanation is still under discussions. The most used approach is that there are two partial reactions

which are related to each other and taking place at the same time: anodic oxidation reaction of the reducer and cathodic reduction reaction of metal ion, as shown in Figure 8 [57]. The main driving force of the autocatalysis process is the reducer oxidation reaction which appears only on the catalyst and produces electric potential necessary for the reduction reaction of the metal ion. Formally in the catalysis process, the free electron has an interim role like shown in Figure 8. An electron can move freely on the surface of the catalyst. Therefore, the reduction reaction takes place not by the direct contact of the particles (electron), but by exchanging an anonym electron, as shown in Figure 8.

#### 2.4.1 Autocatalytic copper deposition

The general equation of autocatalyst reaction for copper is [57]:



Copper (II) ions form complex compounds with ligands. Most known reducer for the reaction is formaldehyde (CH<sub>2</sub>O). During the process, side reaction can also take place. Formaldehyde reacts with OH<sup>-</sup> ions and produces formate anion and methanol. Actually, the general equation does not describe the whole process. For example, formaldehyde initially is hydrated to methanediol before its oxidation reaction. Following, methanediol reacts with OH<sup>-</sup>, and as results, methamediol anion appears. An alkaline environment is necessary for copper autocatalysis process – for reducer oxidation catalysis reaction. Ligands also play a crucial role – it prevents copper ions from reaction with OH<sup>-</sup>. Otherwise, solid insoluble Copper (II) hydroxide could be formed [57]. Ligands usually are sodium potassium tartrate and EDTA [55].

#### 2.5 Techniques of circuit formation on dielectrics

There are many laser-based circuit formation techniques. However, only a few of them are applied in real production [19, 27]. There are destructive or non-destructive circuit formation techniques. Destructive can be assumed those which uses etching procedures for fabrication – photolithography, microscopic integrated processing technology (MIPTEC). Non-destructive methods can be classified into two groups. The first one is selective conductor deposition, like inkjet printing, aerosol printing, and laser-induced forward transfer (LIFT). The second one is selective plating by local surface modification, like laser direct structuring (LDS), selective deposition on the

local roughened surface by a laser – laser-induced selective activation, laser modification of ink paste layer on the surface and the last one – in situ surface modification and metal deposition in the liquid phase. Most of them have advantages and disadvantages for specific application areas.

### 2.5.1 Photolithography

Photolithography is the most widely applicable method for printed circuit board fabrication. There is a lot of literature about photolithography [58, 59, 60]. The main principle of photolithography is exposure to photoresist through the mask on the conductive layer and chemical etching procedures. The process itself can be divided into several main steps: a substrate (textolite) covered by a conductive layer (copper foil, electroless plating or PVD); photosensitive resist layer deposition; pattern formation by laser exposure through a photomask; resist development; chemical etching of metal film; resist removal. The method is very suitable for mass production. However, prototyping with photolithography is very expensive, since the mask has a high cost. Another problem with photolithography is that the conventional (industrial) technology can be applied only on the flat surface. There are few investigation works of the photolithography on the curved surface [61, 62]. However, patterning only on the regular surface like sphere [61] or 2.5 D [62] was shown. The structures were fabricated using an elastomeric mask. The placement of the mask had to be done very precisely, what could complicate the upscaling process for industrial application. Therefore, the application of mask photolithography for moulded interconnect devices, where the parts have a complex 3D geometry is very complicated or even not possible.

### 2.5.2 MIPTEC

Microscopic integrated processing technology (MIPTEC) is a circuit formation technology developed by PANASONIC [27].

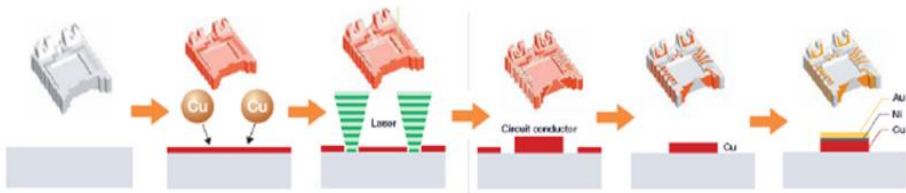


Figure 9. processing steps for MIPTEC technology [27]



materials for printing, based on silver nanoparticles. Moreover, there are many technological issues for printing on 3D complicated geometries.

#### 2.5.4 LIFT

Laser-induced forward transfer (LIFT) is the process which enables deposition of the liquid or solid material in small droplets and affords a high resolution. The technology was first demonstrated by Bohandy et al. [66] It is not widely applied in the industry yet, but a lot of research activities is carried out by the time.

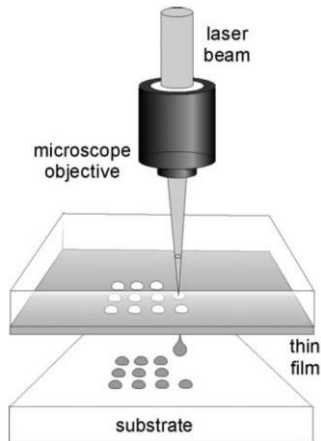


*Figure 11. The principle of the LIFT technique [67].*

Laser-induced forward transfer method relies on the absorption of laser energy in the material of interest causing local vaporisation and expulsion of material from a donor substrate to a receiver substrate on which patterns are formed [68]. Solid state, simple rheological, multiphase, multicomponent can be used for the transfer process. The general process of LIFT is shown in Figure 11. Uniform layer of the material to transfer is covered on a glass slide by spin coating or just by the special blade. The donor substrate is mounted near the substrate, usually about 100  $\mu\text{m}$  above. The process is very sensitive to the distance between the substrate and donor plates. For the transfer process, a laser beam is focused on the interface of the donor material and donor glass plane. The Nd:YAG nanosecond laser is mostly used for the process. The wavelength of the radiation is chosen depending on the material. In the case of silver ink, the 1064 nm wavelength can be used. The light is absorbed by the donor material and generates a rapid increase of the local pressure at the interface. As a result, small droplets of the thin film are ejected from the donor and deposited onto a substrate. This techniques also enables the deposition of

transparent material, using a so-called dynamic release layer (DRL) between the substrate and the film to be transferred [69]. Technology can be an alternative technique for various processes like electronic components placement, such as organic thin film transistors or organic light emitting diode, microelectromechanical systems (MEMS), sensors [70] and also for medical applications such as tissue engineering. LIFT can also be used for circuit trace formation on a flexible substrate. Usually PI or PET is a substrate material. The problems of LIFT technology application for the flexible circuit is the adhesion since the substrate is weak. Another disadvantage is the cost of the donor. Silver ink is costly comparing with copper sulphate used in plating processes. In addition, LIFT has some unresolved problems for 3D surfaces applications [71].

### 2.5.5 Laser sintering of ink paste

There are several methods for ink paste sintering [72], but all of them have many similar procedures. Nonconductive ink solution based on metal compounds is reduced to metal atoms by laser irradiation. Kang et al. [4] made ink paste by dispersing Copper oxide (CuO) particles into a reducing agent solution. The solution consisting of polyvinylpyrrolidone (PVP Mw 10 000, Aldrich, 13 wt. %) and ethylene glycol (Aldrich, 27 wt. %) was mixed with nanoparticles by an ultrasonic wave. Finally, the CuO NP solution with a viscosity of 5000 cps was achieved [4]. The solution was deposited on polyimide (PI) by a spin-coating technique.

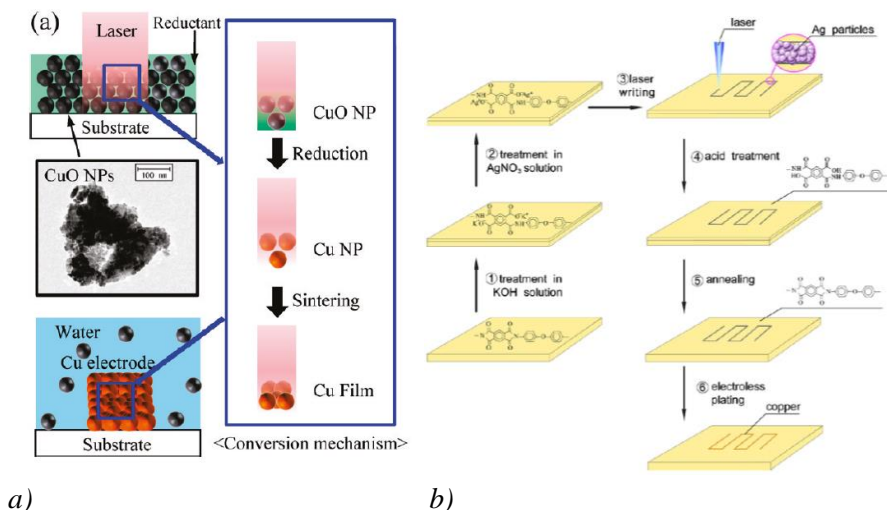


Figure 12. Laser sintering of ink paste: ink paste with copper oxide nanoparticle a)[4]; silver ion ink paste b)[5].

Following, the laser writing procedure was performed. Ytterbium-doped fiber laser was used for irradiation of the deposited layer. Both pulsed nanosecond and CW lasers have been applied.

The whole process chain is shown in Figure 12 a). The irradiating laser beam has photons with energy high enough to brake Cu-O bond. After bond breaking, a reduction of Cu ions by ethylene glycol takes place. Results have been checked by Energy Disperse Spectroscopy (EDS). 90 percent of Cu ions could be reduced by pulse laser irradiation.

Another work has been carried out by Chen et al. [5]. PI films were treated by KOH solution. As a result, PI became hydrolysed, and potassium polyamine was generated. Following, the specimen was immersed in the AgNO<sub>3</sub> solution. Therefore, Ag ions exchanged the potassium ions (Figure 12 b). Laser writing was performed by Nd:YAG laser nanosecond laser with the IV harmonic wavelength. After laser irradiation, the Ag ions were reduced to Ag<sup>0</sup> [5]. The disadvantages of both processes are very similar concerning with the difficulties of thin layer deposition. In the case of the complex 3D surface, it becomes almost impossible. Another technological problem is very low laser writing speed in the hundreds of microns/s during the reduction process.

#### 2.5.6 Laser-induced selective activation

Zhang et al. presented a technology [6] for selective copper plating on laser modified areas in a water environment, followed by chemical palladium activation and electroless plating as shown in Figure 13 b). Firstly, polymeric specimen – polycarbonate was immersed in distilled water. The fundamental radiation of an Nd:YAG nanosecond laser was used to modify the polymer surface in the water. After the treatment, a sample was activated in palladium colloidal solution for several minutes. The rinsing after activation with palladium was performed in the distilled water. The last step – electroless copper plating was applied for deposition of conductive circuit. Selective plating process has also been tried by performing laser activation in the air. However, no selective plating has been achieved.

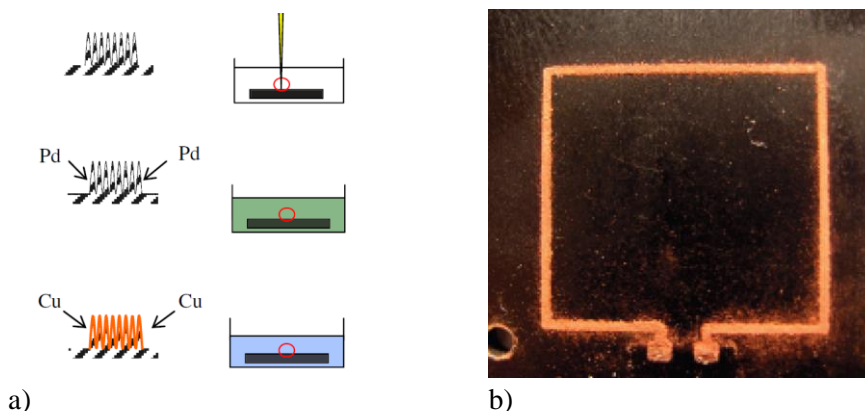


Figure 13. The working principle of selective laser activation a) and metalised sample using this method b) [73]

Authors also investigated the mechanism of activation. They found that selective plating took place due to the increase in the surface roughness of the laser processes areas. The strong correlation between roughness and plating was observed. The explanation of the mechanism is: laser treated polymeric surface in water produces the rough and sponge-like structure. The palladium solution diffuses in these pores during the activation procedure. The washing step rinses all palladium from the untreated surface. The diffusion time from the pores is longer, and thus the palladium stays in laser-modified areas after rinsing [74]. However, the spatial selectivity is not sufficient for many applications since palladium is very active and usually activates also laser not processed areas (see Figure 13 b). Moreover, laser processing of the sample in a liquid complicates the application for 3D objects.

### 2.5.7 Laser-assisted metal deposition from the liquid phase

Promising, one step process of local metal deposition was shown by K. Kordas et al. [75]. Continuous wave  $Ar^+$  laser exposed polyimide (Kapton) film immersed in the copper electroless plating solution. Plating bath was filled with a standard commercial solution (CUPRO-T-ECHO), which contains copper ion source, reducer (formaldehyde), ligand and  $OH^-$  source. Multiples translation of laser beam has been performed to the surface of PI in a copper bath. Deposition of metal started only after several passes of the laser beam over the sample. The mechanism of the local copper deposition, according to the authors, is that the local heating of the polyimide surface initiates oxidation of formaldehyde (reducer). At the same time, laser-treated polyimide can also generate free electrons for copper reduction. Therefore, localised electrons on the laser-treated surface attract copper-ligand complex, and the copper

reduction occurs in situ. The author applied EDX analysis to determine purity of the deposited copper. However, not only pure copper but CuO was also produced. Moreover, the copper line writing speed reached only several tens of micrometres per second. Such a slow fabrication cannot be accepted by real industrial applications.

#### 2.5.8 Laser direct structuring

State of the art in laser-based selective metal plating on polymers is the LDS method from LPKF Laser and Electronics, Germany developed in 1997 [1]. The structuring is performed using a laser beam that exposes and activates special additives in the plastic compound. Metal oxide (copper oxide spinel) additives are dispersed in a concentration of 4-10% wt. depending on the polymer matrix. These precursor additives are activated during the laser writing process in order to convert them into a catalyst for electroless deposition of the metal, and the laser-scanned area can be selectively plated. This activation process induces physical-chemical and thermal reactions under the focal point of the laser beam. Due to the laser effect, the polymer bonds are broken, and the chemical connections of the metal oxide molecules are released [19]. Metallization of the laser-treated parts starts with a cleaning step, followed by an additive build-up of the tracks typically 5-8  $\mu\text{m}$  thick utilising the electroless copper bath. The last procedure is plating with catalytic nickel and immersed gold. The process steps except for final metallisation with nickel and gold are shown in Figure 14 [19]. High-temperature thermoplastics such as PEEK or LCP, technical materials such as PA, PPA or PET/PBT, and standard plastics such as PC/ABS are available for LDS on the market. Conductor paths with a width of 100  $\mu\text{m}$  and spacing between them of 100  $\mu\text{m}$  are produced with the current technology. The standard system writes at a speed of 4 m/s. In special cases with optimised focusing, more delicate structures with a linewidth of up to 40  $\mu\text{m}$  are possible. Typical layer thicknesses are 7  $\mu\text{m}$  Cu, 7  $\mu\text{m}$  Ni and 0.1  $\mu\text{m}$  Au.

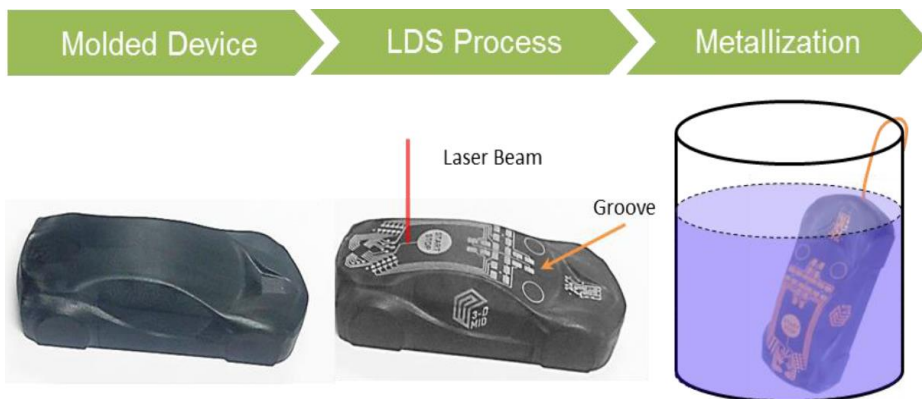
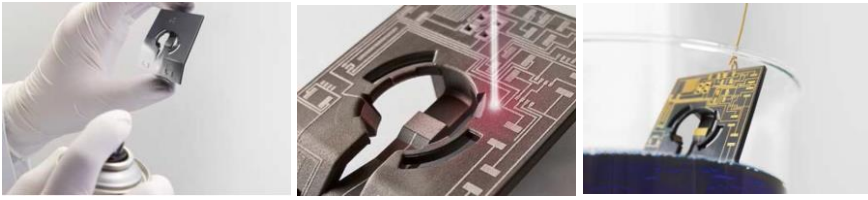


Figure 14. LDS process steps [19].

The advantages of this technology are a rapid ability to change the layout by varying the CAD data, a shorter process chain comparing with conventional PCB fabrication and almost unlimited freedom of the shape. However, usage of LDS additives in polymers rises fundamental limitations for a broad range of industrial application of the LPKF-LDS technology:

- High concentration of the additives 4-8% alters properties of polymers significantly, and an inorganic filler (talk, etc.) is additionally added to the material;
- Polymer price for LDS materials is high since additives used in the whole volume of a part are expensive [8];
- Signal damping and distortion in the radiofrequency application, since LDS additives are metal-based particles. Therefore, the spread into high gigahertz range device is not possible [9].

There are a few commercial materials for LDS available on the market, but most of them are based on expensive metal-organic fillers [8]. In addition, multi-wall carbon nanotubes can also be applied for the LDS material as a catalytic additive [11]. LPKF has also offered a chemical solution for prototyping. The 3D printed part can be coated with a special spray lacquer which contains LDS additives for electroless plating; an example is shown in Figure 15.



a)

b)

c)

*Figure 15. LDS spray technique: Special paint-lacquer is deposited on the surface by spraying a), painted part with a lacquer containing LDS additives are activated by a laser b) and finally plated by electroless plating c)[76].*

There is no free-available scientific information or technical characterisation about LDS proto-paint process.

### 2.5.9 Comparison of the methods

All methods were compared, as shown in Table 1. Eight different criteria were used for comparison: 1) processing speed (H- high, M – medium, S – slow, V refers to very); 2) capabilities of 3D surfaces processing (regular – refers to simple – regular geometry, like sphere or cylinder, free-form allows processing on very complicated 3D geometry; 2.5 D – 2.5 dimensional); 3) the use of expensive materials in the method (Y-yes, N- no); 4) spatial resolution of circuit traces (H- high, M – medium, L – low, V refers to very); 5) capabilities for radio frequency applications at high gigahertz range (5-35 GHz); 6) circuit design capabilities (N. L. –no limitation; L - limited); 7) number of steps for first layer deposition; 8) If the method is destructive or not.

Table 1. Comparison of circuit formation on dielectrics techniques

Method	Speed	3D geometrical capabilities	Expensive materials	Spatial resolution	RF at high GHz	Circuit design	Steps	Destructive
Photolithography	H	Regular 3 D	N	V. H	Y	N. L.	6	Y
MIPTEC	H	Free-form	N	H	Y	L	5	Y
Aerosol jet printing	M	Free-form	Y	H	Y	N. L.	1	N
Inject printing	M	Free-form	Y	H	Y	N. L.	1	N
LIFT	H	Regular 3 D	Y	H	Y	N. L.	1	N
Ag organic paste reduction and sintering	V. S	2.5 D	N	H	Y	N. L.	4	N
CuO paste reduction and sintering by laser	S	2.5 D	N	H	Y	N. L.	3	N
Laser-induced selective activation	H	2.5 D	Y	L	Y	N. L.	4	N
Laser-assisted metal deposition from the liquid phase	V. S	2.5 D	N	L	Y	N. L.	1	N
LDS	H	Free-form	Y	H	N	N. L.	3	N
LDS spray	H	Free-form	Y	H	N	N. L.	3	N

### 3. EXPERIMENTAL SETUP

#### 3.1 Samples preparation for LDS

Polymeric granules specially prepared for masterbatch were heated up to the melting temperature in a chamber. The injection of melted masterbatch was performed through the nozzle to the clamped mould under very high pressure (50-1500 bar).

To guarantee high quality in the injection moulded parts the following points have to be considered:

- The material has to be plasticised and injected carefully to avoid adverse effects on the material properties.
- The process settings (such as pressures and temperatures) concerning the machine and mould have to remain constant concerning time and space.

A blend of polypropylene (PP) plastic (Lyondell Basell Hostacom CR1171G black) and industrial MWCNT (XNRI-7 from Mitsui and Co. LTD) was used for injection moulding. Grains of PP were previously mixed with MWCNT in an extruder at the concentration of 2.5%; 5.0% or 7.5% (of MWCNT) by mass. The PIOVAN mixer tool was used together with the Sandretto 330 tonnes injection moulding tool. The extruding temperature ranged 165-175 °C. The injection pressure was 74 bars, and the temperature in a chamber ranged 175-195 °C. Injected polymeric plates in size of 100x150x3 mm<sup>3</sup> were used as a substrate for laser-induced selective metallisation experiments.

#### 3.2 Samples preparation for SSAIL

For SSAIL process following material has been used:

- PC/ABS compound - LNPT<sup>TM</sup> THERMOCOMPT<sup>TM</sup> Compound NX10302, 3 mm thick;
- PA - Ultramid B2S, carbon filled, BASF, 3 mm thick;
- PVC - filled with talc and titanium dioxide, SKZ institute, 3 mm thick;
- PMMA- 140 HF SABIC, 3 mm thick;
- PET –R120416A1 from IT4IP, 100 µm thick;
- PEEK 450FE20, VIKTREX, 1 mm thick;
- PPA – DUPONT HTNF8200 NC010, 3 mm thick;
- Soda lime glass 2 mm thick, TED PELLA;

- Fused silica glass, SigertWafer, 2 mm thick.

All the samples, except the glass and fused silica, were fabricated by injection moulding. The roughness of the surfaces was  $< 0.5 \mu\text{m}$ .

### 3.3 Laser experimental setup for LDS

Two lasers: Baltic HP and Atlantic from Ekspla with different pulse durations of 10 ns and 10 ps at full width at half maximum (FWHM), respectively, were used for the polymer surface activation. The Nd:YVO<sub>4</sub> picosecond laser Atlantic (Ekspla) with the pulse duration of 10 ps, pulse repetition rate of 400 kHz - 1 MHz and maximum average power up to 60 W and the Nd:YAG nanosecond laser Baltic HP (Ekspla) with the pulse duration of 10 ns, pulse repetition rate of 100 kHz and maximum power of 12 W were used for surface modification of PP. Pulse picker has been used for pulse repetition rate reduction for Atlantic laser.

Translation of the laser beam was performed with a galvanometric scanner (Scanlab AG). The experimental setup is shown in Figure 16 (a). The F-theta lens of 80 mm focal length was used to focus the laser beam on the surface of the polymer sample. The laser beam was scanned over the area to be metallised by hatching as shown in Figure 16 (b). The spatially selective activation was tested depending on the used laser wavelength (1064 or 532 nm), scanning speed (from 0.1 to 3 m/s), and the number of scans (from 1 to 50). 50% overlapping of the scanned lines was used, and the average laser power was varied from 0.1 to 1 W. The pulse repetition rate was set to 50 or 100 kHz. In all tests except the tests on spatial selectivity, a defocused laser beam with the spot size of 120  $\mu\text{m}$  in diameter (Gaussian intensity level  $1/e^2$ ) was used.

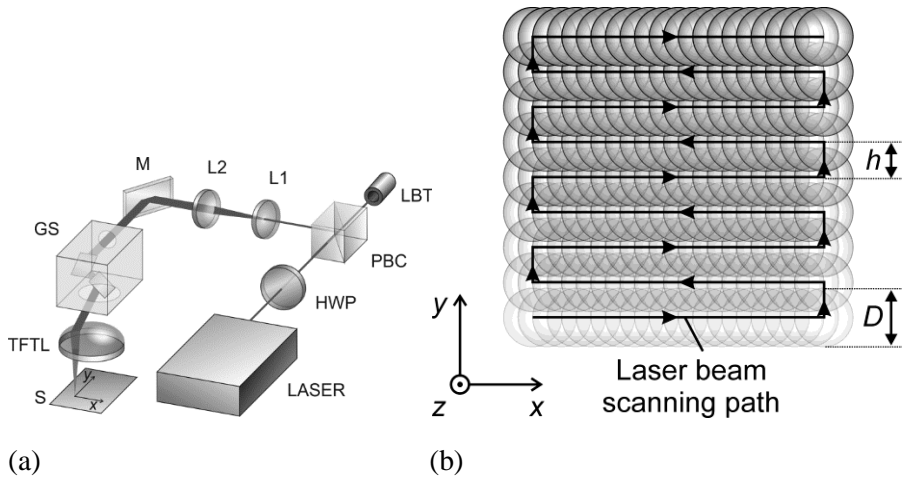


Figure 16 [11]. (a) Experimental scheme of the laser activation of a polymer: LASER - picosecond or nanosecond laser, HWP - half wavelength wave plate, PBC - polarizing beam splitter cube, LBT - laser beam trap, L1 and L2 lens of the beam expander, M - highly reflecting mirror, GS - galvanometer scanner, TFTL - telecentric f-theta lens, S – sample, XY - denotes beam positioning directions: (b) Laser beam scanning path, z - beam propagation direction, D – laser spot size diameter on the sample, h – the distance between overlapping neighbour scan lines (hatch distance).

### 3.4 Laser experimental setup for SSAIL

The same laser processing setup (Figure 16) used for LDS experiment was also applied for the SSAIL tests. Both lasers Baltic HP and Atlantic from Ekspla with different pulse durations of 10 ns and 10 ps at full width at half maximum (FWHM), respectively, were used for the polymer surface activation. The diameter of a focused laser spot of 15-40  $\mu\text{m}$ , laser beam translation speed of 0.1 – 4 m/s, average laser power within 0.1-5 W and hatch – 50% (scanned lines overlap) were controllable parameters for the nanosecond laser processing. In the case of the picosecond laser processing, the pulse repetition rate was 10 – 400 kHz, average laser power was in the range of 0.1 – 40 W and laser beam translation speed: 0.1 – 4 m/s. Both lasers were applied using the 1064 nm fundamental wavelength or second harmonic at 532 nm.

### 3.5 Metal plating for LDS

After the laser activation, samples were copper-plated by immersing them in a chemical bath. Wayne Mayers [77] solution which composition is presented in Table 2 was used for the plating. The temperature of the bath was set to 40° C, and the laser-activated samples were immersed for 30 min.

*Table 2. Composition of the copper electroless plating bath.*

<b>Ingredient</b>	<b>Assignment</b>	<b>Formula</b>	<b>Concentration</b>
Potassium sodium tartrate	Complexant	NaKC <sub>4</sub> H <sub>4</sub> O <sub>6</sub> ·4H <sub>2</sub> O	0.35 M
Copper sulphate	Copper donor	CuSO <sub>4</sub> ·5H <sub>2</sub> O	0.12 M
Sodium hydroxide	Buffer	NaOH	1.25 M
Sodium carbonate	Buffer	Na <sub>2</sub> CO <sub>3</sub>	0.3 M
Formaldehyde	Reducing agent	HCOH	3.41 M

### 3.6 Chemical activation and plating procedures for SSAIL process

After the laser treatment, samples were washed with ethanol 99.8% (Sigma-Aldrich) and rinsed with distilled water afterwards. For chemical activation, a highly diluted silver nitrate (Sigma-Aldrich) solution ( $\sim 10^{-5}$  M) was used. Activation step followed by rinsing in distilled water for 5 min. Finally, electroless copper deposition was performed for 30 min at 30°C. The copper plating bath contained copper (II) sulphate pentahydrate (0.12 M), formaldehyde (0.3 M), sodium hydroxide (1.2 M), sodium carbonate (0.3 M) and sodium-potassium tartrate (0.35) (all Sigma-Aldrich) and pH = 12.7. All steps of the SSAIL method are shown in Figure 27.

### 3.7 Sheet resistance measurements for quality evaluation

The quality of the surface activation was investigated by testing samples after the copper plating. The technique was used for both methods of metallisation (LDS and SSAIL). The sheet resistance was measured using the four-probe method [78]. The results of sheet resistance measurement were used in optimisation of laser processing and chemical plating parameters. The scheme of the measurements is shown in Figure 17.

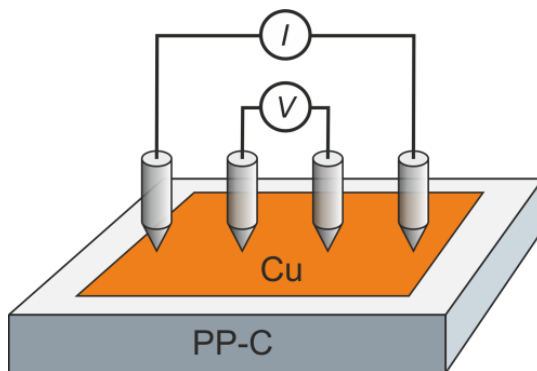


Figure 17 Scheme of sheet resistance measurements using the four-probe method.

The technique uses 4 probes aligned in one line as shown in the scheme. The distance between adjacent probes is 2 mm. Electric current is applied to the outer probes while the voltage is measured by inner probes. Average sheet resistance is calculated by equation 3 [78]:

$$R_s = \frac{\pi}{\ln 2} \frac{V}{I} = 4.532 \frac{V}{I} \quad (3)$$

where  $I$  is the electric current,  $V$  is the voltage.

### 3.8 Morphology analysis with SEM and optical microscopes

Scanning electron microscope (JEOL JSM-6490LV) and optical microscope (Olympus BX52) with digital camera were used to analyse the surface after the laser irradiation and metallisation steps. Optical microscope contains objectives in the range of 5-50 of magnification. Bright and dark field modes were used. Before the SEM analysis, samples, were covered by 50 nm gold layer with the magnetron sputter coater Q150T ES (Quorum Technologies) to avoid charging of polymer surface.

SEI (secondary electron emission) mode (at high vacuum) was used in SEM analysis. Voltage was 20 kV, the working distance was 11 mm.

### 3.9 XPS analysis

X-ray photoelectron spectroscopy (XPS) analysis was performed with the Thermo Scientific ESCALAB 250Xi spectrometer equipped with a monochromatic Al  $K\alpha$  radiation ( $h\nu = 1486.6$  eV).

### 3.10 Surface wetting of water measurements

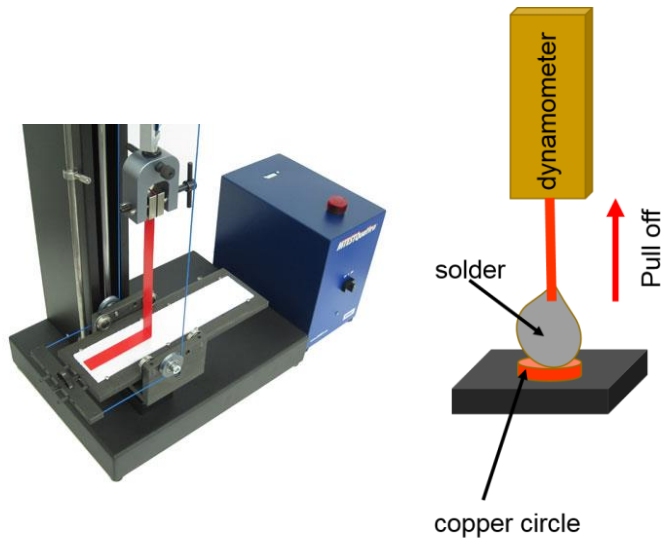
Water drop dynamics was measured by a contact angle meter (KRUSS DSA25). The volume of the drop has been calculated from the cross-section of a drop photo. Transient analysis of wetting dynamics has been made.

### 3.11 Raman spectroscopy

Raman spectroscopy was used to investigate a mechanism of the polymer activation. Raman spectrometer/microscope inVia (Renishaw, UK) has been used. A continuous-wave laser with a power of 10 mW and the wavelength of 632.8 nm was applied for excitation of a sample. A microscope objective with the magnification factor of 50X was used to focus the excitation beam on the surface of the specimen. Each spectrum was averaged by collecting it ten times. The spectra were measured in the range of 250-3200  $\text{cm}^{-1}$  using four different detectors. Analysis of the D and G Raman band before and after the laser treatment of a specimen was utilised to investigate the crystalline structure of the PP with MWCNT (PP-MWCNT) additives.

### 3.12 Adhesion measurements

For adhesion measurement, a standard Scotch tape test: ASTM D3359 – 17 [79] has been applied for LDS samples (see Figure 18 a). The copper patterns for the scotch tape test were modified into a net structure with the line width of 1 mm and the same gap between them. Samples which passed the Scotch tape test were checked by another technique. The adhesion has been checked by soldering the wire onto the deposited copper pad with an area of 1  $\text{mm}^2$  and pulled off with a mechanical dynamometer as shown in Figure 18 b.



a)

b)

*Figure 18. Measurements techniques applied for plated copper adhesion strength measurements: a) scheme of scotch tape test [80] and b) solder measurements with a dynamometer.*

### 3.13 Profile measurements

Profile measurements of the surface after the laser process and the plating were measured with mechanical profiler Dektak 150. Resolution to Z component (perpendicular to the surface) was 5 nm. 50 nm needle has been used for the test. The profile was measured by layout of 1600  $\mu\text{m}$  length lines (measuring time 12 s).

## 4. LDS EXPERIMENTS WITH PP DOPED MWCNT

**The material related to this chapter has been published in [A2], [A5], [A6], [P2], [C1-C7].**

In this chapter, a selective metallization for polypropylene doped with multiwall carbon nanotubes using the LDS approach has been investigated. The idea to test new additives for the LDS process came from the industrial request to find a cost-effective solution for LDS polymers. The work was started in collaboration with FIAT Research Center in FP7 project APPOLO. Pico- and nanosecond laser were tested for laser activation of PP-MWCNT. After the activation step, the electroless metal deposition procedure was applied. The mechanism of activation was investigated using the sheet resistance measurement of laser-processed and plated surfaces with copper. Raman spectroscopy was used to define structural changes of the polymer after laser irradiation. Selective activation and plating mechanism were suggested based on experimental results. The investigated process for the new LDS material was applied to produce working demonstrators.

### 4.1 Analysis of plated surfaces for different parameters of laser activation

Laser processing parameters used for investigation are described in the experimental section. First, surface areas (3x10 mm) were irradiated by nanosecond and picosecond lasers by changing average laser power and scanning speed. The hatch distance in the area was kept equal to the radius of a focused beam. Polymer samples after the laser processing were immersed in to chemical bath for electroless copper deposition procedure.

Initial results for laser treatment of PP doped with MWCNT additives showed that electroless plating took place only after the surface was irradiated with nanosecond laser pulses at 1064 and 532 nm wavelengths, 0.1-2 W average power of the irradiation and 50 kHz of pulse repetition rate, scanning speed 0.1-1 m/s. Despite extensive investigations, no plating was observed for samples structured with the picosecond laser in the investigated irradiation range. Therefore, the later experiments were continued only with the nanosecond laser. As known from the literature [13], picosecond pulses (in the range of tens of ps) refer to “cold” photo-chemical ablation process, while the interaction of nanosecond pulses with the material leads to its thermal decomposition. The laser-activation process of PP with MWCNT additives

seems to be based more on thermal effect than selective ablation of PP, leaving the additives of MWCNT un-ablated as claimed in [81].

Initially, the influence of the average laser power (0.1-0.9 W) and scanning speed (0.1-1 m/s) for the surface activation was investigated at the pulse repetition rate of 50 kHz. A single scan of the laser beam was used. The sheet resistance measurements were performed for the laser-treated areas after their electroless metallisation to estimate the effect of laser processing parameters on the surface activation. The test results are presented by plots for both used wavelengths in Figure 19, where the sheet resistance is replaced by the sheet conductance ( $1/R_s$ ).

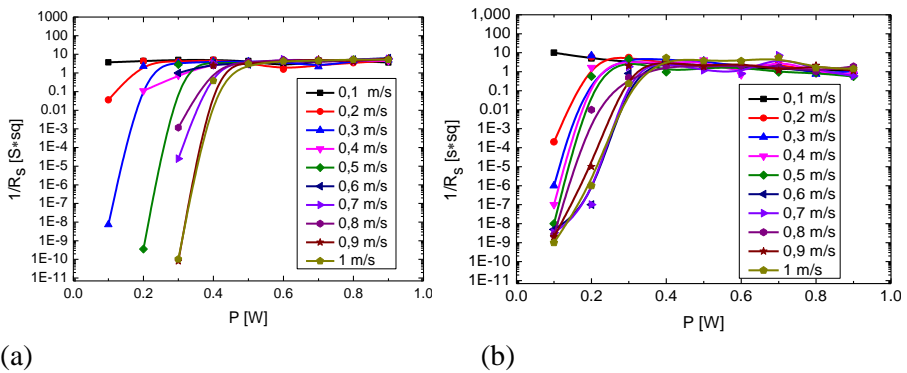


Figure 19. Dependence of the sheet conductivity on the average laser power for various scanning speeds. The chemical plating parameters were fixed. The measurement data were fit with spline curves. (a) represent the results of the laser activation using the 1064 nm and (b) of 532 nm wavelengths [11].

The sheet conductance increased with the growing laser fluence (power) until it reached the saturation. The sheet conductance stopped growing and saturated when the whole laser-activated surface was completely covered by a metal (Figure 20 d), while, in the growing stage of the curve, not whole laser-modified surface area was covered by copper as shown in Figure 20 (a, b, c). It is clearly seen from Figure 19 that for each scanning speed, there was a particular laser power value when the sheet conductance saturated.

The relation between the scanning speed, average laser power, and hatching distance were combined into a single parameter – the irradiation dose in  $J/cm^2$  which accumulate the whole laser irradiation per spot (4)

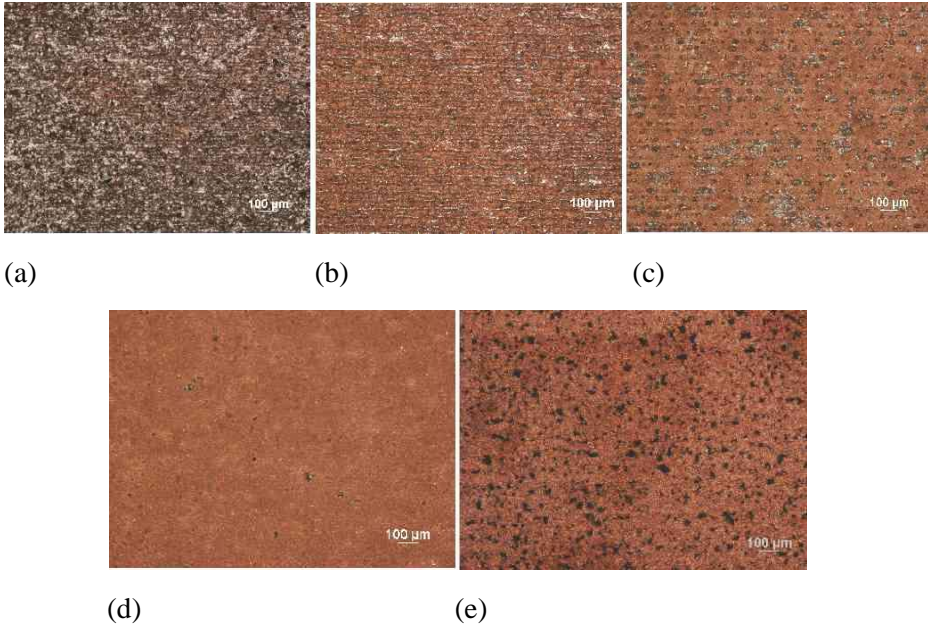


Figure 20. Optical microscope images of metallised PP-MWCNT surfaces structured with the 532 nm wavelength at the 0.8 m/s scanning speed and various settings of average laser power: (a) 0.1 W, (b) 0.2 W, (c) 0.3 W, (d) 0.4 W and (e) 4 W [11].

$$D = \frac{P \cdot h}{V \cdot \pi \cdot w^2} \cdot 10^8 \quad [\text{J}/\text{cm}^2] \quad (4)$$

$D$  is the irradiation dose,  $P$  is the average laser power,  $V$  is the laser scanning speed,  $h$  is the hatch distance,  $w$  is the radius of the focused laser beam. All measurement results were combined and presented as the sheet conductance in dependence on the irradiation dose (Figure 21).

Although the same equivalent irradiation dose values were calculated from different parameter sets of laser processing (scanning speed and laser power), the samples processed at those regimes exhibited similar values of the sheet conductance. That results indicate that the laser-activation of the polymer surface has a threshold character on the absorbed laser energy. The drastic increase in the sheet conductance started at the dose of  $0.55 \text{ J}/\text{cm}^2$  and stabilised at the high ( $S \cdot \text{sq}$ ) value when the irradiation dose was higher than  $1.4 \text{ J}/\text{cm}^2$ . The laser activation threshold value was considered to keep at  $0.55 \text{ J}/\text{cm}^2$ , where the linear growth of the sheet conductance started.

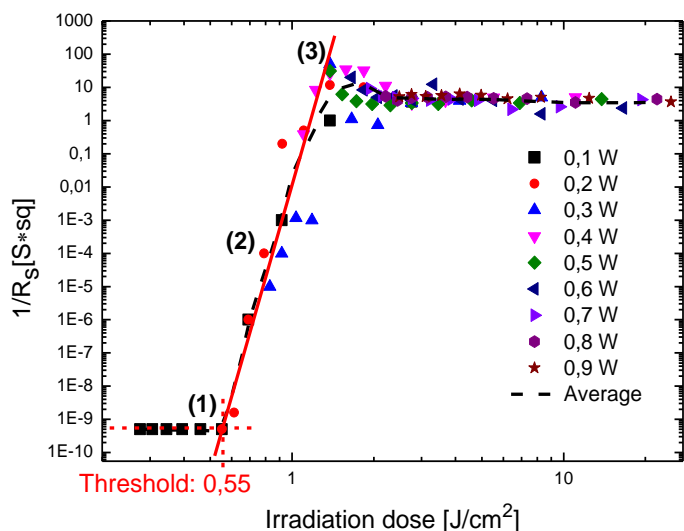


Figure 21. Dependence of the sheet conductance on the irradiation dose. Laser radiation wavelength was  $1064\text{ nm}$  [11]. MWCNT concentration was 2.5%.

For a better understanding of the laser-activation step, the scanning electron microscope (SEM) imaging of the surfaces treated with various laser irradiation doses before the metallisation step was performed. Any noticeable changes in the polymer surface were observed for the doses below the threshold value. However, SEM pictures revealed the melting of the polymer surface when the irradiation dose was above the threshold.

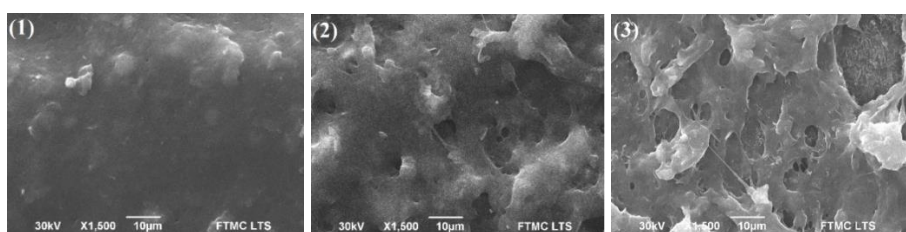


Figure 22. Top-side SEM images of polymer surface processed with the indicated irradiation dose value around the activation threshold. Numbers 1-3 in the pictures correspond to the irradiation dose values numbered in Fig.21 [11]. Dose of irradiation dose: 1 -  $0.6 J/cm^2$ ; 2 -  $0.9 J/cm^2$ ; 3 -  $1.3 J/cm^2$ .

The steep increase in the sheet conductance started at approximately  $0.55 J/cm^2$  and ended at  $1.4 J/cm^2$ . In this range of irradiation doses (from  $0.55$

to  $1.4 \text{ J/cm}^2$ ), the growing amount of re-melted PP-MWCNT material was evident on the surface by increasing the irradiation dose (Figure 22).

The sheet conductance was the highest when the surface of PP-MWCNT looked totally re-molten. The SEM analysis proved that irradiation conditions leading to the surface activation also induce melting of the surface. The laser activation threshold of the irradiation dose correlated with the melting temperature (as seen from SEM images in Figure 22) of the PP-MWCNT composite surface.

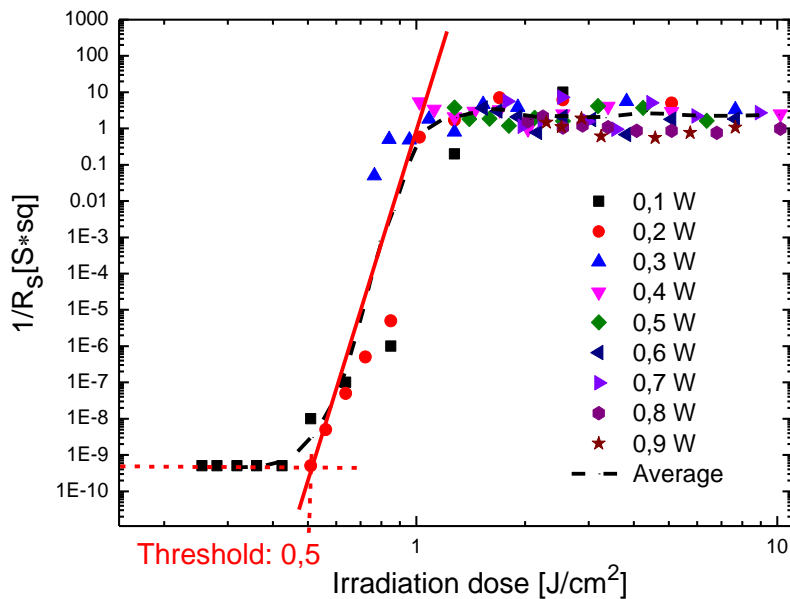


Figure 23 Sheet conductance dependence on the irradiation dose when laser irradiation was made by the 532 nm wavelength [11].

Both used laser wavelengths showed a similar behaviour of the activation. We suggest that the activation process is related to polymer surface melting. However, the threshold irradiation dose for the 532 nm wavelength was slightly lower as is shown in Figure 23. This difference in the irradiation dose threshold could be affected by the absorption coefficient of PP which is higher for the shorter 532 nm wavelength [82].

The maximum sheet conductance of the copper-plated samples was found after activation with the dose of  $1.4 \text{ J/cm}^2$  in the case of 1064 nm and  $1.3 \text{ J/cm}^2$  for the 532 nm wavelength (Figure 21 and Figure 23, respectively). The slight

decrease in the sheet conductance with further increase of the irradiation dose was, probably, related to the rougher surface of the polymer after its activation using a higher dose of irradiation. Using much higher irradiation dose ( $\sim 13 \text{ J/cm}^2$ ), burning of the polymer surface took place, and, as a result, the surface was not fully covered by a metal (see Figure 20 (e)).

The sheet conductance measurement of the metal-plated specimens for various concentrations of MWCNT additives (from 2% to 7.5% by mass) did not show distinct changes in the final resistance value of the plated copper film.

Influence of the number of scans on the polymer surface activation was also investigated in our experiments. The same investigation method was used – measuring the sheet resistance of the finally plated samples. Multiple scanning over polymer surface varying irradiation dose did not provide any benefits. Several passes by a laser beam reduced the conductivity of a coated surface for the irradiation doses above the threshold. However, it increased also the conductivity of metallised copper for irradiation dose below the laser-activation threshold for a single scan. The reason is that later scans accumulated modifications of the surface and thus surface exceeded the melting point with lower fluence. Unfortunately, multiple scanning for the doses below the threshold did not allow to reach better metal plating quality comparing with a single scan when using the laser irradiation dose above the activation threshold.

For optimisation of the laser processing time, the maximum scanning speed of 3 m/s (limited by the used galvoscaner) was tested for activation as well. The pulse repetition rate was increased to 100 kHz in order to have sufficient overlap of laser pulses. Irradiation dose value was kept optimal for the 1064 nm wavelength –  $1.4 \text{ J/cm}^2$ . No significant changes in sheet resistance were observed after the copper plating. That indicates further potentials for upscaling the laser activation process speed.

The sheet resistance tests of the laser-treated but non-metallised and untreated surfaces were performed as well. The PP without MWCNT was also measured as a reference sample (0% in Table 3). The results indicated a decrease in the resistance more than 130 times after the laser activation step for PP-MWCNT (see values in Table 3). The equivalent reduction in the resistance was observed for all tested concentration of MWCNT additives in PP (2; 5; 7.5 %).

Table 3. Value of sheet resistance of non-metalized polymer surface.

Concentration of additives	0 %		2.5 %		5.0 %		7.5 %	
Laser treatment	yes	no	yes	no	yes	no	yes	no
Sheet resistance, $[\Omega \cdot \text{sq}] \cdot 10^5$	230	230	1.66	230	1.65	220	1.63	220

#### 4.2 Raman spectroscopy for analysis of laser-activated surfaces

In order to understand what happens with the polymer surface during the laser activation, Raman spectroscopy was applied. Differences in the Raman spectra of the polymer before and after laser activation were analysed. Raman spectra of the initial and treated with laser polymer surfaces are presented in Figure 24.

Raman spectrum of the PP with MWCNT sample before the laser treatment shows a well-recognisable pattern of PP modes (Figure 24 (a)). The middle-intensity band near  $398 \text{ cm}^{-1}$  belongs to the deformational vibration of the C-C-C network [83]. The Raman bands sensitive to the crystalline phase of PP appear at  $808$  and  $840 \text{ cm}^{-1}$  [84]. The presence of the band near  $808 \text{ cm}^{-1}$  indicates that the studied sample contains a crystalline phase, while the line near  $840 \text{ cm}^{-1}$  is a marker of the defected phase which contains helical chains [83]. A stretching vibration of the C-C bond is visible at  $1166 \text{ cm}^{-1}$  [83]. The doublet near  $1439/1458 \text{ cm}^{-1}$  is associated with the deformation scissoring modes of methylene and methyl groups, respectively. In the high frequency spectral region, the C-H stretching vibrational modes are located at  $2848 \text{ cm}^{-1}$  ( $\text{CH}_2$  symmetric),  $2869 \text{ cm}^{-1}$  ( $\text{CH}_3$  symmetric),  $2883 \text{ cm}^{-1}$  ( $\text{CH}_3$  symmetric),  $2906 \text{ cm}^{-1}$  ( $\text{CH}_2$  symmetric),  $2923 \text{ cm}^{-1}$  ( $\text{CH}_2$  asymmetric), and  $2958 \text{ cm}^{-1}$  ( $\text{CH}_3$  asymmetric) [84]. The presence of MWCNT in PP can be recognised from three broad features located at  $1329$  (D band),  $1597$  (G band), and  $2654 \text{ cm}^{-1}$  (2D band) [85]. The intensity of these bands is enhanced due to the resonant Raman scattering.

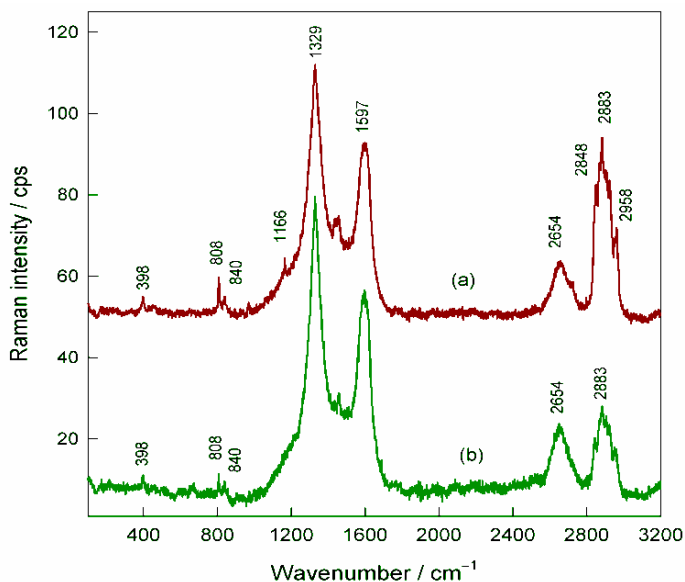


Figure 24. Raman spectra of the PP-MWCNT composite: (a) before, and (b) after laser treatment (0.2 W, 0.2 m/s, 1064 nm). The Raman excitation wavelength was 632.8 nm. Spectra were corrected by using polynomial baseline function fit [11].

Treatment of the PP-MWCNT sample with the laser radiation (Figure 24 (b)) resulted in several apparent changes of the Raman bands. The relative intensity of the PP crystalline phase-sensitive bands  $I_{808}/I_{840}$  decreased from 2.30 to 1.26. Thus, the laser treatment increased the relative amount of the defected phase of PP comparing to the crystalline one. However, the laser treatment induced a substantial decrease in the relative intensity of the PP bands comparing with the carbon-related Raman features. Thus, the relative intensity  $I_{2883}/I_G$  decreased from 1.05 to 0.44.

For analysis of the MWCNT precursor activation, the changes in the D and G Raman band intensities, responsible for carbon structure were investigated. Analysis of the D and G bands, characteristic to carbon allotropes, showed several observable alterations in the spectra after the laser irradiation. Firstly, the relative intensity  $I_D/I_G$  increased after the activation, and, according to Ferrari et al.[85], that indicates the growth in the crystalline cluster size and formation of disordered nanocrystalline structure [85].

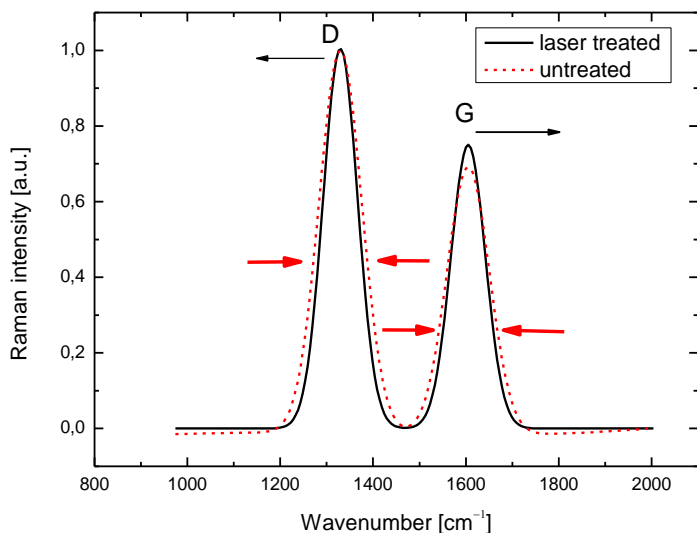


Figure 25. The Gaussian fit of the normalised spectral D and G bands, a surface treated with the laser (black colour), untreated (red colour). Arrows indicate the behaviour of the spectra after the laser activations [11].

Secondly, the narrowing of the D and G bands was observed. This result refers to the decrease in the number of defects (in carbon crystalline phase) – increased structural order. Narrowing of the bands was found by measuring FWHM of the fitted Gaussian curves as shown in Figure 25.

Moreover, a positive shift of the G band and negative shift of the D band were observed. The positive shift of the G band also indicates clustering of the carbon structure [86]. Characteristics of the Raman spectra before and after activation are presented in Table 4.

Table 4. Characteristics of the carbon D and G bands before and after the activation with a laser (0.2 W, 0.2 m/s, 1064 nm).

	Untreated	Treated
I(D)/I(G)	1.37	1.46
D <sub>position</sub>	1337.2 cm <sup>-1</sup>	1333.6 cm <sup>-1</sup>
G <sub>position</sub>	1586.4 cm <sup>-1</sup>	1592.4 cm <sup>-1</sup>
D <sub>FWHM</sub>	108.4 cm <sup>-1</sup>	97.3 cm <sup>-1</sup>
G <sub>FWHM</sub>	108.5 cm <sup>-1</sup>	95.1 cm <sup>-1</sup>

### 4.3 Test of the plating spatial selectivity

Selectivity of metal plating was tested by the varying diameter of the laser beam affecting the polymer surface. The experiments were performed by scanning lines with a defocused laser beam on PP (2.5 % of MWCNT). A sample position was vertically shifted relative to the focus position. Therefore, lines with different width were modified on the polymer surface. The laser irradiation dose was kept constant during these experiments. After the metal plating procedure, the width of the metal lines was measured. The distance out of focus was varied by 1 mm up to 18 mm. The diameter of the activated area diameter was determined from the defocused laser spot size used in all previous tests. The diameter of the activated area was considered to set the width of the plated metal line, and for the 134  $\mu\text{m}$  beam (diameter at Gaussian intensity level  $1/e^2$ ) and the 1.4  $\text{J}/\text{cm}^2$  irradiation dose (averaged over a spot area), it was 60  $\mu\text{m}$ . Precise control of the line width was performed by adjusting the defocussing distance. The width of the line from 22  $\mu\text{m}$  to more than 100  $\mu\text{m}$  was achieved in a single laser scan without hatching as shown in Figure 26.

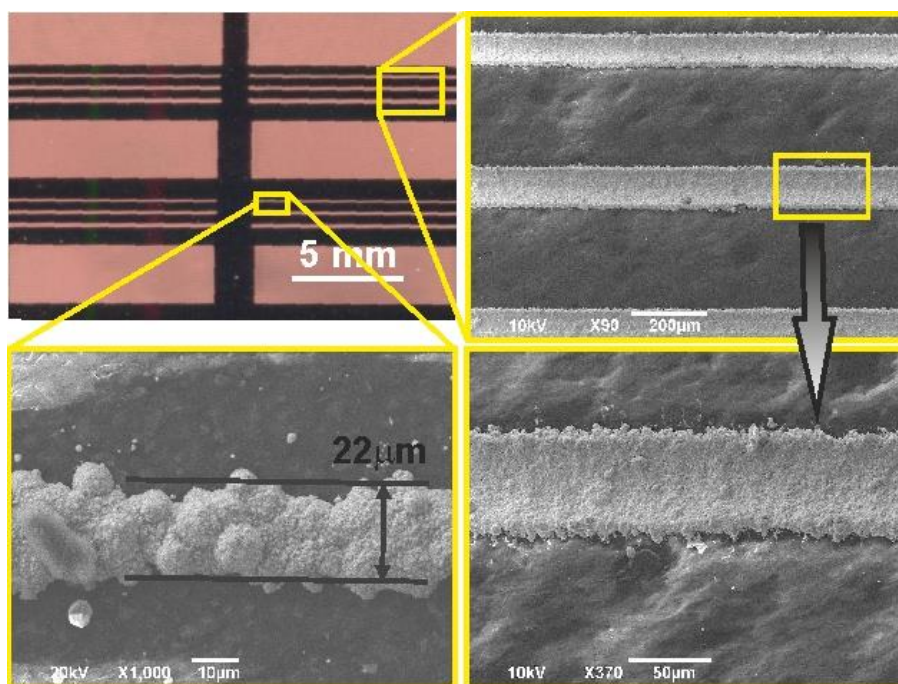


Figure 26. Results of the spatial selectivity of plating by changing the focus position [11].

The narrowest plated line (22  $\mu\text{m}$ ) was fabricated, when the scanning of the laser was done not at the focal point. Further reducing of laser spot size (shifting z to the focus direction) resulted in discontinuity of plated line, the trace contained under-plated part.

#### 4.4. Discussion of the activation mechanism

All analysis results indicate structural changes in the material during the laser activation step. The destruction of the crystalline PP polymeric order was observed in Raman spectra. However, the convincing results necessary for the selective plating were obtained from analysis of the D and G bands behaviour. It was shown that the average size of the crystalline MWCNT clusters was increased, and the formation of disordered nano-crystalline carbon structure was initiated by the laser activation. The necessity of surface melting for activation was proofed by the SEM images at and above the laser activation threshold of the irradiation dose.

Moreover, the change in conductance after the laser activation was shown as well. Therefore, all these results refer to the MWCNT reorientation (reorganisation) in a molten pool of PP at the surface. When the laser beam melted the surface of the composite, MWCNT started to interact in a liquid PP and forms interconnected MWCNT structure resulting in an increase of the surface conductivity by 130 times. The sheet resistance is still too high for application in electronics directly, but it can be a crucial parameter for selective catalytic metallisation of the surface.

The electroless plating procedure which was applied after the laser activation of the surface is a catalytic process. The main driving force in the electroless plating is the formaldehyde oxidation reaction. This reaction is catalytic, and the final product of this oxidation is a free electron on the catalyst surface. The following reaction is a reduction of the metal ion. For this reaction, the free electron reduces the metal ion and a ligand (sodium potassium tartrate) from the complexant compound is released. Therefore, the surface for the plating should be not only catalysing but also electro-conductive in order the electron could freely move on the surface of the catalyst. The increase in conductivity of the laser-activated surface more than 130 times is the key factor for a highly selective metal deposition using the catalytic electroless plating method.

#### 4.5 Results and conclusions

- Selective electroless plating of the polypropylene (PP) doped with multiwall carbon nanotubes (MWCNT) was achieved after its surface activation with nanosecond laser pulses, but no metal plating was obtained after the picosecond laser treatment.
- Activation of the polymer with a nanosecond laser has a threshold for the irradiation dose, and this activation threshold is related to the melting of the polymer surface.
- The final sheet resistance values of the plated metal line did not show any significant differences between the specimens with various concentration of the MWCNT additives in the tested range of 2.5 to 7.5% by weight.
- The surface treatment with the ns-laser also resulted in a decrease of the electrical sheet resistance of the non-metallised PP-MWCNT.
- Raman spectroscopy used in the activation chemistry analysis of PP-MWCNT revealed narrowing of the D and G bands, corresponding to vibration modes of carbon allotropes after the treatment with the ns-laser, indicating a decrease in the number of defects in crystalline phase of carbon. The increase of the I(D)/I(G) ratio after the laser activation referred to the growth in the crystalline cluster size and formation of disordered nano-crystalline structure. The positive shift of the G band confirmed the clustering of MWCNT as well.
- Raman spectroscopy results, SEM analysis, and sheet resistance measurements confirmed reorientation of the MWCNT additives into the interconnected structure when PP was melted by the laser. The increased electrical conductivity of the laser-activated areas enabled the catalytic reaction of reducer in the electroless plating bath.
- The conductive copper lines as narrow as 22  $\mu\text{m}$  were achieved using PP-MWCNT. Polypropylene doped with MWCNT was shown to be suitable for applications in electronics, and that was proved by making several prototypes of functional electronic circuits.

## 5. SELECTIVE SURFACE ACTIVATION INDUCED BY LASER (SSAIL) METHOD FOR SELECTIVE PLATING OF POLYMERS

**Material related to this chapter has been published in [A4], [P1], and [C7-C9].**

Tremendous efforts were put by many researchers in order to eliminate the harm caused by LDS additives (palladium-based metal organic or copper oxide spinel crystal particles) in the injected plastic parts [9, 87, 88]. The idea of this research was to find the method of electric circuit fabrication on LDS-additives-free plastics. Therefore, extended experimental procedures described in Chapter 4 were applied to pure polymers. As the starting point, selective laser activation was chosen [6]. The electroless copper plating procedure requires the catalyst. Since the pure polymer does not contain LDS additives, the activation step with a catalyst has to be done. Palladium colloidal activation has been used in case of selective laser activation. The palladium particles are very active for the copper deposition. Therefore, it is very hard to achieve selective plating. Moreover, the laser processing of the polymer in the liquid is complicated. Initially various catalysing solution has been tested: silver colloid, palladium-tin colloid, palladium ionic, gold nanoparticles, carbon black, however none of them showed appropriate results. After the intensive research, another catalysing solution was found which works well for the selective metallisation process –  $\text{AgNO}_3$ . As a result, a new approach for the laser-based selective plating has been developed and called SSAIL (Selective Surface Activation Induced by Laser).

Technology contains 4 main steps: 1) laser surface excitation and modification, 2) catalyst chemical activation – in  $\text{AgNO}_3$  solution, 3) rinsing, 4) electroless copper deposition in the electroless plating bath (Figure 27).

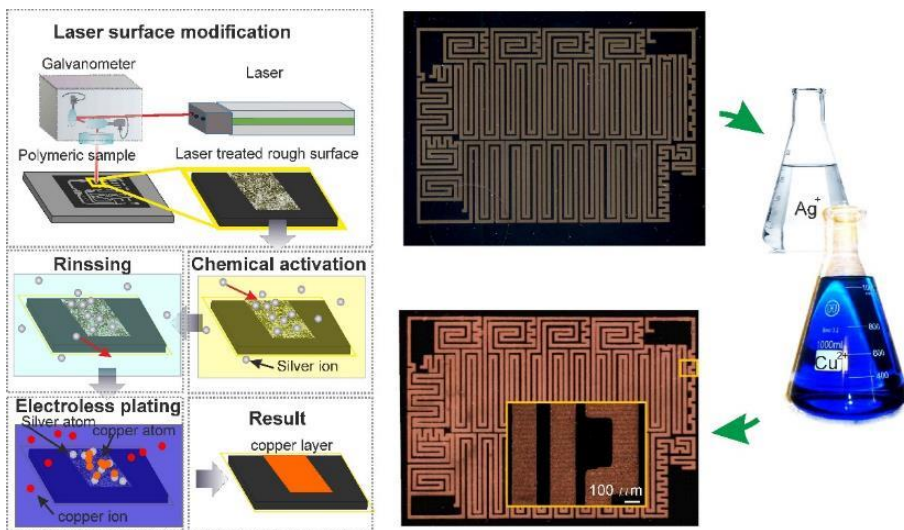


Figure 27 Scheme of the SSAIL process.

In this chapter, the results of an investigation of SSAIL for PA6 are presented. A unique selective plating mechanism was discovered.

### 5.1 Surface activation with pico- and nanosecond laser pulses

Two types of laser (pico- and nano-second lasers described in the experimental setup) were applied for polyamide PA 6 surface modification utilising various sets of laser process parameters for surface irradiation. The pulse repetition rate (for picoseconds: 10-400 kHz, for nanoseconds: 10-100 kHz), the diameter of a focused laser spot (for picoseconds 30 – 50  $\mu\text{m}$  and 40 – 55  $\mu\text{m}$  for nanoseconds), laser beam translation speed (0.1 – 4 m/s for both lasers), the average laser power (for picoseconds: 0.1 – 40 W and 0.1 – 10 W for nanoseconds) and hatch (for picoseconds: 15 – 25  $\mu\text{m}$  and 20 – 27  $\mu\text{m}$  for nanoseconds) were controllable parameters for laser processing. Laser fluence, pulse overlapping, irradiation dose were cumulative process parameters depending on the combination of mentioned parameters and were used for the process analysis.

Both lasers were applied using the 1064 nm fundamental wavelength or second harmonic at 532 nm. The first result revealed that plating is not feasible after the nanosecond laser modification of PA 6 using the SSAIL approach within the whole broad range of parameter window. However, a spatially selective layer was successfully coated only on areas processed by the picosecond laser (Figure 28).

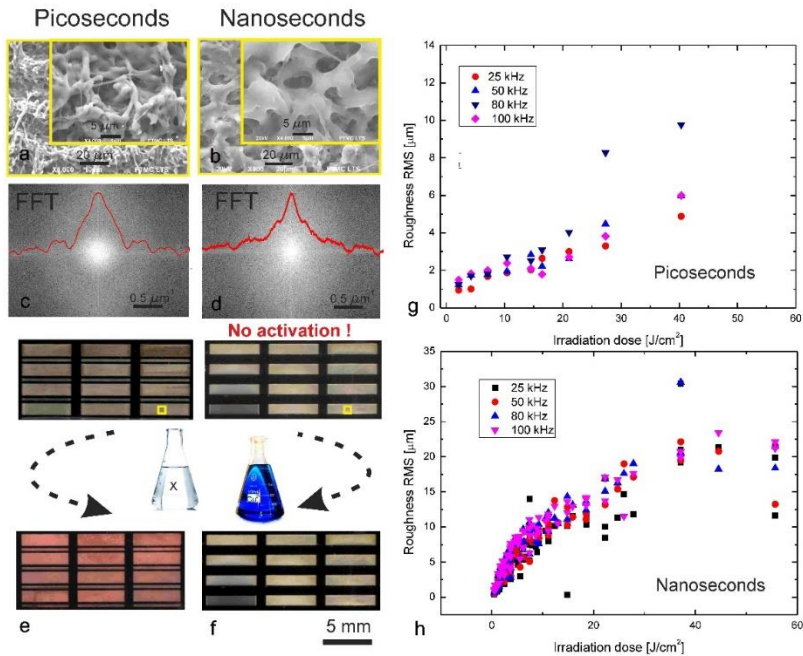


Figure 28. SEM images of PA 6 surface treated by the picosecond a) and nanosecond b) lasers at 10 kHz; 0.6 W and 0.3 m/s scanning speed at 1064 nm of wavelength. Fast Fourier Transformation (FFT) picture of SEM images (c, d). The pictures of the samples after laser processing and final electroless is represented below SEM images (e, f). Plots on the right side indicate the surface roughness after laser processing with nanosecond h) and picosecond g) pulses.

It can be easily seen that the morphology of PA 6 surface is similar after processing with ps- and ns-pulse duration. Both treated samples have a rough, porous surface. The roughness by RMS is higher for nanosecond pulses. However, no correlation was found when comparing the sheet resistance measurements results with the processed surface roughness (see Figure 29). However, the roughness of the surface does not fully describe the structure after laser processing. Therefore, the Fast Fourier Transformation (FFT) of SEM images was calculated for the surfaces processed with nano- and picosecond lasers. FFT images are presented in Figure 28. The red curve in the FFT figure represents the intensity of the image bright pixels in arbitrary units. First noticeable difference in the FFT images is that the central part has a dark ring in case of the picosecond-laser processed surface. This result reveals about quasi-periodic structure in micron scale and disorder, chaotic – orientated distribution (Figure 28). For the sample treated by picosecond

pulses, a fraction of the surface pattern is smaller and thin wire-like structures are formed as seen from the SEM image with a higher magnification. Although both surfaces are porous and rough after laser structuring, the electroless copper deposition after the activation appears only on the surface processed by the picosecond laser pulses.

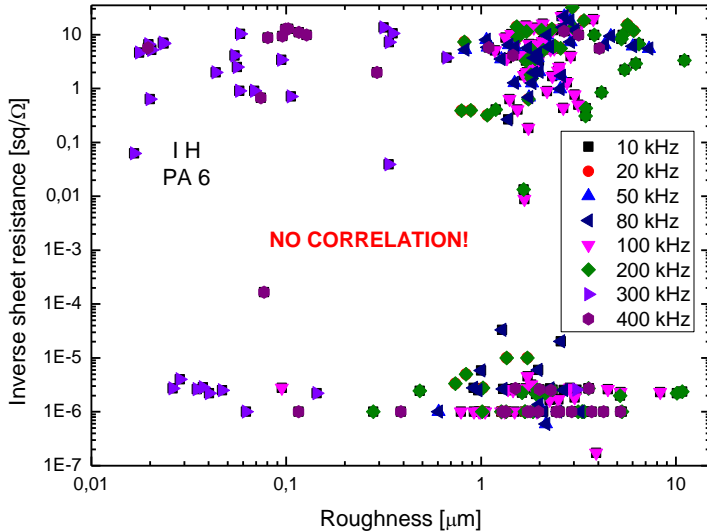
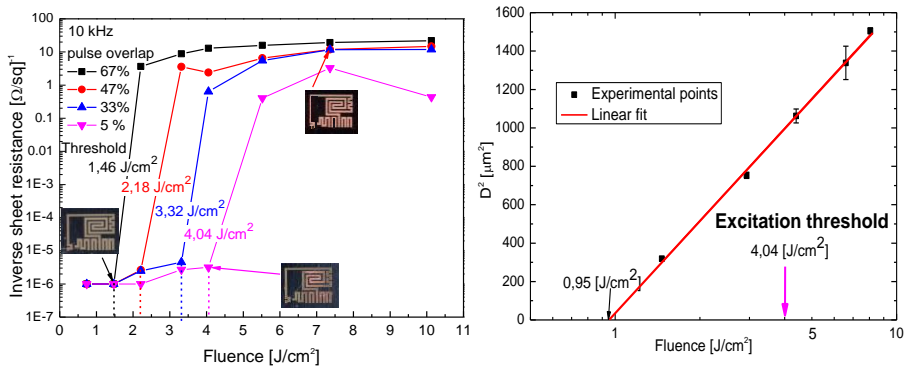


Figure 29. Inverse sheet resistance dependence on the roughness of PA 6 surface processed with picosecond pulses at 1064 nm.

The reason for opposite results utilising the picosecond and nanosecond laser activation could be explained by the different mechanism of the laser light interaction with thermoplastic material for ultra-short pulses. The same pulse energy and irradiation dose were applied in both cases. However, the peak intensity ( $\sim 5 \cdot 10^{11}$  W/cm<sup>2</sup>) was 1000 times higher for the picosecond laser pulses. In the case of the picosecond pulses, the different process can appear due to the high peak intensity of the pulse. Short pulse can transfer light energy to the material very fast. The nonlinear absorption of the polymer becomes significant and important. Therefore, photochemical process can take place leading to a decomposition of polymer and new chemical compounds can be formed. These new chemical groups can be an essential factor for selective activation after the picosecond laser processing. In this case, a hypothesis can be assumed that reducing groups such as aldehydes can be produced on the laser-processed surface.

While after the nanosecond laser processing, the surface microstructure is developed mainly by melt formation and the thermochemical process is

dominant. Therefore, the mentioned differences resulted in different PA 6 modification behaviour both morphological and chemical.



a)

b)

Figure 30. a) Dependence of the inverse sheet resistance on the laser fluence for various settings of the pulse overlapping. Dependencies for different pulse overlapping are presented in colours. Photo inserted in the picture represents plating quality – grey colour appears after laser processing, red colour – plated copper; b) The 'Liu plot' for the ablation threshold of PA 6 at 1064 nm wavelength estimation (red line – linear fit).

However, in the SSAIL process, the laser-induced physical surface morphology (roughness) does not explain selective activation and plating mechanism since the polymer surface is highly rough and has porous (sponge-like) structure after nanosecond laser treatment as well.

All further investigations were performed with the picosecond laser. Polymer surface after the picosecond laser modification and copper plating steps was analysed by measuring the sheet resistance with the four-probe method. The measurement results for various ps-laser fluencies and pulse overlapping settings are presented in Figure 30 a). For convenience, the inverse sheet resistance (conductance) is shown. Every curve in the graph has a region of a steep growth of the conductance starting at a particular laser fluence value. The starting point of the steep growth in the electric conductance of the deposited copper layer corresponds to the threshold of laser fluence for the PA 6 surface excitation. This threshold increases with the decreasing the pulse overlapping (increasing scanning speed). Therefore, it testifies that the origin of the threshold can be shifted by the accumulation of pulse energy. The ablation threshold for a single pulse was also measured for PA 6 (see Figure 30 b) However, the threshold of surface excitation does not coincide with the ablation threshold of PA 6 which is equal to 0.95  $\text{J}/\text{cm}^2$  as shown in Figure

30 b. Consequently, the local copper deposition was induced not only by structural changes related to the ablation process and required more than four times higher laser fluencies.

In addition, the experiments with the 532 nm laser wavelength were also carried out. Decrease in the excitation threshold value down to  $1.45 \text{ J/cm}^2$  was observed in the case of the shorter 532 nm wavelength for the 10 kHz pulse repetition rate. However, the ablation threshold for 532 nm is ( $0.72 \text{ J/cm}^2$ ) also lower.

Morphology of the PA 6 surface after the laser treatment with fluences below and above the threshold was checked by SEM. In Figure 31, the SEM images of the processed surfaces above and below the threshold are presented. The fluences which were used for the surface processing are indicated by numbers in the plot of the inverse sheet resistance dependence on the laser fluence. The surface structure (morphology) of the polymer as seen from SEM images in Figure 31 slightly differs for different pulse repetition rate. However, the surfaces treated with laser below and above threshold value looks similar. No significant changes in morphology were observed after applying the laser fluences above the threshold for all pulse repetition rate shown in Figure 31.

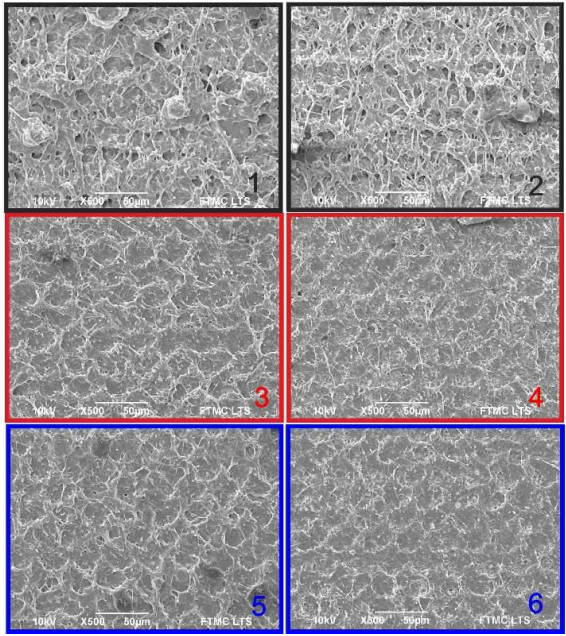
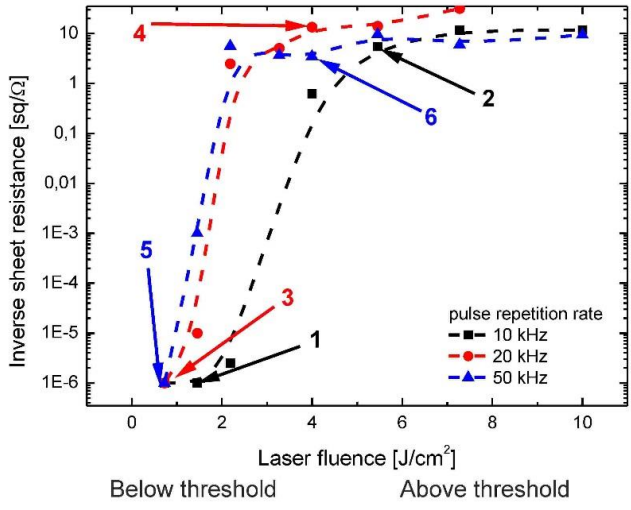
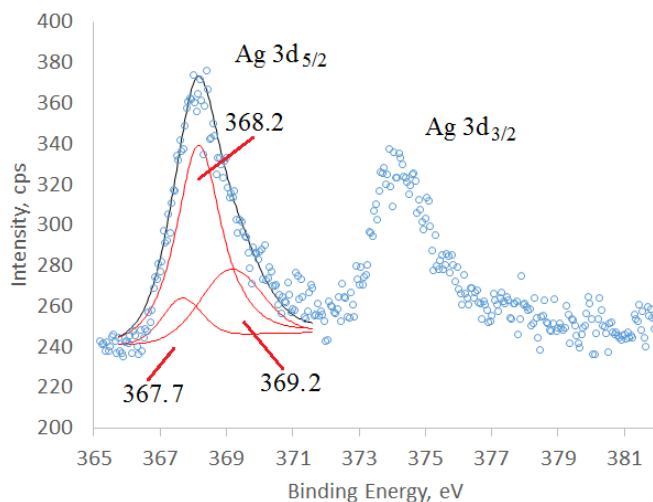


Figure 31. Inverse sheet resistance dependence on laser fluence for various pulse repetition rates: 10 kHz, 50 kHz, 100 kHz. SEM images below the plot present the surface morphology of the PA6 polymer surface after laser treatment with fluence below the and above the threshold. 1064 nm wavelength was used for modification.

Minor differences in the morphology again confirms the fact that the selective plating process is caused not by physical structural changes in surface morphology after laser processing.

## 5.2 XPS analysis of samples

For a better understanding of the SSAIL process, the XPS studies were applied. Three different samples were tested: original, unprocessed by the laser (reference) surface of PA 6; laser-processed PA 6; PA 6 laser-processed and activated with silver. After the laser modification, a slight change in the percentage of atomic composition was observed – a decrease of carbon from 81.45% to 77.86% (atomic) and an increase of nitrogen from 7.5% to 10.2%. Analysis of the laser-modified and silver-activated areas is extremely important for the SSAIL process understanding. XPS spectrum for silver bonds of the laser-processed and the activated surface is shown in Figure 32.



*Figure 32. High-resolution XPS spectrum of the laser-treated PA 6 area after its activation with silver: circles - raw data; red lines – fitted peaks, black line - envelope data. The peak 367.7 eV corresponds to the silver bounds with oxygen ( $\text{Ag}_2\text{O}$ ), 368.2 eV - metallic silver, 369.2 eV - other unresolved silver bounds ( $\text{AgNO}_3$ ?) or Ag bounds with the polymer.*

Positions of fitted peaks shown in Figure 32 are in good agreement with known data of the Ag  $3d_{5/2}$  positions for oxidised silver 367.47 eV ( $\text{AgO}$ ) and 367.7 eV ( $\text{Ag}_2\text{O}$ ) [89], and 368.2 eV for metallic silver [90]. Therefore, the peak at 367.7 eV can be assigned to silver bounds to oxygen ( $\text{Ag}_2\text{O}$ ); peak at 368.2 eV - to metallic silver and peak at 369.2 eV – to other unresolved silver

bounds ( $\text{AgNO}_3$ ) or Ag bounds with the polymer. From Figure 32, it can be easily seen that the intensity of the metallic silver  $3d_{5/2}$  peak (368.2 eV) is dominant. Therefore, it can be considered that most of the silver ions (from the activation step) are reduced to metallic silver. The silver nitrate solution which was used for the activation step does not contain any additional reducing agent. Hence, the silver ions have been reduced on the laser-processed PA 6 surface by the chemical products which could appear during the laser modification; e. g. the picosecond laser irradiation introduced oxygenated carbon-containing functional groups [91], (Figure 33) which can enhance adsorption of Ag (I) as well as act as reducing groups, reducing the adsorbed Ag(I) ions to neutral atoms. The metallic Ag acts as an initial catalyst for autocatalytic electroless copper deposition.

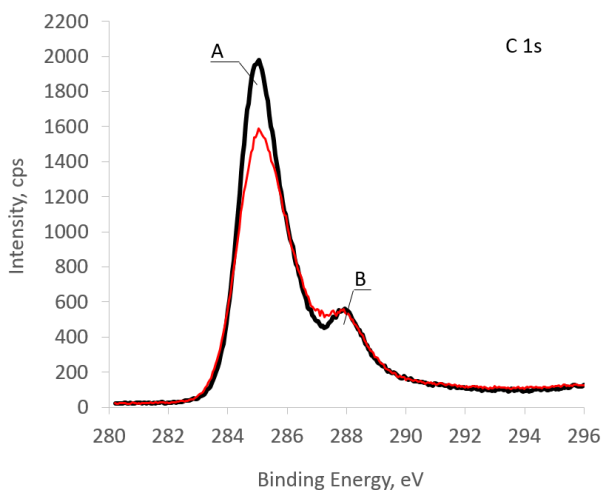


*Figure 33. High-resolution XPS spectrum of the C 1s region acquired for the untreated surface of PA (thick black line) and laser processed PA area (thin red line).*

The main peak “A” in Figure 33 at 284.6 eV can be assigned to overlapping C-C, C-H and C-N bonds [92]. The peak at 288 eV was attributed to CONH bonds in PA 6 [92] overlapping with carbonyl C=O (288 eV) bonds [91] and partly overlapping with O-C=O bonds (approximately at 288.8 eV) [92]. The calculated ratio of these peaks (A/B) was approximately 3.5 and 2.8 for untreated, and laser processed PA 6. The same increase of C=O peak intensity was found in [92] for UV laser-irradiated Polyetheretherketone (PEEK) surface, where C-C and C=O peak ratio was about 8.6 and 4.4 for the untreated and laser-processed area, respectively. Calculated ratio difference of the sample and data found in the literature [91] could arise due to differences in

processed polymers since CONH bonds are present in PA 6 and but not present in PEEK [92]. Similar results are reported in [92] for plasma treated PA 6 where A/B ratio was about 6.3 and 3.6 for the untreated and plasma-treated area, respectively. It is also worth to mention that in both cases described above [91], surface composition changes were reported as well. Namely, increased oxygen and nitrogen content and decreased carbon content on the laser-treated surfaces correlates with surface composition changes in the present work.

### 5.3 Wetting dynamics analysis of processed surface

Surface interaction with ionic solution strongly depends on the surface energy [93]. Wetting properties of the PA 6 surface were tested before and after laser modification by investigation of a water droplet dynamics. A video camera was used to capture the droplet on the PA 6 surface. In addition to the picosecond laser processing, nanosecond treatment was also analysed.

Water droplet volume was calculated from a cross-section picture of a water droplet at different moments after the droplet contact with the surface. Figure 34 shows the results of five different samples: PA 6 washed with ethanol and rinsed with water afterwards (as ethanol was used to clean the sample after the laser processing); PA 6 processed by the ps-laser; PA 6 prepared by the ps-laser and washed with ethanol, rinsed with water afterwards and the last two cases have been repeated using ns-laser. Figure 34 shows that wetting results are different for each surface. Unprocessed surface shows almost no changes in wettability. The volume of a droplet changes insignificantly as well as the contact angle. Different behaviour shows the PA 6 surface processed by a laser (without ethanol rinsing). Similar results were also after the ns-laser processing. The decrease in the droplet volume and the growth in the contact angle were observed.

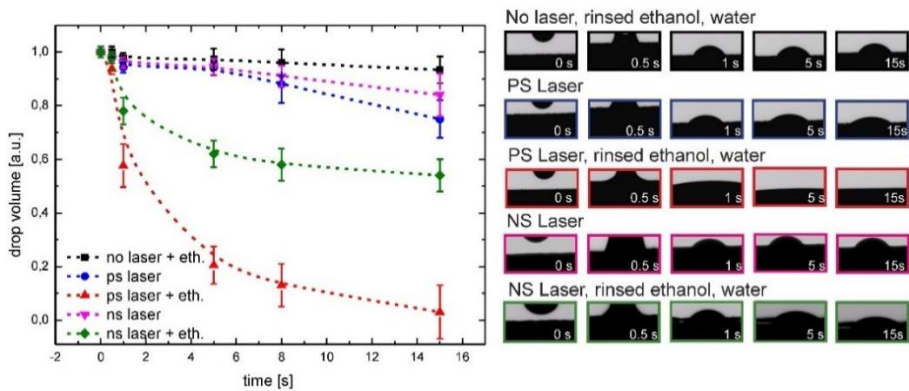


Figure 34. Dynamics of the PA 6 surface wetting. Photos of the water droplet on PA (on the right), from the top: PA 6 surface rinsed with ethanol and water after; PA 6 surface modified with picosecond (PS) laser; PA 6, ps-laser-modified and rinsed with ethanol and water after, PA 6 surface modified with nanosecond (NS) laser, NS-laser-modified and rinsed with ethanol and water after. The plot (on the left) presents time-depended dynamics of the droplet volume for all five surfaces of PA 6 shown in photos.

Reduction in the droplet volume could be caused by water spreading over the structured PA 6 surface (Figure 34). As the surface of PA 6 modified by the picosecond laser has a rough and porous structure, the liquid can diffuse inside the cavities and distribute uniformly. The laser-modified and rinsed with ethanol and water sample showed complete different wetting dynamics. The surface was super-hydrophilic, and water droplet disappeared after a few seconds.

As known from [94], the ethanol enhances the interaction (wetting properties) with water. The nanosecond laser processing and ethanol washing have shown less hydrophilic properties, but still, the increase in water droplet absorption was significant. Different wetting behaviour after the ethanol rinsing for the laser-modified and unmodified areas could be explained that water easily washes away ethanol from a smooth surface. However, that does not happen from the laser-structured areas.

Rinsing of the whole plastic surface (pre-treated with the picosecond laser radiation and not) with ethanol and later with water plays a crucial dual role in the overall process of metallic coatings formation:

- 1) rinsing with ethanol enhances the wetting properties of the surfaces dramatically (see above);

2) sequential rinsing with water eliminates ethanol from the untreated by a laser surface, which wettability again decreases dramatically, whereas some amounts of diluted ethanol-water mixture remain in rough and porous surface areas of the laser-ablated plastic and secure the wettability of the surfaces to be activated by silver and later plated with copper.

However, the mentioned mechanism of the increased wettability for laser-treated areas cannot explain the whole SSAIL process, because only roughening of the surface does not enable to activate the surface for electroless copper deposition. This was proofed by the SEM image in Figure 28 of the laser modified PA 6 surface with nanosecond pulses or SEM images of the surface after picosecond laser processing below the activation threshold Figure 31.

The selective plating mechanism can be explained by the combined process of silver ion adsorption by increased wettability of the laser-treated surface and ability of the laser-modified surface to reduce silver ions to neutral atoms

## 5.4 Results and conclusions

- A new method of laser-induced selective electroless polymer plating by copper was developed, including the additional step of chemical surface activation after the laser treatment.
- The SSAIL method works with the picosecond pulse irradiation and has a threshold of irradiation dose but does not work with a nanosecond laser irradiation.
- No correlation between selective plating and surface roughness after the laser structuring was observed.
- XPS spectra of the laser-excited and catalyst-activated areas have shown that silver ions can be reduced to silver atoms by PA6 polymer surface treated with picosecond laser pulses above the threshold of irradiation dose.
- Wetting dynamics tests disclosed an essential role of rinsing with ethanol, which increased adsorption of silver ions from water solution to the laser exposed areas.
- The selective plating mechanism can be explained by the combined process of silver ion adsorption by increased wettability of the laser-treated surface and ability of the laser-modified surface to reduce silver ions to neutral atoms.

## 6. EVALUATION OF SELECTIVELY-PLATED SURFACE QUALITY, RELIABILITY AND OPTIMISATION OF THE SSAIL PROCESS

**Material related to this chapter has been published in [A1, A3, C10, C11, and C12].**

Practical implementation of the SSAIL technology into industry forced us to make special validation of the technology on selectivity and reliability of plating and optimisation of the process for different materials.

It is not easy to evaluate selective plating quality. Firstly, the required properties should be described. As the selective plating technology aimed for electronic circuit application, the necessary properties are as follows: good electrical conductance, the selectivity of plating, adhesion of metal to the substrate, and resistance to the temperature variation. All these properties could be influenced by many other factors of the plated track. For example, the conductance of the plated surface depends on deposited metal thickness, line width, the morphology of the layer and many other factors.

### 6.1 Sheet resistance

One of the best evaluation parameters is electrical resistance. In this work, a sheet resistance was measured using the four-probe method, as described in the Setup section. One resistance test can detect plated surface irregularities, which can be caused by many processes. The typical properties which can affect the sheet resistance of plated copper:

- The thickness of the deposited layer;
- The geometrical shape of the conductive trace;
- Plated surface morphology;
- Plated surface roughness;
- Plated surface irregularities;
- Purity of the plated material (part of pure metal compared with oxide compounds);
- Under-plating (please see explanation in Figure 35).



*Figure 35. Examples of underplating (left) and overplating (right) using various regimes of the SSAIL process.*

Laser processing, chemical activation, rinsing procedures and chemical plating include many parameters which can affect mentioned properties of the plated metal layer. The geometrical shape could be kept constant for the experiments. The thickness of the plated surface can be controlled by choosing identical plating conditions. For optimisation of the SSAIL method, the influence of specific parameter was checked by keeping constant the others. Firstly, the plating quality dependency on laser processing was investigated. Therefore, the sheet resistance measurements of the plated surface with constant chemical bath conditions for various laser machining parameters has been carried out.

The influence of laser parameters could be seen from Figure 31. It is shown that laser excitation has a threshold of laser fluence, and depends on the scanning speed. However, after comparison of the sheet resistance measurement results with the irradiation dose, the minimum dose was observed when the plating starts. Figure 36 shows the inverse sheet resistance dependence on the irradiation dose for various pulse energies at 10 kHz. It can be easily seen that even for different pulse energies the same threshold value of irradiation dose was observed.

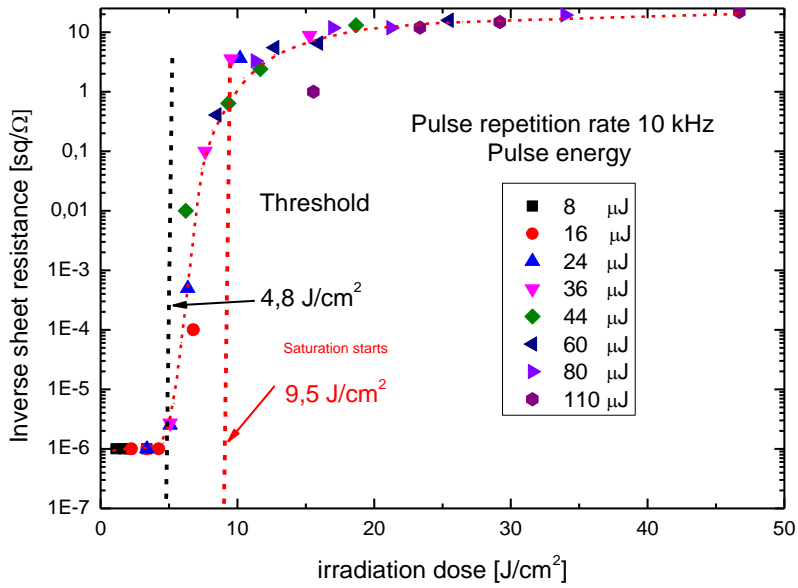


Figure 36. Dependence of inverse sheet resistance on irradiation dose for various ps-laser pulse energies at 10 kHz of pulse repetition rate. Polymer PA 6. Wavelength: 1064 nm. Scanning speed 0.1 – 0.4 m/s.

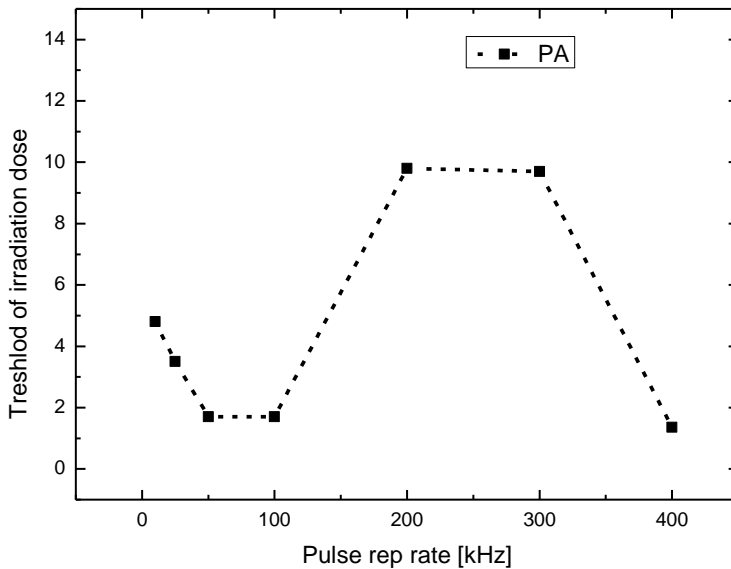


Figure 37. Threshold values of the surface excitation for different pulse repetition rates. Polymer PA 6. The threshold values were extracted from the inverse sheet resistance dependence on the irradiation dose for various pulse repetition rates.

In the sheet resistance dependence on the laser fluence, the accumulation effect could be seen. Therefore, a conclusion can be assumed from the data shown in Figure 31 and Figure 36 that polymer surface excitation has the threshold of irradiation dose. The inverse sheet resistance dependence on the irradiation dose has a steep growth above the laser-excitation threshold until it starts saturating as indicated in Figure 36. The growth of inverse sheet resistance is steep but still has a slope, and it complicates the analysis. Therefore, it has a threshold point and the point where the saturation starts as shown in Figure 36. Both points were used for quality analysis of the PA6 polymer plating. The saturation starting point can be assumed as a point where the surface is fully covered by copper, and there are no under-plating areas. Mathematically, it was evaluated as approximated Heaviside function intersection point with a curve. The samples processed with the irradiation dose values above the saturation starting point has sufficient electrical conductivity for electronic applications. The subsequent increase in conductivity is achieved by building up the thicker copper layer, which is a simple task for electroless plating technology.

Further investigation has been performed with different pulse repetition rate. The threshold values for different pulse repetition rate is shown in Figure 37. The threshold behaviour of the laser excitation has been observed for all pulse repetition rate values used in the experiment.

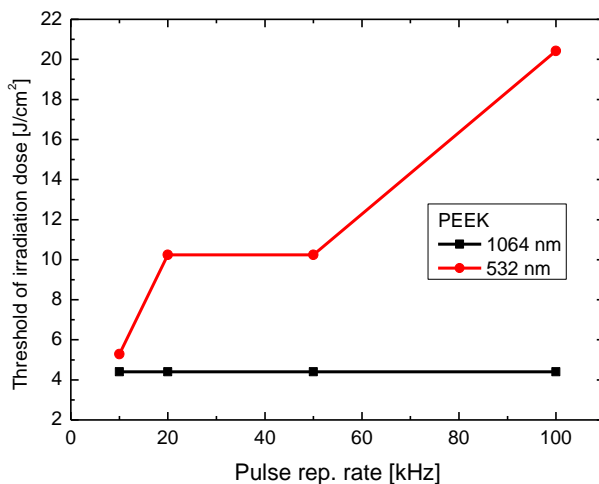
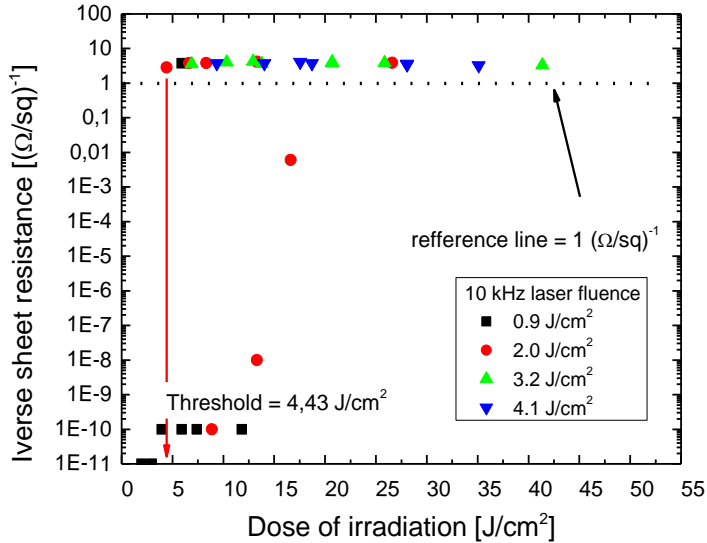
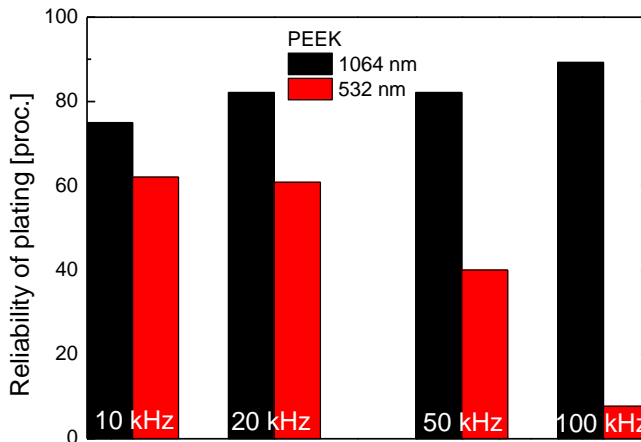


Figure 38. Dependence of the excitation threshold of irradiation dose on pulse repetition rate for the 1064 nm and 532 nm wavelengths of the picosecond pulse irradiation for PEEK polymer.

However, the threshold values disorderly varied depending on the pulse repetition rate for PA6. For high-performance plastic material like PEEK, the threshold behaviour for various pulse repetition rates was different from PA6. The threshold was almost constant for all repetition rates until 100 kHz, when the 1064 nm wavelength of the ps-laser was applied (see Figure 38).



a)



b)

Figure 39. a) Inverse sheet resistance dependence on irradiation dose at 10 kHz pulse repetition rate for PEEK polymer for 1064 nm wavelength; b) Reliability of plating for different pulse repetition rate, for 1064 nm and 532 nm of laser wavelength, material – PEEK.

For higher pulse repetition rates, the laser-excitation of the surface for catalyst activation was not achieved. Further investigation of the excitation threshold has shown that not all values of irradiation dose above the threshold provided surface plating. The inverse sheet resistance remained very low even when the irradiation dose above the threshold was applied. This could be seen in Figure 39 a), where the inverse sheet resistance values above the threshold are very low. In this case, the plating does not start even if the irradiation dose is high enough. Due to this problem, the reliability of plating depending on laser parameters has been evaluated.

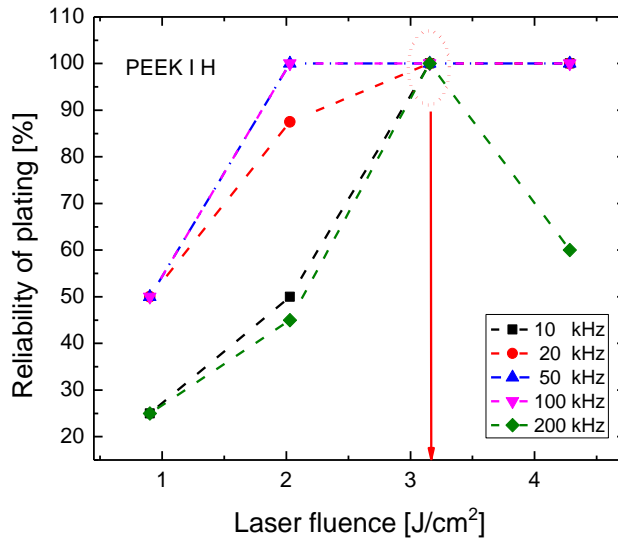
140 different samples processed with various irradiation doses above the threshold of excitation were copper-plated at the same conditions, and plating quality was evaluated. Pulse repetition rates were 10, 20, 50 100, 200 and 400 kHz. Scanning speed varied 0.1-3 m/s. The pulse energy was kept in the range of 8-110  $\mu$ J. Pulse density (pulse number per scanned length) has been kept constant when changing the pulse repetition rate, by modifying the scanning speed.

The parameter of the reliability of plating in % was estimated as the part of samples which were sufficiently plated after the SSAIL procedure when the irradiation dose is above the threshold. The sufficiently plated surface was considered to keep a surface which has a low sheet resistance – at the point (like shown in Figure. 36) where the saturation of the inverse sheet resistance starts with a further increase in the irradiation dose. The sufficient inverse sheet resistance was considered to keep the average value of saturation point, which was at  $\sim 1 \text{ sq}/\Omega$  as shown in Figure 39 a).

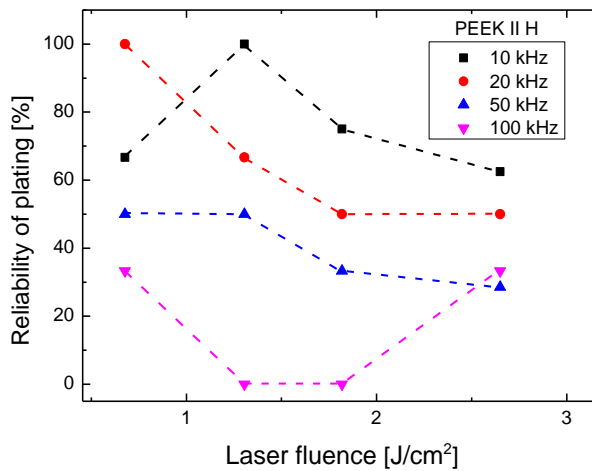
Reliability of plating was analysed in order to define the impact of the pulse repetition rate when laser fluence and scanning speed were not constant, and the impact of laser fluence, when scanning speed was not constant for different pulse repetition rates and for various irradiation doses above the threshold of excitation. Reliability of plating for various pulse repetition rates is represented in Figure 39 b). From data presented in Figure 39 b), it could be seen that the reliability of plating slightly increases with increasing pulse repetition rate for the 1064 nm wavelength. However, the opposite behaviour was observed for the 532 nm wavelength. Activation threshold for the 532 nm wavelength was also higher than for the 1064 nm wavelength and increased with the increasing pulse repetition rate (see Figure 38).

The reliability of plating can also be influenced by laser fluence or pulse energy (if the focus spot size is kept constant). The mentioned effect is shown

in Figure 39 a), where the inverse sheet resistance values for doses above the threshold are still low for some laser fluence values: 0.9 and 2 J/cm<sup>2</sup>. This result indicates that laser fluence is also an important parameter in the laser activation process.



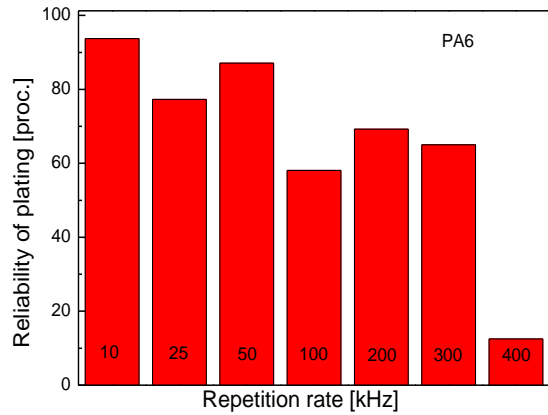
a)



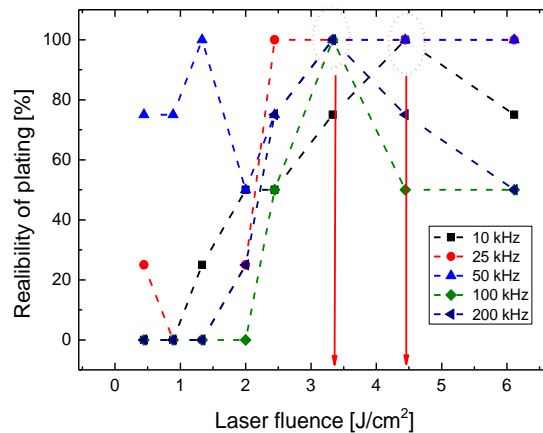
b)

Figure 40. Reliability dependence on pulse energy for different pulse repetition rates for a) 1064 nm and b) 532 nm wavelengths in PEEK polymer.

In order to indicate the impact of laser fluence on the laser activation process, the results of the reliability of plating were presented depending on a laser fluence in Figure 40. Despite the different scanning speed and pulse repetition rate were applied, the reliability of plating reaches 100 percent, when 3.2 J/cm<sup>2</sup> (or higher for 10, 20, 50, 100 kHz pulse repetition rate) laser fluence was applied for surface activation, as shown in Figure 40 a). Therefore, there is an optimal laser fluence for the activation. However, results for the 532 nm wavelength are different.



a)



b)

Figure 41. Reliability of PA 6 polymer depending on a) pulse repetition rate and b) pulse energy. Wavelength was 1064 nm.

The reason for this could be that the range of applied pulse energy is lower than in the case of 1064 nm, and the optimal laser fluence was not reached even with the highest value applied. Application of higher pulse energy for the 532 nm wavelength radiation was limited by the laser system.

Reliability of plating for the PA6 polymer is presented in Figure 41. Results reveal that the reliability of plating was lower for higher pulse repetition rates. The optimal laser fluence was 4.45 J/cm<sup>2</sup> (see Figure 41 b) for the pulse repetition rate of 10 – 100 kHz. In the case of 100 and 200 kHz pulse repetition rates, the optimal fluence was 3.41 J/cm<sup>2</sup>. However, for higher frequencies, no optimal pulse energy was revealed, and the regime was unstable (see Figure 42).

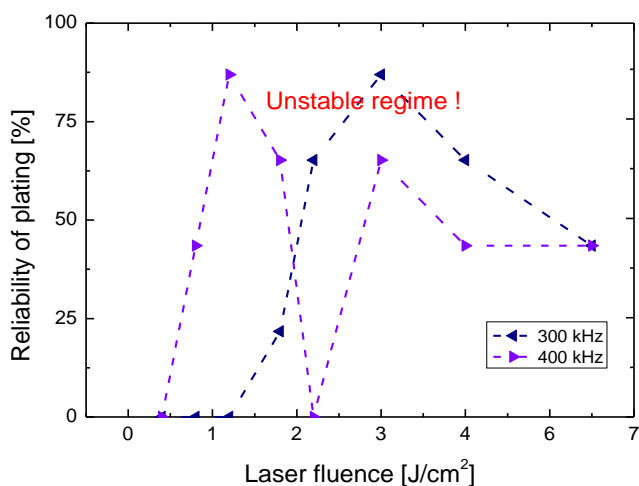


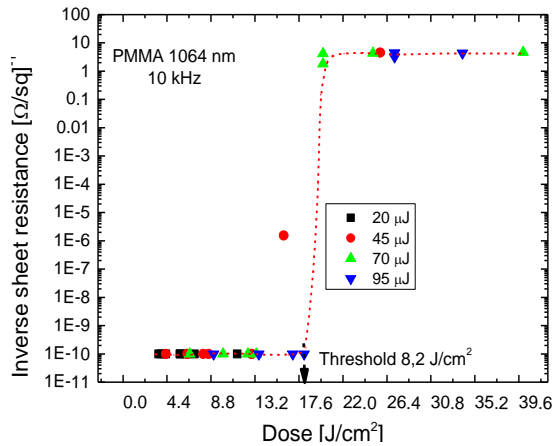
Figure 42. Reliability of plating for PA 6 at high pulse repetition rates. Wavelength was 1064 nm.

Opposite to the LDS technology, the SSAIL process can also be applied for transparent polymers. The SSAIL experiments were carried out with transparent PMMA plates. 1064 nm, 532 nm and 355 nm wavelengths have been used for laser excitation. Preliminary results enclosed the threshold behaviour of the irradiation dose for excitation similar to the case of opaque materials (Figure 43 a).

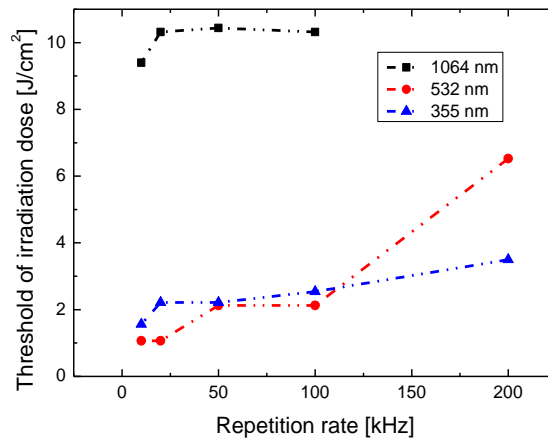
The threshold values have been indicated for different pulse repetition rates using 1064; 532 and 355 nm of laser wavelengths and are shown in Figure 43 b. Threshold values presented in the plot reveals that for the 532 nm and 355 nm wavelengths the laser excitation threshold is more than five times lower. This could be influenced by nonlinear absorption in the transparent material.

For the shorter wavelength, the absorption is higher. Unfortunately, by increasing pulse repetition rate, the higher threshold was obtained. The activation with the pulse repetition rate higher than 100 kHz could be not achieved.

From the reliability chart, a slight decrease with increasing pulse repetition rate was observed for all three wavelengths (Figure 44 a).



a)



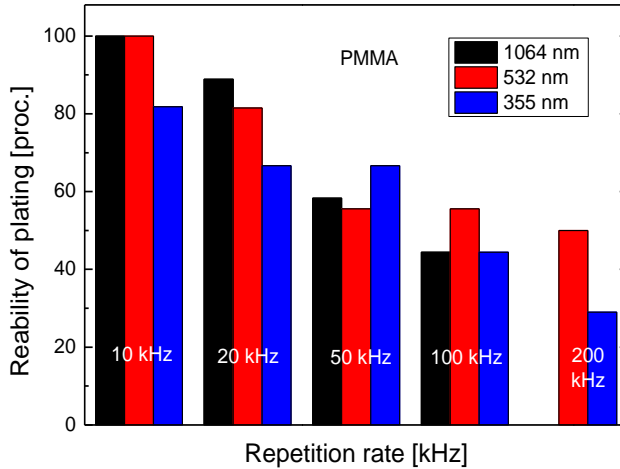
b)

Figure 43. Results of sheet resistance measurements for transparent PMMA polymer: a) inverse sheet resistance dependence on the irradiation dose and presented the threshold for excitation using the 1064 nm wavelength at 10 kHz; b) the laser excitation threshold for 1064 nm, 532 nm and 355 nm wavelengths depending on the irradiation dose.

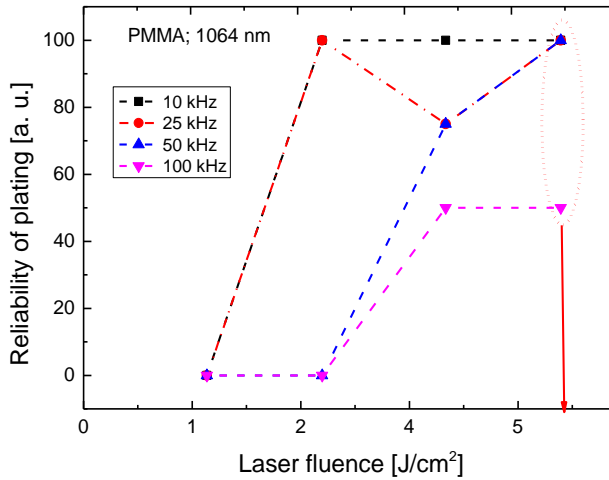
In addition, optimal laser fluence was determined from the plating reliability dependence on the laser fluence plots in Figure 44 b and b)

Figure 45 a, b. As shown in Figure 44 b and b)

Figure 45, the optimal laser fluence provided 100 percent reliability only for low frequencies: 10-50 kHz for the 1064 and 355 nm of the wavelengths and 10-20 kHz for 532 nm.

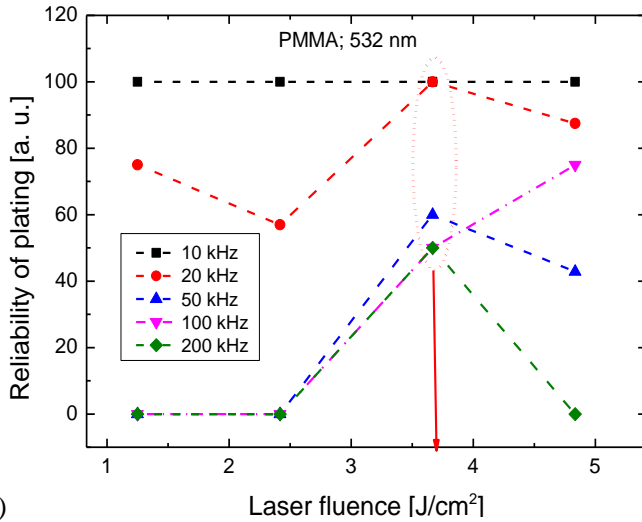


a)

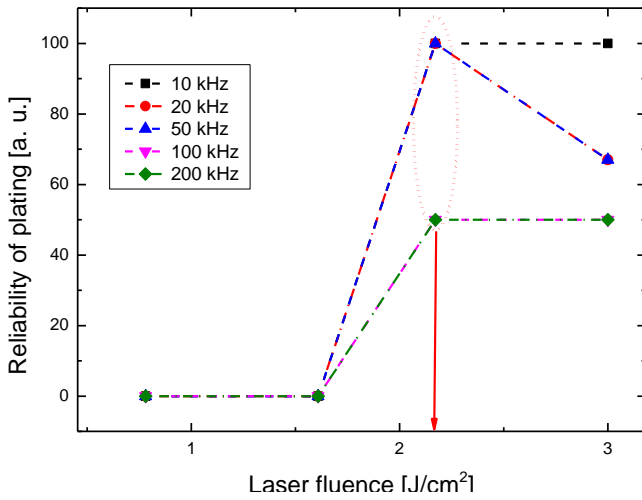


b)

Figure 44. a) Reliability of PMMA plating for various pulse repetition rates and wavelengths; b) and laser fluences for PMMA 1064 nm. The arrow in the plot indicates optimal laser fluence.



a)



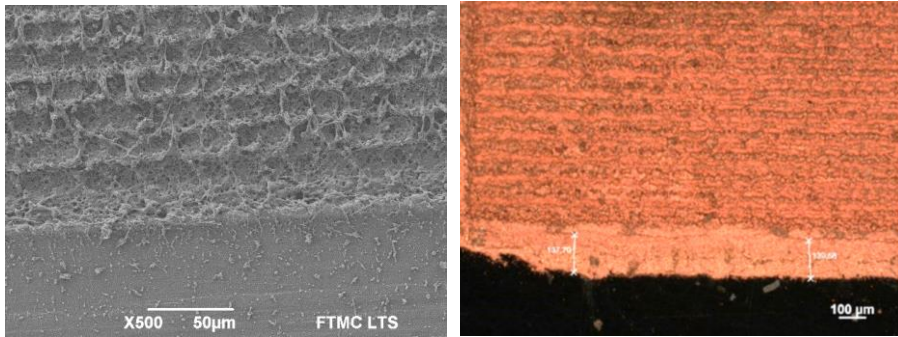
b)

Figure 45. a) Reliability of PMMA plating depending on laser fluences for PMMA a), 532 nm and b) 355 nm of wavelength. The arrows in the plots indicate optimal laser fluence.

## 6.2 Selectivity

Another critical parameter for electrical circuit formation is spatial plating selectivity. Generally, selectivity cannot be measured by sheet resistance tests.

Selectivity can cause two types of unwilling consequences for the circuit: overplating when the not-irradiated surface is covered by copper layer and underplating when the laser-treated surface is not fully covered. Both cases are shown in Figure 35. Over-plating and under-plating problems can be influenced by several factors: 1) laser processing parameters 2) surface preparation for plating; 3) chemical activation; 4) rinsing and 5) plating parameters. Under-plating usually can be easily detected by the sheet resistance measurements. However, there are specific cases which are discussed here. In this section, the influence of laser processing parameters to the plating selectivity is analysed. Incorrect laser processing regime can cause over-plating out of the boundaries of the laser-irradiated area as shown in Figure 46. Such over-plating is driven by debris (see Figure 46) of the polymer after the laser-material interaction.



*Figure 46. Over-plating out of the boundaries (on the left after laser processing, on the right after plating).*

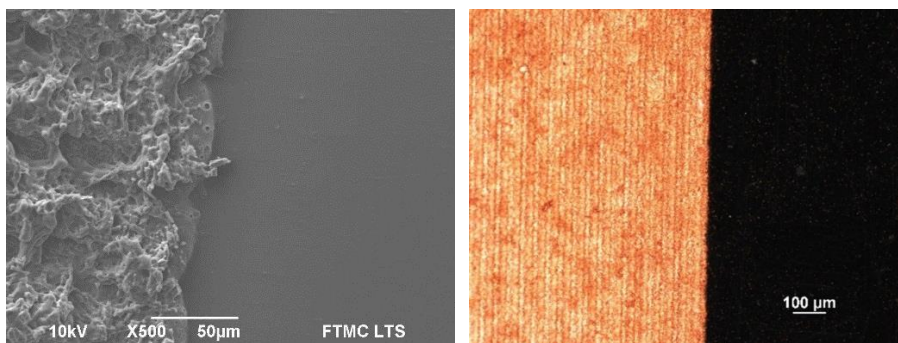


*Figure 47. Elimination of over-plating with correct laser processing parameters (on the left after laser processing, on the right after plating).*

Debris appears due to the ablation process. However, it can be controlled by laser processing parameters – pulse repetition rate, laser fluence, scanning

speed and hatching. Figure 47 shows the surface borders processed with the correct parameters. The measurements of over-plating width, as shown in Figure 46 was carried out. The over-plating width dependency on the irradiation dose for PA 6 polymer is shown in Figure 48. Over-plating was observed to be increased with increasing the irradiation dose for pulse repetition rate up to 100 kHz.

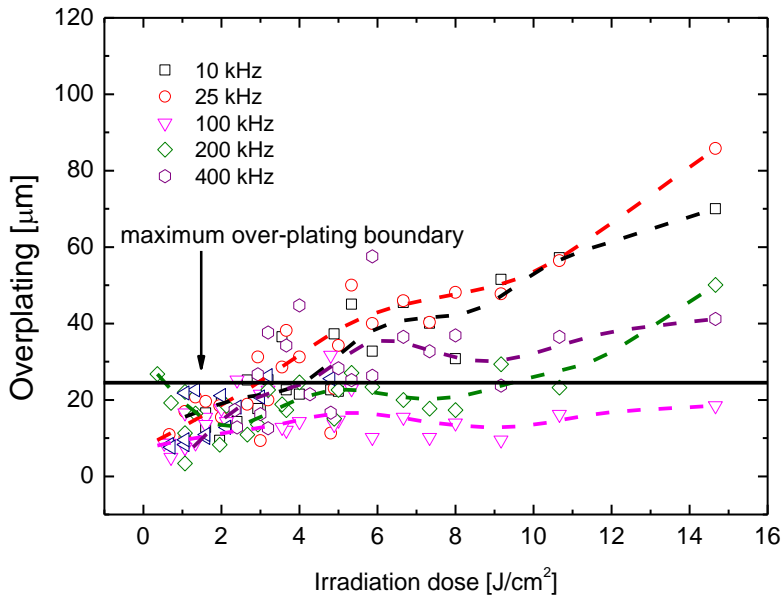


Figure 48. The over-plating width dependence on the irradiation dose for various pulse repetition rates. Dash lines are fitted average functions of experimental points. The PA6 polymer was used as a substrate. Wavelength was 1064 nm.

When the pulse repetition rate was 100 kHz, it insignificantly increased with the irradiation dose. The maximum allowed over-plating width was chosen for evaluation of the laser parameters for selectivity, as shown in Figure 48 (maximum over-plating boundary).

Two boundaries were shown for the processing parameters determined from the tests of the sheet resistance (good plating layer) and over-plating (plating selectivity). To simplify the analysis, only values of the processing parameters with high reliability for plating should be analysed. That means the values above the irradiation threshold with optimal laser fluence were chosen (see Figure 41 b.). The 25  $\mu\text{m}$  limit for over-plating (as shown in Figure 49) has been chosen as sufficient for the applications. Only two values of the optimal laser fluence fall into the region of processing window which is limited by the

threshold of irradiation dose and the boundary of maximum over-plating. The processing speed increases with decreasing the irradiation dose for the constant pulse repetition rate. Therefore, the leftmost value, in this case, is optimal (as indicated in Figure 49).

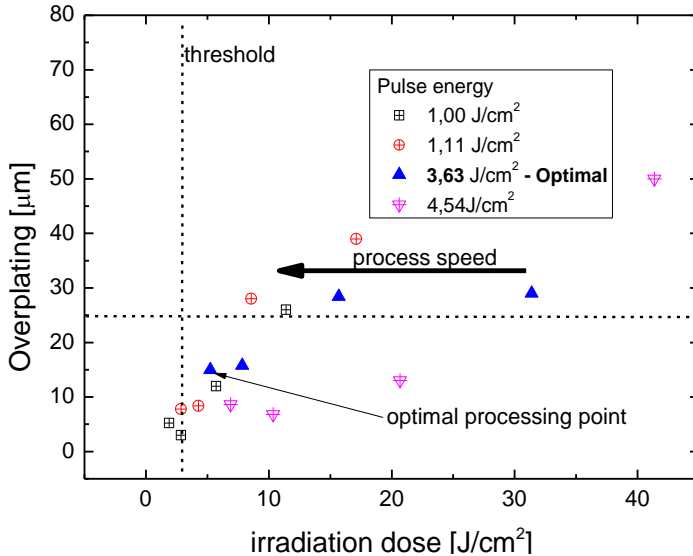
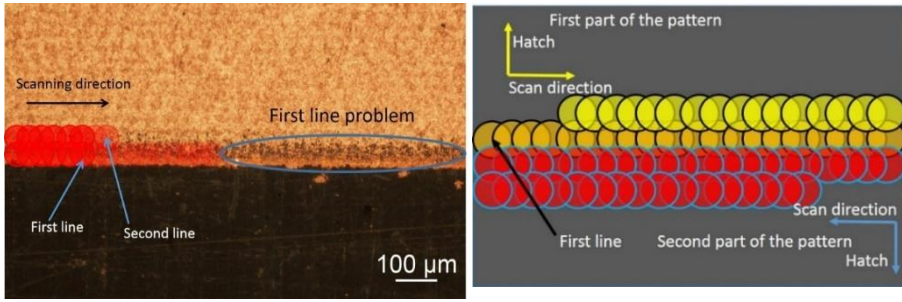


Figure 49. Over-plating dependence on irradiation dose with indicated boundary for selectivity and irradiation threshold. 20 kHz, PMMA. The 532 nm wavelength was used.

Another problem in the plating selectivity – a first line problem, more precisely saying – the underplating of the first line. The first line where the scanner starts hatching the surface quite often is under-plated like shown in Figure 50. This problem was found with PEEK, PMMA, PET, and PPA polymers. In order to avoid this problem, two different scanning approaches were investigated. The first one – multiple scanning of the first line, the second one – start scanning from the middle of the pattern, as shown in Figure 50 b. Results of the test revealed that the first line problem could be eliminated when the scanning starts in the middle of the pattern for PET, PMMA and PEEK as shown in Figure 51. However, multiple scanning of the line does not work for all material. A slight increase in the plating was observed only for PET polymer (see Figure 52).



a)

b)

Figure 50. First line problem a) and pattern for the problem solution b).

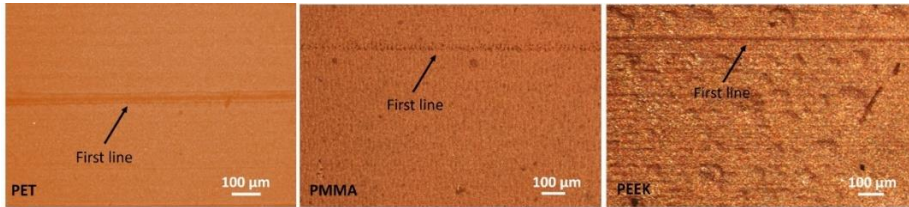


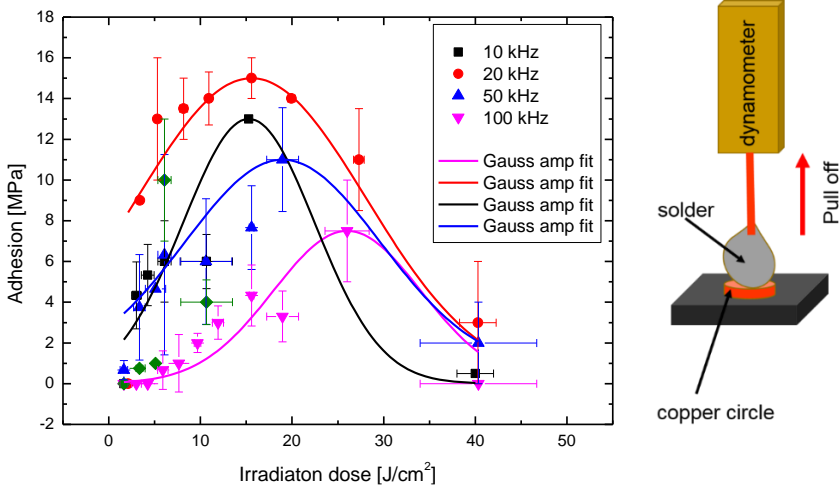
Figure 51. First line problem solution for PMMA; PET; PEEK starting scanning from the middle of the pattern.



Figure 52. First line problem solution for PET by using multiple scanning of the line.

### 6.3 Adhesion

Another critical factor for circuits is adhesion of metallic trace to the substrate. We used two methods of testing. Initially, the standard scotch tape test was applied for the plated surface. The result was that all the samples had passed this test at 100 percent. The second method – a wire was soldered to the small area of the plated surface (2 mm<sup>2</sup>) and has been pulling off with a dynamometer. The measured adhesion for the copper-plated PA6 after irradiation with the 1064 nm wavelength of the laser is presented in Figure 53. The dependence on the irradiation dose has been observed for adhesion strength. Firstly, the adhesion force increases with increasing the irradiation dose until it reaches the maximum value and starts to decrease.



a)

b)

Figure 53. a) Adhesion of copper to PA 6 dependence on irradiation dose for various pulse repetition rates. Error bars indicate standard deviation, the points in the plot represents average value. The picture b) shows the measurement technique. Wavelength was 1064 nm.

The data were fitted by the Gaussian function. Although the roughness of laser treated surface increases with increasing irradiation dose (as shown in Figure 28), the adhesion strength has its maximum point and is not driven only by the roughness of the surface. Pulse repetition rate has a very high impact on adhesion strength. For low pulse repetition rate of 10 – 20 kHz, adhesion is higher in comparison with higher pulse frequency. FWHM of the fitted Gaussian function varied with the pulse repetition rate and could be applied to evaluate the irradiation dose parametric range for the adhesion strength. However, the values of the adhesion force are very different for various pulse repetition rates. For example, the first experimental point for 20 kHz is above the maximum value for 100 kHz. Therefore, the application of FWHM as parametric window could not be applied. In this case, the minimum adhesion boundary has been applied as shown in Figure 54. The minimum adhesion strength value was considered to keep 2 MPa as a sufficient for electronics application with a high reserve ratio. The evaluation of sufficient adhesion range of irradiation dose is shown by arrows. Boundaries of the range are at a cross-section of Gaussian function with the minimum adhesion strength line. For those curves which start or finish above the minimum adhesion line, the boundary is indicated as the experimental point with minimum and maximum irradiation doses (limited by plating quality) as shown in Figure 54.

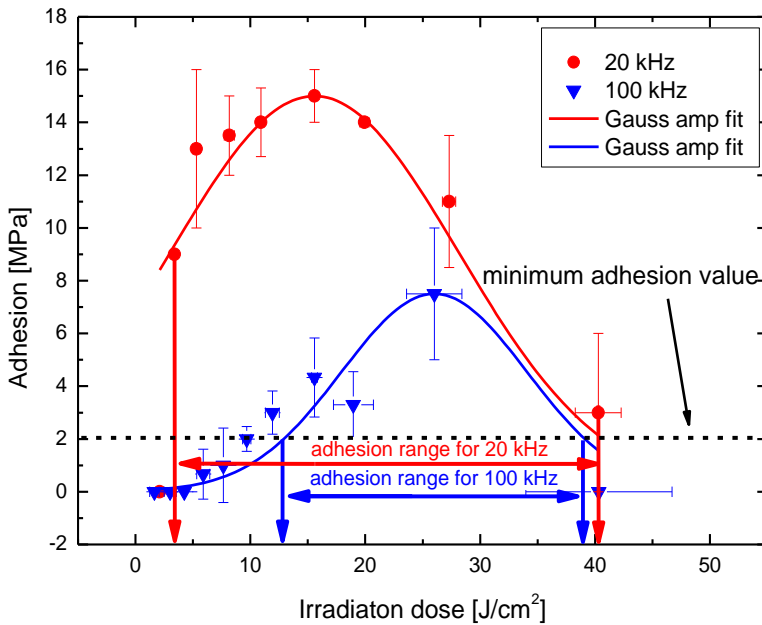


Figure 54. Evaluation of adhesion parametric window for circuit trace.

#### 6.4 Evaluation of optimal laser processing parameters

As mentioned before in the quality evaluation section, the most important properties of the circuit trace are plated surface conductance, the spatial selectivity of plating (resolution) and plated surface adhesion to the substrate. The threshold of the irradiation dose, optimal laser fluence and range of irradiation dose define sufficient sheet conductance of the plated metal layer with high reliability of plating as described previously. Irradiation dose also defines the over-plating out of the borders due to ablation debris. Adhesion range was indicated in the adhesion section. The evaluation of the optimal processing point should combine all mentioned properties of the plated metal layer. In this case, the processing parameters represented as the irradiation dose are firstly limited by boundaries: the threshold of irradiation dose, the range of irradiation dose for sufficient plating selectivity, the range of irradiation of sufficient adhesion to a substrate as shown in Figure 55. Within these boundaries, there are 17 processing points in the plot for the 20 kHz pulse repetition rate processing of the PA6 polymer. However, for reliability, the optimal laser fluence should be taken into account. Therefore, the processing window is narrowed to 8 points. The very important factor for application is the processing time. For constant pulse repetition rate and

constant laser fluence, the lower irradiation dose indicates the higher processing speed. Therefore, the leftmost point is chosen as the optimal processing point.

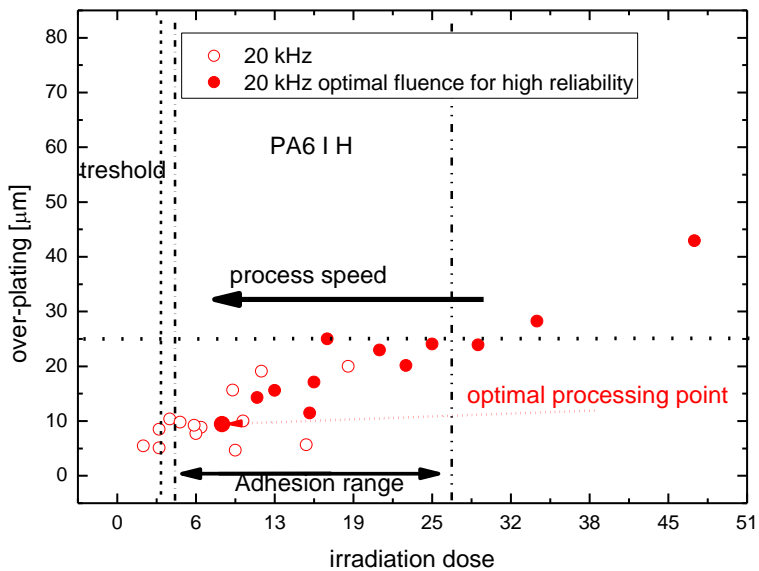


Table 5. Optimal laser processing parameters for polymeric materials.

Material	Laser Wavelength [nm]	Pulse repetition rate [kHz]	Irradiation dose [J/cm <sup>2</sup> ]	Laser fluence [J/cm <sup>2</sup> ]	Adhesion strength [MPa]	Reliability [%]	Over-plating [μm]	Scan Speed [m/s]	Surface roughness RMS [μm]
PA6	1064	50	8.4	7.8	7.2	100	16	1.5	2.1
PPA	1064	50	8,49	8,16	8	100	12	1.5	2.3
PC/ ABS	1064	100	1,63	1,13	8.3	100	11	2	1
PMMA	532	50	5.23	2.3	3.8	100	8	1.0	1.0
PEEK	1064	50	10.3	4.7	3.3	100	16	1	1.2
PET	532	400	11.82	1.37	1.2	100	10	1.6	1.1
PVC	532	100	6.82	2.86	2	100	38	3	2.4
ABS 3D printed	1064	100	11.82	4.7	3.4	100	39	3	5.3
Float glass	355	400	35.4	4.7	18	100	5	1.6	0.97

### 6.5 Alternative method for plating quality evaluation

The electrical and optical properties of the semi-transparent films were investigated in numerous works [<sup>95</sup>, <sup>96</sup>, <sup>97</sup>]. However, the analysis of the sheet resistance dependence on the optical transmittance can be applied only for films with the thicknesses smaller than the absorption depth. Such kind of measurements cannot be realised with a relatively thick metal layer on the porous opaque substrate. A fast and easy method to indicate the quality of plated copper layer is on demand from industry for inline process monitoring in a factory. Therefore an alternative method was developed for evaluating the quality of copper plating based on colourimetry [<sup>98</sup>]. The method compares colour images taken through an optical microscope in the dark field mode on samples before and after plating procedures. Colour differences are analysed.

All tested samples were photographed before and after copper deposition. The average colour was calculated from five sections of the surface. The colour

difference  $\Delta E$  was calculated between images after the plating  $E_p$  and after laser processing  $E_l$  by using an equation 5:

$$\Delta E = \sqrt{(R_p - R_l)^2 + (G_p - G_l)^2 + (B_p - B_l)^2} \quad (5)$$

where  $R_p$ ,  $G_p$ ,  $B_p$ ,  $R_l$ ,  $G_l$ ,  $B_l$  are average, normalised red, green and blue components of the sample images after the plating and laser treatment procedures. The average colour difference and the standard deviation of it were calculated from the data achieved. All plated samples for colour difference measurement were also tested with the sheet resistance measurements.

### 6.5.1 Percolation model of the sheet resistance

The conductivity of the polymer and metal mixture is divided into the three regions according to the percolation model [<sup>99</sup>, <sup>100</sup>, <sup>101</sup>]:

$$\sigma_m(\phi_{frac}) = \begin{cases} \sigma_m(\phi_{frac} - \phi_{crit})^t & \text{if } \phi_{frac} > \phi_{crit} \\ \sigma_m \left( \frac{\sigma_m}{\sigma_p} \right)^s & \text{if } \phi_{frac} = \phi_{crit} \\ \sigma_m(\phi_{crit} - \phi_{frac})^{-q} & \text{if } \phi_{frac} < \phi_{crit} \end{cases} \quad (6)$$

where  $\phi_{frac}$  is the surface fraction of metal plated polymer surface;  $\phi_{crit}$  is the percolation threshold when the conductivity is tending to zero;  $\sigma_m$  and  $\sigma_p$  are the conductivities of the metal and polymer constituents respectively;  $t$ ,  $s$  and  $q$  are the exponential factors that depend on the dimensionality of the system. The percolation model used to describe optical and electronic properties of nano-porous layers [<sup>102</sup>, <sup>103</sup>, <sup>104</sup>] then can be generalised for all range of area fraction  $\phi_{frac}$  values: below, above and at the percolation threshold. Therefore, the sheet resistance  $R_s$  is a function of  $\phi_{frac}$ :

$$R_s = R_s(\phi_{frac}) = \frac{1}{h\sigma(\phi_{frac})} \quad (7)$$

where  $h$  is the layer thickness of the conductor and insulator mixture.

### 6.5.2 Area fraction of copper dependence on the colour difference

The obtained colour of the sample was affected by the fraction of the surface area plated by the metal  $\phi_{frac}$ . Openings in the polymer surfaces presented the colour of laser structured polymer. The copper-covered part of the polymer

produced the colour of copper (Figure 56). In the case of a poorly plated surface, the copper plated areas did not have interconnection with each other, and, therefore, it possessed small average colour difference and high sheet resistance (Fig. 56 a). The moderate plating quality represents the case when more than a half of polymer surface is covered by the metal islands, and they have a continuous net of interconnections between them through all the surface area (Figure 56 b). The well-plated case appears when almost all surface area of the polymer is covered by the metal deposition, and an only a small part of the polymer is left open (Figure 56 c). The measured area fraction  $\phi_{frac}$  of the copper-plated polymer versus the colour difference  $\Delta E$  of the non-plated and plated surface is given in Figure 57 a. In the particular case with the threshold value of 0.27 the area fraction had a linear dependence on the colour difference (Figure 57 a):

$$\phi_{frac} = +0.06 + 1.55\Delta E \quad (8)$$

Similar linear dependence has been reported for the semi-transparent copper nanowire film in the area fraction versus transmittance representation by J. W. Borchert et al.<sup>[105]</sup> and by S. M. Bergin et al.<sup>[106]</sup>. However, in the general case, our measured fraction of the sample surface covered by the metal was a function of the colour difference and the threshold value of luminance. The measurement of the area fraction is sensitive to the threshold value  $Y_{th}$  and obtains linear relationship only with particular the value of 0.27. The determination of the correct threshold value requires additional calculations. The way to avoid this is to use colour difference instead of area fraction. Taking into account that the percolation model of electrical conductance of isolator-conductor mixture can be adapted to our experimental conditions. The sheet resistance from Equations (5, 6, 7) becomes a function of colour difference  $R_s = R_s(\Delta E)$ .

Firstly, experimental sheet resistance measurement results were compared with the areal fraction of deposited copper (Figure 56). For areal fraction measurements digital RGB optical microscope images of copper plated areas were converted to the grayscale mode by using a formula based on the NTSC standard <sup>[107]</sup>:

$$Y' = 0,299R_p + 0,587G_p + 0,114B_p \quad (9)$$

where  $Y'$  is the luminance of the image after the ECP procedure. The area fraction  $\phi_{frac}$  of the copper was evaluated by calculating the ratio of a number of pixels above certain threshold  $Y_{th}$  to the total number of the picture pixels.

The average area fraction and the standard deviation of it were evaluated from the five sections of the image. The areal fraction has been calculated from optical images transferred to the black & white mode using chosen threshold value  $Y_{th}$ .

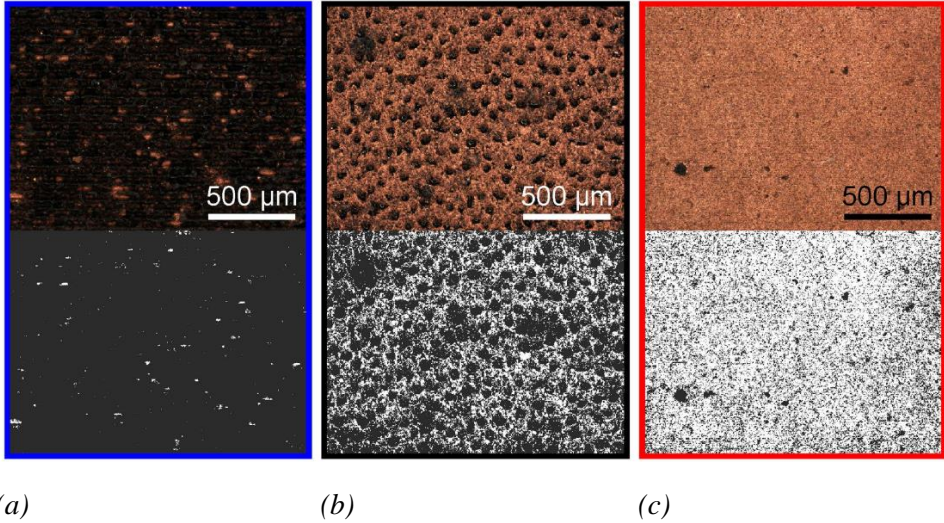


*Figure 56. Copper on the polymer. The dark field optical microscope images of deposited copper on the polymer (top row) and conversion of images to black and white mode at the threshold value  $Y_{th}' = 0.27$  (bottom row). The naked polymer is given by the black colour and copper deposition by the white colour. The areal fraction of under-plated copper: low areal fraction high under-plating range (a), moderate areal fraction and under-plating range (c), high areal fraction and no under-plating [98].*

### 6.5.3 Sheet resistance dependence on the colour difference

The sheet resistance  $R_s$  of the metal-plated polymer areas versus the colour difference  $\Delta E$  of the non-plated and plated surface is given in Figure 57 b. The sheet resistance of copper on the polymer surface has a power law dependence on the colour-difference of the non-plated and plated areas described by the percolation model equations (5, 6, 7). The exponents  $q = 1.4$ ,  $s = 0.5$  and  $t = 1.5$  of the power law in the generalised percolation model of sheet resistance were found from the fits of the experimental data for poorly, moderately and well-plated areas, respectively (Figure 57 b). The decrease of sheet resistance with the colour difference occurs because the higher is the amount of copper deposited on the sample, the bigger the colour difference is, and therefore, results in the lower sheet resistance. This power law relationship can be

converted to the quantity of copper plated onto the polymer. In this way, the quality of copper plated areas by the electroless copper plating (ECP) procedure can be evaluated from optical microscope images, by simple calculation of colour difference.

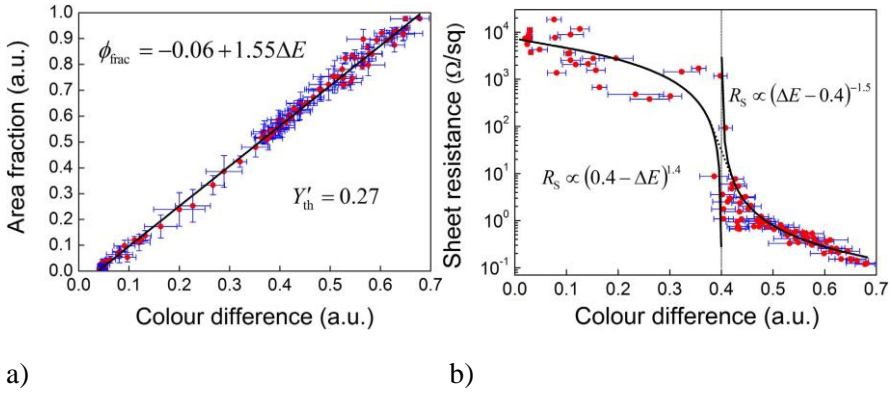


Figure 57. a) Red circles - the measured area fraction of copper versus the colour difference between images of the non-plated and copper plated polymer surface. The area fraction  $\phi_{\text{frac}}$  was calculated by using Equation (8) with the threshold value of the luminance  $Y_{\text{th}} = 0.27$ . b) The colour difference  $\Delta E$  was calculated by using Equation (5). The horizontal and vertical blue error bars indicate the standard deviation in the colour-difference and area fraction measurements taken from 5 sections of the microscope images, respectively. The solid black line is the linear least square fit of the experimental data points [98].

The sheet resistance of copper layers decays by the power-law with increasing of the colour difference. The percolation theory of electrical conductance of insulator-conductor mixture has been adopted in order to explain the experimental results. The colour difference method is a fast and inexpensive method to evaluate the plated surface quality for an areal fraction and indicate an underplating problem. Thus, the fast evaluation method has a high potential for an industrial application using fast online quality control.

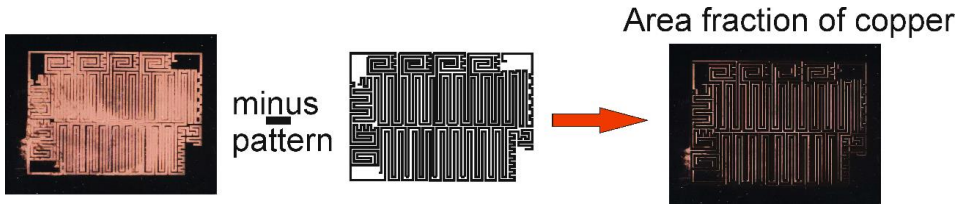
## 6.6 Influence of parameters in activation and plating

The SSAIL method includes a few chemical steps activation, rinsing and plating, and parameters of chemical treatment have a high impact on the results. The list of parameters includes the concentration of activation solution, activation time, rinsing time and temperature after activation, the concentration of reagents in the copper plating bath, etc. Preparation of the

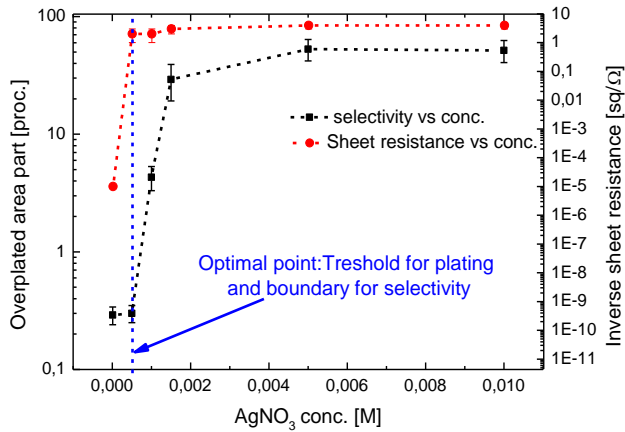
sample after laser processing is also an essential task. As previously stated in the SSAIL process investigation section, better-quality of the plated surface could be achieved by immersion of the sample in ethanol before the activation procedure. During this procedure, the surface energy increases and silver ions are absorbed stronger. Moreover, the sample, prepared for the plating and activation steps, should be well rinsed in an ultrasonic bath in order to wash the debris (ablation product) as better as possible (shown in selectivity section).

#### 6.6.1 Concentration of reagents and temperature of the bath

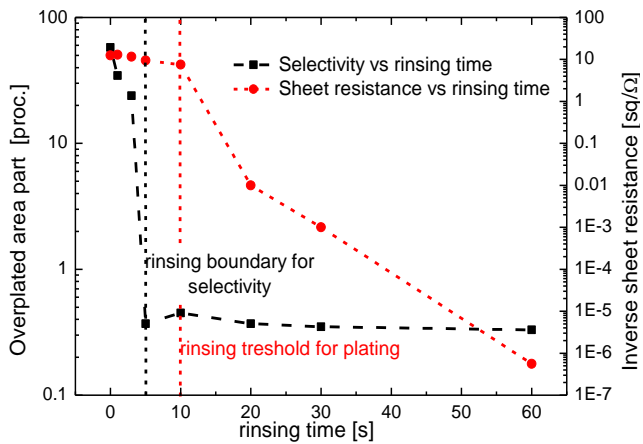
When the concentration of silver nitrate solution is too low or too high, over-plating or under-plating could be observed. Incorrect rinsing of the activated sample can lead to similar problems. Therefore, the impact of concentration of silver nitrate to the plating selectivity was analysed. There are two boundaries which limit the concentration of the activator and rinsing time after activation from both sides. Higher concentration and shorter rinsing time lead to over-plating of non-processed areas and under-plating (or even no plating) when the concentration is too low or rinsing time is too long. Under-plating (or no plating) could be found by the sheet resistance measurement. The overplating could be estimated by image analysis of plated samples comparing them with CAD data of the circuit to be plated. The principle of area fraction measurement is shown in Figure 58 a. Plated copper area part has been measured by Corel Draw X6 software. PA 6 sample used for a test was black colour with the orange colour of the copper plated pattern. In order to exclude only over-plated areas of copper, the draw of pattern of the circuit has been joined with the photo of the sample at the same scale by eliminating the copper pattern on laser-treated areas as shown in Figure 58. As a result, only copper part of over-plating included into the count. All results of sheet resistance and area fraction dependence (over-plated part) on the silver nitrate concentration and rinsing time after the activation are presented in Figure 58 b and c, respectively. The optimal concentration has been determined for silver nitrate. In Figure 58 b, blue dash line presents the optimal concentration of  $5 \times 10^{-4}$  M for high selectivity (low over-plating area part) and high conductance (inverse sheet resistance). While in the rinsing case there is wider rinsing time window. The region between 5 and 10 seconds could be applied for the process (see Figure 58 c).



a)



b)



c)

Figure 58. The principle of the over-plated area part measurements for the plating selectivity measurements a) Selectivity and sheet resistance dependence on silver nitrate concentration b) and rinsing time after activation c).

Further investigation has been performed to identify the influence of copper sulphate concentration; formalin concentration; silver nitrate solution temperature and washing temperature before the activation for sheet resistance of the plated sample. The saturating concentration of copper hydrated sulphate ( $\text{CuSO}_4 \cdot 5\text{H}_2\text{O}$ ) can be kept 0.08 M as shown in Figure 59 a. However, a further increase in concentration insignificantly affects the conductance of the plated copper. The 0.08 M of concentration is optimal, because, the lower as the possible concentration of copper in the solution ensures better stability of the solution [56].

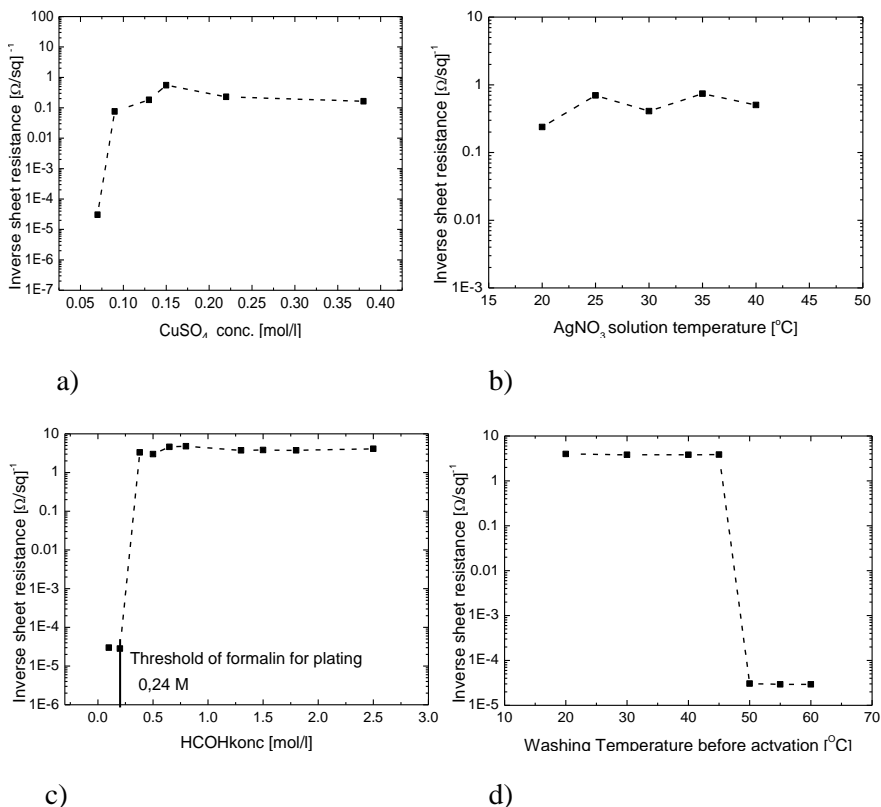


Figure 59. Inverse sheet resistance dependence on chemical parameters: a) copper sulphate concentration; b) silver nitrate temperature; c) formalin concentration; d) washing temperature before the activation.

Similar behaviour was observed for reducer – formalin (Figure 59 c). The threshold concentration of formalin for the plating was 0.24 M. The further increase in concentration does not provide any positive results. Therefore, the concentration should be kept near the threshold since a higher concentration

of reducer can lead to instability of the plating bath, and the in-volume copper reduction could start [77].

Silver nitrate solution temperature in the range 20-40° C did not have any effect on the activation step as shown in Figure 59 b). From 20 to 40° C, no effect in the conductance of the plated surface was observed. However, when the temperature reaches 45° C inverse sheet resistance decreases drastically indicating no plating regime. This could be explained that hot water remains in the laser-processed rough surface and does not allow activator to adhere to the surface. Therefore the 20° C (room temperature) is the most convenient to keep for washing.

#### 6.6.2 Double activation procedure

An improvement in the plating quality was observed after application of the double activation process. The procedure includes one additional activation step. It was initially observed that those samples which did not induced plating could be plated after repeating all the steps except the laser treatment. Thus, laser processing window could be wider. Steps of double activation are as follows: laser processing, rinsing with ethanol, silver nitrate activation, water rinsing, copper plating solution, water rinsing, silver nitrate activation and finally copper plating solution. The double activation procedure was investigated in order to determinate which compound in the plating bath plays a significant role in the process. As a result, it was found that NaOH – is necessary after the first activation step instead of the copper plating solution. In the case of PC/ABS polymer, the plating after single activation appears only for very narrow laser processing parametric window at low pulse repetition rate values. As shown in Figure 60, double activation allows using higher pulse repetition rate for fast processing of PC/ABS. Another benefit from the double activation procedure is solving the first-line problem and improvement of spatial plating resolution for many polymers. Under-plating is a very common problem when writing narrow traces, and the use of the double activation procedure could help here.

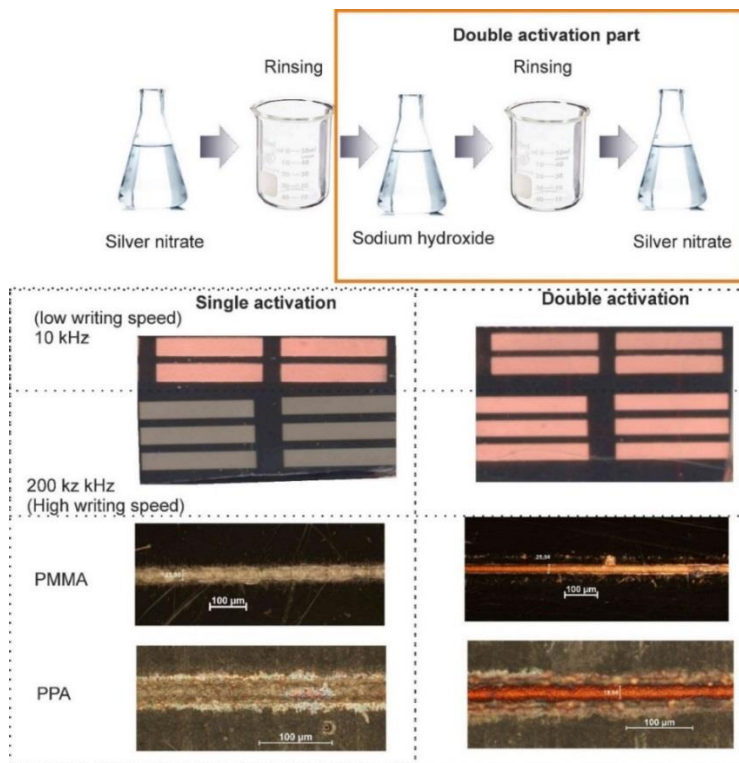


Figure 60. Scheme of the double activation process and plated PC/ABS samples below, showing extended laser processing window after the double activation. Single line plating improvement for PMMA and PPA polymers after double activation is presented below.

The increase of plating quality was observed even only after pre-treatment in NaOH before the silver nitrate procedure in a single activation process. However, better results were achieved after the double activation step. The reason for better plating quality – electrical conductance – can be explained by additional chemical reaction of silver and hydroxide ions.

The alkaline solution contains a high concentration of hydroxide ions. They are localised on the surface due to the induced polarisation of the polymer surface [108]. The laser-processed area has a higher positive surface potential [109] comparing with the rest of the surface. After treating with sodium hydroxide, the sample is rinsed and immersed in the activation solution.

Weakly adhered OH<sup>-</sup> ions on the untreated area are washed away during the rinsing procedure. However, the high amount of hydroxide ions remains on the laser-treated areas. The mechanism of hydroxide localisation on the

processed areas could be explained by the combined process. Firstly, they are held mechanically by rough and porous surface and thus could not be easily removed during rinsing. The second, a stronger surface potential is created due to larger surface area. Moreover, the laser processing leads to chemical decomposition of polymeric chains, and new functional groups which contain electric charge appears on the polymer surface [110].

After NaOH<sup>-</sup> treatment sample is immersed in AgNO<sub>3</sub> activation solution and localised OH<sup>-</sup> ions on laser treated areas reacts with Ag<sup>+</sup>. As a result, insoluble silver hydroxide is formed, which immediately is decomposed to silver oxide:



Freshly formed Ag<sub>2</sub>O reacts with aldehydes very actively (aldehydes groups, which appears after surface modification with a laser or formaldehyde from the copper bath) and as a result, metallic Ag is produced.

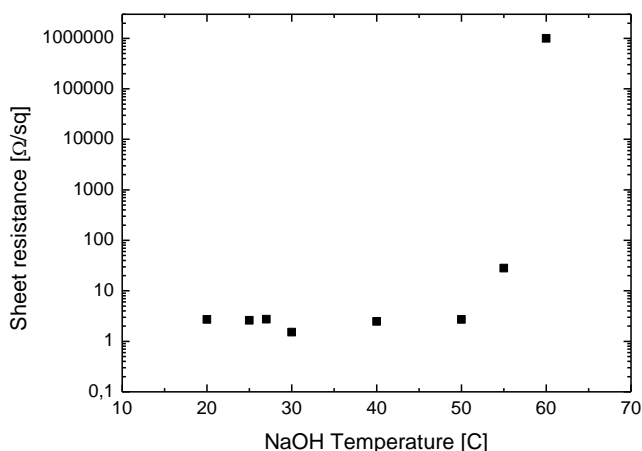


Figure 61. Dependence of the sheet resistance on NaOH- temperature.

Increased metallic Ag concentration on the surface enables effective copper deposition on laser treated areas. Such a process can work independently of a sequence of procedure applied.

Influence of the NaOH- solution temperature was evaluated as well. The sheet resistance measurements of finally plated samples treated at various sodium hydroxide temperatures were carried out. The results revealed that no significant change in the sheet resistance appears in the temperature range of

20-50° C. (see Figure 61), however, further increase in temperature results in a steep increase of the sheet resistance.

### 6.7 Spatial resolution of SSAIL

An important part of the technology is spatial selectivity or resolution of the metal plating. We tested that by checking the limits of narrowest plated line and the shortest gap between plating lines (as shown in Figure 62) for polymers used in the experiments: PA, PPA, PC/ABS, PVC, ABS 3D print, PET, PEEK and soda lime glass.

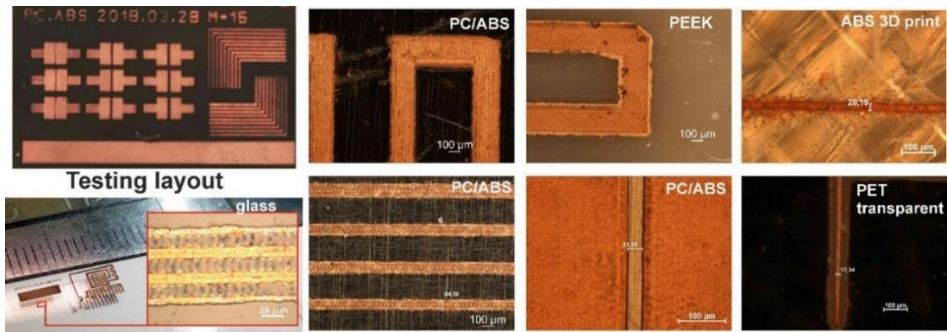


*Figure 62. Layout for testing of plating selectivity for various materials.*

The gap between plating contacts ranged from 20 to 200  $\mu\text{m}$ , and the width of the line was modified by overlapping of lines starting with a single scan at the focal point. All improvements as double activation or multiple scanning procedures were used (if necessary) to increase the selectivity of plating. Evaluation of samples was performed with an optical microscope. The microscope images for various materials are shown in Figure 62, and measured results are presented in Figure 63.

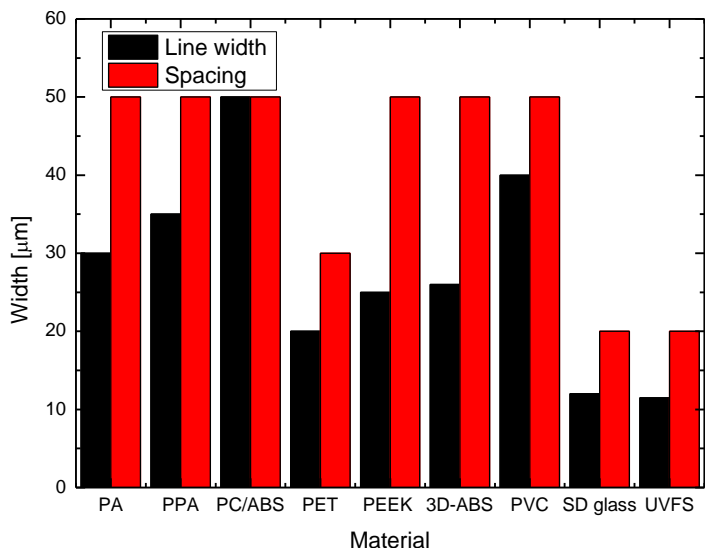


Figure 63. Selectivity of copper plating: the narrowest width of the metal line and spacing (narrowest gap between plated lines).

As seen from Figure 63, the spatial plating selectivity – resolution strongly depends on the material, the lowest resolution was achieved for PC/ABS and the highest one for glasses.

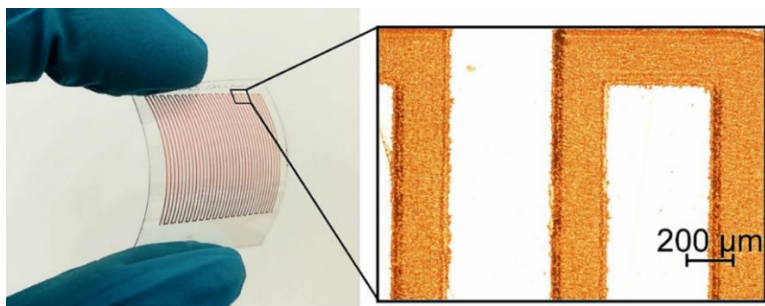


Figure 64. A flexible PET with a circuit pattern made by SSAIL.

High resolution can be achieved on transparent and flexible materials like PET as shown in Figure 64. Narrow plating line and small pitch can extend application areas for the SSAIL technology on transparent materials. Very narrow structures could be transparent for the naked eye. Therefore, such plating net as shown in Figure 65 can substitute the ITO electrodes used for touch screens or other applications which need transparent electrodes.

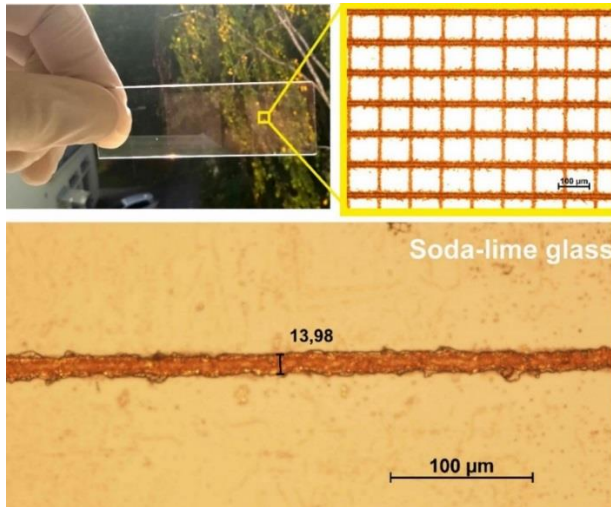


Figure 65. The fine copper structure on glass produced using the SSAIL technology.

## 6.8 Demonstrators

As laser-induced selective electroless metal plating technologies are intended for industrial applications, demonstrators on MID devices were prepared by various steps of the technology validation. The new PP-MWCNT material with the laser direct structuring approach was applied for making the working prototypes of electronic circuits. Moulded interconnect device demonstrator for FIAT 500 gloves box cover was prepared. The electronic circuit layout of the touch button for the cover opening mechanism was fabricated using the PP-MWCNT material and the LDS process. Examples of conductive tracks for the touch-sensitive button are shown in Figure 66.



Figure 66. Conductive traces for the FIAT gloves box cover touch button demonstrator [11].

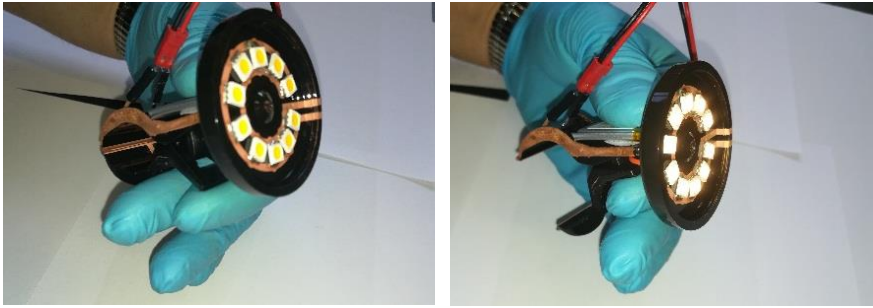
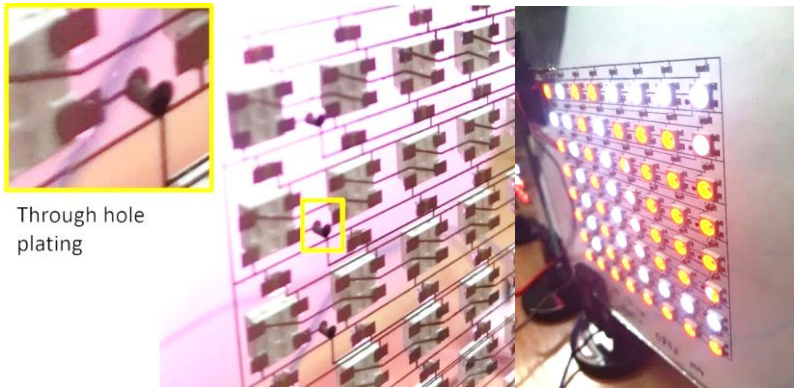
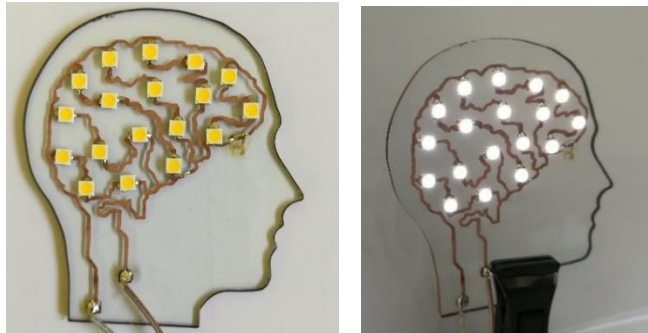


Figure 67. Real demonstrators of the SSAIL technology - a LED illuminator with the wiring on the 3D surface (PA 6).



Through hole plating

a)



b)

Figure 68. Demonstrators on a glass substrate. a) LED display matrix 8x8 with the circuit on both glass substrate sides, connected via through-hole plating; b) LED demonstrator of the human brain.

Another demonstrator was built using the SSAIL technology on complex 3D designed PA 6 part. The LED lighter start lighting when tongs are open as shown in Figure 67. The 3D laser processing was performed using Intelliscan scanner from SCANLAB mounted on the YASKAWA Motoman MH5S robot hand. LED soldering procedure was performed in an industrial SMD reflow oven under 160°C temperature.

For electronics on glass demonstration, a programmable LED 8x8 matrix display was fabricated. Circuitry design contains two layers on both sides of a glass substrate with connection through-hole plating as shown in Figure 68 a). In Figure 68 b), demonstration of LED on the glass with contacts representing a shape of human brains is shown.

## 6.9 Results and conclusions

- Laser processing parameters have a high impact on the final properties of the plated copper layer. Electrical conductance of the metal layer, plating selectivity and adhesion of the layer to a substrate can be controlled by the processing parameters.
- Laser fluence is a very important parameter for the quality of the electroless copper plating. The optimal laser fluence value for high reliability of plating was determined for a set of polymers.
- Spatial selectivity of plating depends on the laser irradiation dose. Higher irradiation dose can cause overplating of copper on the areas, which are not processed by a laser. The problem probably arises due to the debris after laser ablation.
- There is an optimal irradiation dose for the highest copper layer adhesion to the polymer substrate and the method to find it was proposed.
- Quality of the plated surface can be evaluated by the colour difference measuring technique.
- An additional procedure such as multiple scanning or double activation process can improved plating quality in the case of plating narrow lines. Moreover, the double activation procedure can broaden the range of laser processing parameters for activation, thus allowing to increase the processing speed.
- The functionality of the SSAIL technology has been proved on working electronic demonstrators.

## LIST OF CONCLUSIONS

1. Raman spectroscopy results, SEM analysis, and sheet resistance measurements tests confirmed reorientation of the MWCNT additives into the interconnected structure when polypropylene was melted by the laser. The increased electrical conductivity of the laser-activated areas enabled the catalytic reaction of reducer in the electroless plating bath, implementing selective copper deposition on laser treated areas.
2. The mechanism of selective plating by using SSAIL method can be explained by the combined process of silver ion adsorption by increased wettability of the picosecond laser-treated surface and ability of the picosecond laser-modified surface of PA6 polymer to reduce silver ions to neutral atoms.
3. Laser processing parameters have a high impact on the final properties of the plated copper layer. The optimal laser fluence for high reliability of plating, plating selectiveness and adhesion of deposited metal to a substrate strongly depends on the irradiation dose. The method to find optimal process parameters was proposed.

## SUMMARY

In this thesis, laser-assisted selective chemical copper deposition on dielectrics, and its application for electric circuit traces was investigated. Two approaches of selective plating methods were proposed and tested: laser direct structuring (LDS) of Polypropylene with carbon nanotubes additive and newly-developed technology Selective Surface Activation Induces by a Laser (SSAIL).

Laser direct structuring is based on special additives called LDS additives mixed in vole volume of the polymeric part. Laser beam activates those additives, making them an active catalyst for electroless copper plating in the bath. Thus only laser written areas are deposited. In this work new type of additives, Multiwall carbon nanotubes were investigated. Experimental studies of activation process were performed with sheet resistance measurements, scanning electron microscope analysis and Raman spectroscopy. Results revealed that activation is caused by melting process during which carbon nanotubes are reorganised to the conductive pattern. The boundaries of the processing parameters have been shown. Laser activation writing speed reached 4 m/s and plating pitch down to 25  $\mu\text{m}$ .

SSAIL is a new technology developed during PhD studies period. The method contains steps: laser excitation of the surface, wet chemical activation with catalyst, rinsing and electroless copper deposition in the bath. The main advantage of the method is that no special additives are needed as in the case of LDS. Experimental results showed that the selective plating process is not caused only by surface roughness. Sheet resistance measurement, XPS analysis and microscope images have been used to analyse the process after laser excitation, activation and plating steps. Results of activation mechanism revealed that process works only after picosecond laser excitation. XPS analysis has shown that PA6 after laser processing has reducing properties of metals ions. Investigation of wetting dynamics revealed the importance of sample preparation prior activation procedure. Part of the experiments was related to optimal laser and chemical parameters investigation. Several types of polymers were tried for the SSAIL approach: PA, PC/ABS, PPA, PVC, PMMA, PET, PEEK and two types of glass: soda-lime and fused silica. High processing speeds up to 4 m/s and plating pitch down to 25  $\mu\text{m}$  has been achieved.

## REFERENCES

- (1) Franke, J. *Three-Dimensional Molded Interconnect Devices (3D-MID): Materials, Manufacturing, Assembly and Applications for Injection Molded Circuit Carriers*; Franke, J., Ed.; Hanser Publications: Munich, 2014.
- (2) Biver, E.; Rapp, L.; Alloncle, A.-P.; Serra, P.; Delaporte, P. High-Speed Multi-Jets Printing Using Laser Forward Transfer: Time-Resolved Study of the Ejection Dynamics. *Opt. Express* **2014**, *22* (14), 17122.
- (3) Rapp, L.; Ailuno, J.; Alloncle, A. P.; Delaporte, P. Pulsed-Laser Printing of Silver Nanoparticles Ink: Control of Morphological Properties. *Opt. Express* **2011**, *19* (22), 21563.
- (4) Kang, B.; Han, S.; Kim, J.; Ko, S.; Yang, M. One-Step Fabrication of Copper Electrode by Laser-Induced Direct Local Reduction and Agglomeration of Copper Oxide Nanoparticle. *J. Phys. Chem. C* **2011**, *115* (48), 23664–23670.
- (5) Chen, D.; Lu, Q.; Zhao, Y. Laser-Induced Site-Selective Silver Seeding on Polyimide for Electroless Copper Plating. *Appl. Surf. Sci.* **2006**, *253* (3), 1573–1580.
- (6) Zhang, Y.; Hansen, H. N.; De Grave, A.; Tang, P. T.; Nielsen, J. S. Selective Metallization of Polymers Using Laser Induced Surface Activation (LISA)—characterization and Optimization of Porous Surface Topography. *Int. J. Adv. Manuf. Technol.* **2010**, *55* (5–8), 573–580.
- (7) Huske, M.; Kickelhain, J.; Muller, J.; Eber, G. Laser Supported Activation and Additive Metallization of Thermoplastics for 3D-MIDs. *Proc. 3rd LANE* **2001**.
- (8) Račiukaitis, G. *Appolo, 7 Framework Project Public Report, Y3*; Vilnius, 2016.
- (9) Fischer, A. J.; Meister, S.; Drummer, D. Effect of Fillers on the Metallization of Laser-Structured Polymer Parts. *J. Polym. Eng.* **2017**, *37* (2), 151–161.
- (10) Friedrich, A.; Geck, B.; Fengler, M. LDS Manufacturing Technology for next Generation Radio Frequency Applications. In *2016 12th International Congress Molded Interconnect Devices - Scientific Proceedings, MID 2016*; 2016.
- (11) Ratautas, K.; Gedvilas, M.; Stankevičiene, I.; Jagminienė, A.; Norkus, E.; Pira, N. L.; Sinopoli, S.; Račiukaitis, G. Laser-Induced

- Selective Metallization of Polypropylene Doped with Multiwall Carbon Nanotubes. *Appl. Surf. Sci.* **2017**, *412*, 319–326.
- (12) Gordiz, K.; Menon, A. K.; Yee, S. K. Interconnect Patterns for Printed Organic Thermoelectric Devices with Large Fill Factors. *J. Appl. Phys.* **2017**, *122* (12), 124507.
  - (13) Bäuerle, D. *Laser Processing and Chemistry*. Springer: Berlin; New York 2011, pp 105–210.
  - (14) Islam, A.; Hansen, H. N.; Tang, P. T.; Sun, J. Process Chains for the Manufacturing of Molded Interconnect Devices. *Int. J. Adv. Manuf. Technol.* **2009**, *42*(9):, 831–841.
  - (15) Lam po Tang, S. Recent Developments in Flexible Wearable Electronics for Monitoring Applications. *Trans. Inst. Meas. Control* **2007**, *29*(3–4), 283–300.
  - (16) Wong, W. S.; Salleo, A. *Flexible Electronics: Materials and Applications*; Wong, W. S., Salleo, Eds.; Springer US: New York, 2009.
  - (17) Heininger, N.; John, W.; Boßler, H. Manufacturing of Molded Interconnect Devices from Prototyping to Mass Production with Laser Direct Structuring. In *6th International Congress MID*; 2004.
  - (18) Eberhardt, W.; Buckmüller, P.; Kück, H. MID Prototyping. In *Three-Dimensional Molded Interconnect Devices (3D-MID)*; Franke, J., Ed.; Hanser Publications: Munich, 2014; pp 201–215.
  - (19) Bassim Bachy. Experimental Investigation, Modeling, Simulation and Optimization of Molded Interconnect Devices (MID) Based on Laser Direct Structuring (LDS), Friedrich-Alexander-Universität Erlangen-Nürnberg, 2017.
  - (20) Franke, J.; Goth, C.; Kuhn, T. MID Technology and Mechatronic Integration Potential. In *Three-Dimensional Molded Interconnect Devices (3D-MID)*; Franke, J., Ed.; Munich, 2014; pp 1–21.
  - (21) Automotive Seminar Registration <http://www.lpkfusa.com/register/> (accessed Jul 12, 2018).
  - (22) The future of electronics with MID's <https://www.autodesk.com/products/eagle/blog/future-electronics-mids/> (accessed Apr 16, 2016).
  - (23) Marcori, F.; Antonipieri, M.; di Vora, I.; Padovani, S.; Riolino, I. Study of MID Technologies for Automotive Lighting and Light Signaling Devices. *Adv. Mater. Res.* **2014**, *1038*, 97–103.
  - (24) Direct laser structuring [https://www.lpkf.de/\\_mediafiles/1963-lpkf-laser-direct-structuring-de.pdf](https://www.lpkf.de/_mediafiles/1963-lpkf-laser-direct-structuring-de.pdf) (accessed Jan 16, 2015).

- (25) Kaddour, D.; Tedjini, S.; Djamel, A. 3D Antenna for UHF RFID Tag on Molded Interconnect Device. In *IEEE Antennas and Propagation Society, AP-S International Symposium (Digest)*; 2013.
- (26) Fuchs, M. Materials for 3D-MID. In *Three-Dimensional Molded Interconnect Devices (3D-MID)*; Franke, J., Ed.; Hanser Publications: Munich, 2014; pp 23–61.
- (27) Panasonic MIPTEC for molded interconnect devices <https://www3.panasonic.biz/ac/e/tech/mid/miptec/index.jsp> (accessed Feb 8, 2015).
- (28) Nathan, A.; Ahnood, A.; Cole, M. T.; Lee, S.; Suzuki, Y.; Hiralal, P.; Bonaccorso, F.; Hasan, T.; Garcia-Gancedo, L.; Dyadyusha, A.; et al. Flexible Electronics: The next Ubiquitous Platform. In *Proceedings of the IEEE*; 2012.
- (29) What is thin film transistor? <https://www.quora.com/What-is-thin-film-transistor> (accessed Apr 10, 2018).
- (30) Fagioli, B. LG mass-produces first-ever flexible OLED smartphone display <https://betanews.com/2013/10/07/lg-mass-produces-first-ever-flexible-oled-smartphone-display/> (accessed Jun 3, 2018).
- (31) Fallis, A. . *Hand Book of Printed Electronics Depositions*; 2013.
- (32) Macleod, P. *Technology Watch: A Review of Flexible Circuit Technology and Its Applications*; Macleod, P., Ed.; PRIME Faraday Partnership: Loughborough, 2017.
- (33) Ramakrishnan, R.; Saran, N.; Petcavich, R. J. Selective Inkjet Printing of Conductors for Displays and Flexible Printed Electronics. *IEEE/OSA J. Disp. Technol.* **2011**, 7 (6), 344–347.
- (34) Kopola, P.; Zimmermann, B.; Filipovic, A.; Schleiermacher, H. F.; Greulich, J.; Rousu, S.; Hast, J.; Myllylä, R.; Würfel, U. Aerosol Jet Printed Grid for ITO-Free Inverted Organic Solar Cells. *Sol. Energy Mater. Sol. Cells* **2012**, 107, 252–258.
- (35) Crompton, T. R. *Polymer Reference Book*; Crompton, T. R., Ed.; Smithers Rapra Press: London, 2006.
- (36) Wypych, G. *Handbook of Polymers: Second Edition*, Second.; Wypych, G., Ed.; ChemTec Publishing: Ontario, 2016.
- (37) Young, R. J.; Chung, C. I. Introduction to Polymers. *J. Eng. Mater. Technol.* **1982**, 8, 112–134.
- (38) Biron, M. *Thermoplastics and Thermoplastic Composites*; Biron, M., Ed.; Elsevier, 2007.
- (39) Biron, M. *Thermosets and Composites*; Biron, M., Ed.; Elsevier, 2003.

- (40) Kamal, M. R.; Isayev, A. I.; Liu, S.-J. *Injection Molding : Technology and Fundamentals*; Kamal, M. R., Ed.; Carl Hanser Verlag GmbH & Co, 2009.
- (41) Malek, C. G. K.; Pfleging, W.; Roth, S. Laser Micromachining of Polymers. In *Generating Micro- and Nanopatterns on Polymeric Materials*; Arzt, E., Ed.; Willey-VCH, 2011; pp 141–168.
- (42) Rubinstein, M.; Colby, R. H. Polymer Physics. In *Polymer International*; 2003.
- (43) Lippert, T.; Dickinson, J. T. Chemical and Spectroscopic Aspects of Polymer Ablation: Special Features and Novel Directions. *Chemical Reviews*. 2003, pp 453–485.
- (44) Kruger, J.; Kautek, W. Ultrashort Pulse Laser Interaction with Dielectrics and Polymers. *Adv. Polym. Sci.* **2004**, *168*, 247–289.
- (45) Multiphoton Ionization – New Opportunities at FLASH [http://wof-cluster.desy.de/sites/site\\_photonscience/content/e58/e186104/e186825/e186879](http://wof-cluster.desy.de/sites/site_photonscience/content/e58/e186104/e186825/e186879) (accessed Jul 22, 2018).
- (46) Hanna, D. The Principles of Nonlinear Optics. In *Optics Laser Technology*; Wiley, Y. R. S., Ed.; Wiley-Interscience, 2002; pp 202–235.
- (47) Schlessinger, L.; Wright, J. Inverse-Bremsstrahlung Absorption Rate in an Intense Laser Field. *Phys. Rev. A* **1979**, *10*, 152–169.
- (48) Lippert, T. Interaction of Photons with Polymers: From Surface Modification to Ablation. In *Plasma Processes and Polymers*; Willey-VCH, 2005; pp 517–596.
- (49) Pinho, G. P.; Schittenhelm, H.; Duley, W. W.; Schlueter, S. a.; Jahani, H. R.; Mueller, R. E. Energy Distributions in the Laser Ablation of Metals and Polymers. *Appl. Surf. Sci.* **1998**, *127–129*, 983–987.
- (50) Chichkov, B. N.; Momma, C.; Nolte, S.; Von Alvensleben, F.; Tünnermann, A. Femtosecond, Picosecond and Nanosecond Laser Ablation of Solids. *Appl. Phys. A Mater. Sci. Process.* **1996**, *63*, 109–115.
- (51) Gedvilas, M.; Indrišiuonas, S.; Voisiat, B.; Stankevičius, E.; Selskis, A.; Račiukaitis, G. Nanoscale Thermal Diffusion during the Laser Interference Ablation Using Femto-, Pico-, and Nanosecond Pulses in Silicon. *Phys. Chem. Chem. Phys.* **2018**, *20*, 12166–12174.
- (52) Kerse, C.; Kalaycıođ Lu, H.; Elahi, P.; Çetin, B.; Kesim, D. K.; Akçaalan, Ö.; Yavaş, S.; Aşlk, M. D.; Öktem, B.; Hoogland, H.; et al. Ablation-Cooled Material Removal with Ultrafast Bursts of Pulses.

- Nature* **2016**, 537, 84–88.
- (53) Wen, X.; Tolbert, W. A.; Dlott, D. D. Ultrafast Temperature Jump in Polymers: Phonons and Vibrations Heat up at Different Rates. *J. Chem. Phys.* **1993**, 99, 4140–4151.
- (54) Byskov-Nielsen, J.; Savolainen, J. M.; Christensen, M. S.; Balling, P. Ultra-Short Pulse Laser Ablation of Metals: Threshold Fluence, Incubation Coefficient and Ablation Rates. *Appl. Phys. A Mater. Sci. Process.* **2010**, 101, 97–101.
- (55) Norkus, E.; Vaškėlis, A.; Jačiauskiene, J.; Stalnionienė, I.; Stalnionis, G. Obtaining of High Surface Roughness Copper Deposits by Electroless Plating Technique. *Electrochim. Acta* **2006**, 51 (17), 3495–3499.
- (56) Paunovic, M. Electroless Deposition of Copper. In *Modern Electroplating*; Schlesinger, M., Paunovic, M., Eds.; Wiley Online Library, 2010.
- (57) Prūšinskas, K. Autokatalizinių Cu(II) Redukcijos Procesų Tyrimas Cheminio Variavimo Sistemose Ligandais Naudojant Gamtinius Polihidroksilius Junginius, Center for Physical Sciences and Technology, 2013.
- (58) Leuschner, R.; Pawlowski, G. Photolithography. In *Handbook of Semiconductor Technology*; Jackson, P. K. A., Schröter, P. D. W., Eds.; Wiley, 2000.
- (59) ZORICH, R. *Handbook of Quality Integrated Circuit Manufacturing*; Zorich, R., Ed.; Academic Press, 1991.
- (60) Butterbaugh, J. W.; Muscat, A. J.; Busnaina, A.; Bakhtari, K.; Park, J.; Bearda, T.; Mertens, P. W.; Beaudoin, S. P.; Banerjee, S.; Reidy, R. F.; et al. *Handbook of Silicon Wafer Cleaning Technology*; Butterbaugh, J. W., Ed.; William Andrew, 2008.
- (61) Paul, K. E.; Prentiss, M.; Whitesides, G. M. Patterning Spherical Surfaces at the Two-Hundred-Nanometer Scale Using Soft Lithography. *Adv. Funct. Mater.* **2003**, 13 (4), 259–263.
- (62) Kim, J. G.; Takama, N.; Kim, B. J.; Fujita, H. Optical-Softlithographic Technology for Patterning on Curved Surfaces. *J. Micromechanics Microengineering* **2009**, 19 (5), 055017.
- (63) Reichenberger, M.; Jillek, W.; Hoerber, J.; Franke, J. Functionalization of Thermoplastics Using Inkjet- and Aerosoljet-Printing Technologies. In *10th International Congress MID 2012*; 2012.
- (64) Kurt K. Christenson, Jason A. Paulsen, Michael J. Renn, Kelley

- McDonald, J. B. Direct Printing of Circuit Boards Using Aerosol Jet [http://www.imaging.org/site/PDFS/Reporter/Articles/2011\\_26/REP26\\_5\\_6\\_NIP27DF11\\_CHRISTENSON\\_PG433.pdf](http://www.imaging.org/site/PDFS/Reporter/Articles/2011_26/REP26_5_6_NIP27DF11_CHRISTENSON_PG433.pdf) (accessed Sep 14, 2016).
- (65) Singh, M.; Haverinen, H. M.; Dhagat, P.; Jabbour, G. E. Inkjet Printing-Process and Its Applications. *Adv. Mater.* **2010**, *22*, 673–681.
- (66) Bohandy, J.; Kim, B. F.; Adrian, F. J. Metal Deposition from a Supported Metal Film Using an Excimer Laser. *J. Appl. Phys.* **1986**, *60*, 1538–1549.
- (67) Serra, P. Laser-Induced Forward Transfer: A Direct-Writing Technique for Biosensors Preparation. *J. Laser Micro/Nanoengineering* **2006**, *3*, 236–242.
- (68) Kattamis, N. T.; Purnick, P. E.; Weiss, R.; Arnold, C. B. Thick Film Laser Induced Forward Transfer for Deposition of Thermally and Mechanically Sensitive Materials. *Appl. Phys. Lett.* **2007**, *91*, 171120–171130.
- (69) Delaporte, P.; Alloncle, A.-P. Laser-Induced Forward Transfer: A High Resolution Additive Manufacturing Technology. *Opt. Laser Technol.* **2016**, *78*, 33–41.
- (70) Tsuboi, Y.; Furuhashi, Y.; Kitamura, N. A Sensor for Adenosine Triphosphate Fabricated by Laser-Induced Forward Transfer of Luciferase onto a Poly(Dimethylsiloxane) Microchip. *Appl. Surf. Sci.* **2007**, *532* (20), 8422–8427.
- (71) Nagel, M.; Lippert, T. Laser-Induced Forward Transfer for the Fabrication of Devices. In *Nanomaterials: Processing and Characterization with Lasers*; H.B. Zeng, S. C. S., Ed.; Wiley, 2012.
- (72) Kumpulainen, T.; Pekkanen, J.; Valkama, J.; Laakso, J.; Tuokko, R.; Mäntysalo, M. Low Temperature Nanoparticle Sintering with Continuous Wave and Pulse Lasers. *Opt. Laser Technol.* **2011**, *43* (3), 570–576.
- (73) Zhang, Y.; Hansen, H. N.; Tang, P. T.; De Grave, A. Laser Induced Selective Activation For Subsequent Autocatalytic Electroless Plating, Technical University of Denmark, Department of mechanical engineering, 2010.
- (74) Zhang, Y.; Nørgaard, H. H.; Henri, H. J.; Torben, T. P.; Skov, N. J.; Celal, T. C. An Explanation of the Mechanism for Laser Induced Selective Activation Using Diffusion Theory. *Nami Jishu yu Jingmi Gongcheng/Nanotechnology Precis. Eng.* **2013**, *25* (15), 2101–2111.

- (75) Kordás, K.; Békési, J.; Vajtai, R.; Nánai, L.; Leppävuori, S.; Uusimäki, A.; Bali, K.; George, T. F.; Galbács, G.; Ignác, F.; et al. Laser-Assisted Metal Deposition from Liquid-Phase Precursors on Polymers. *Appl. Surf. Sci.* **2001**, *172* (1), 178–189.
- (76) LDS protopaint [https://www.lpkf.com/\\_mediafiles/3023-brochure-lpkf-protopaint-lds-en.pdf](https://www.lpkf.com/_mediafiles/3023-brochure-lpkf-protopaint-lds-en.pdf) (accessed Nov 9, 2018).
- (77) Bindra, P.; White, J. R. Fundamental Aspects of Electroless Copper Plating. In *Electroless Plating: Fundamentals and Applications*; White, J. R., Ed.; Wiliam Andrew publishing, 1990.
- (78) Smits, F. M. Measurement of Sheet Resistivities with the Four-Point Probe. *Bell Syst. Tech. J.* **1958**, *37* (3), 711–718.
- (79) ASTM. ASTM D3359-17 Standard Test Methods for Rating Adhesion by Tape Test. In *ASTM International*; 1930.
- (80) ASTM D3330 Tape Adhesion Strength Testing <https://www.admet.com/testing-applications/testing-standards/astm-d3330-tape-adhesion-strength-testing/> (accessed Sep 12, 2018).
- (81) A. Zecchina, F. Bardelli, S. Bertarione, G. Caputo, P. C. Process for Producing Electroconductive or Piezoelectrive Traces on Polymeric a Polymeric Substrate. EP2448383 B1.
- (82) Boydag, F. S.; Mamedov, S. V.; Alekperov, V. A.; GKandemir, U. A Study of the Optical Properties of Polypropylene Based Polymer Composite Films. *Macromol. Symp.* **1999**, *1*, 10–21.
- (83) Dollish, F. R.; Fateley, W. G.; Bentley, F. F. *Characteristic Raman Frequencies of Organic Compounds*; Dollish, F. R., Ed.; Willey, 2015.
- (84) Ibrahim, E. E.; Chipara, D. M.; Thapa, R.; Lozano, K.; Chipara, M. Raman Spectroscopy of Isotactic Polypropylene-Halloysite Nanocomposites. *J. Nanomater.* **2012**, *15*, 793084.
- (85) Ferrari, A.; Robertson, J. Interpretation of Raman Spectra of Disordered and Amorphous Carbon. *Phys. Rev. B - Condens. Matter Mater. Phys.* **2000**, *61*, 14095–14107.
- (86) Celiešiute, R.; Trusovas, R.; Niaura, G.; Švedas, V.; Račiukaitis, G.; Ružele, Ž.; Pauliukaite, R. Influence of the Laser Irradiation on the Electrochemical and Spectroscopic Peculiarities of Graphene-Chitosan Composite Film. *Electrochim. Acta* **2014**, *132*, 265–276.
- (87) Now LDS Electronic Circuitry Is Colorable <https://www.ptonline.com/articles/now-lds-electronic-circuitry-is-colorable> (accessed Jan 11, 2019).
- (88) Can LDS plastics be transparent

[https://www.ebinadk.com/en\\_2015/2015/10/lds-transparence/](https://www.ebinadk.com/en_2015/2015/10/lds-transparence/)  
(accessed Jan 11, 2019).

- (89) Moulder, J. F. *Handbook of X-Ray Photoelectron Spectroscopy: A Reference Book of Standard Spectra for Identification and Interpretation of XPS Data*; Chastain, J., Ed.; Perkin Elmer corporation, 1992.
- (90) Evans, S. Energy Calibration Secondary Standards for X-ray Photoelectron Spectrometers. *Surf. Interface Anal.* **1985**, 7 (6), 299–302.
- (91) Kraus, E.; Baudrit, B.; Heidemeyer, P.; Bastian, M.; Stoyanov, O.; Starostina, I. Surface Treatment with Ultraviolet Laser for Adhesive Bonding of Polymeric Materials. *J. Adhes.* **2017**, 93 (3), 204–215.
- (92) Gao, Z. Modification of Surface Properties of Polyamide 6 Films with Atmospheric Pressure Plasma. *Appl. Surf. Sci.* **2011**, 257 (14), 6068–6072.
- (93) Shafrin, E. G.; Zisman, W. A. Constitutive Relations in the Wetting of Low Energy Surfaces and Theory of the Refraction Method of Preparing Monolayers. *J. Phys. Chem.* **1960**, 64 (5), 519–524.
- (94) Yuan, Y.; Lee, T. R. Contact Angle and Wetting Properties. *Springer Ser. Surf. Sci.* **2013**, 51 (1), 3–34.
- (95) Bae, S.; Kim, H.; Lee, Y.; Xu, X.; Park, J. S.; Zheng, Y.; Balakrishnan, J.; Lei, T.; Ri Kim, H.; Song, Y. Il; et al. Roll-to-Roll Production of 30-Inch Graphene Films for Transparent Electrodes. *Nat. Nanotechnol.* **2010**, 5, 574–578.
- (96) Bonaccorso, F.; Sun, Z.; Hasan, T.; Ferrari, A. C. Graphene Photonics and Optoelectronics. *Nat. Photonics* **2010**, 4, 611–622.
- (97) Kim, K.; Lee, H. B. R.; Johnson, R. W.; Tanskanen, J. T.; Liu, N.; Kim, M. G.; Pang, C.; Ahn, C.; Bent, S. F.; Bao, Z. Selective Metal Deposition at Graphene Line Defects by Atomic Layer Deposition. *Nat. Commun.* **2014**, 5, 4781.
- (98) Gedvilas, M.; Ratautas, K.; Kacar, E.; Stankevičiene, I.; Jagminiene, A.; Norkus, E.; Pira, N. L.; Račiukaitis, G. Colour-Difference Measurement Method for Evaluation of Quality of Electrolessly Deposited Copper on Polymer after Laser-Induced Selective Activation. *Sci. Rep.* **2016**, 6, 22963.
- (99) Last, B. J.; Thouless, D. J. Percolation Theory and Electrical Conductivity. *Phys. Rev. Lett.* **1971**, 27, 1719–1721.
- (100) Efros, A. L.; Shklovskii, B. I. Critical Behaviour of Conductivity and Dielectric Constant near the Metal-Non-Metal Transition Threshold.

- Phys. status solidi* **1976**, 78 (2), 475–485.
- (101) Cargnello, M.; Johnston-Peck, A. C.; Diroll, B. T.; Wong, E.; Datta, B.; Damodhar, D.; Doan-Nguyen, V. V. T.; Herzing, A. A.; Kagan, C. R.; Murray, C. B. Substitutional Doping in Nanocrystal Superlattices. *Nature* **2015**, 524, 450–453.
- (102) Marus, M.; Hubarevich, A.; Wang, H.; Smirnov, A.; Sun, X.; Fan, W. Optoelectronic Performance Optimization for Transparent Conductive Layers Based on Randomly Arranged Silver Nanorods. *Opt. Express* **2015**, 23 (5), 6209–6214.
- (103) Marus, M.; Hubarevich, A.; Wang, H.; Stsiapanau, A.; Smirnov, A.; Sun, X. W.; Fan, W. Comparative Analysis of Opto-Electronic Performance of Aluminium and Silver Nano-Porous and Nano-Wired Layers. *Opt. Express* **2015**, 23 (20), 26794–26799.
- (104) Hubarevich, A.; Marus, M.; Fan, W.; Smirnov, A.; Sun, X. W.; Wang, H. Theoretical Comparison of Optical and Electronic Properties of Uniformly and Randomly Arranged Nano-Porous Ultra-Thin Layers. *Opt. Express* **2015**, 23 (14), 17860–17865.
- (105) Borchert, J. W.; Stewart, I. E.; Ye, S.; Rathmell, A. R.; Wiley, B. J.; Winey, K. I. Effects of Length Dispersity and Film Fabrication on the Sheet Resistance of Copper Nanowire Transparent Conductors. *Nanoscale* **2015**, 4, 14496–14499.
- (106) Bergin, S. M.; Chen, Y. H.; Rathmell, A. R.; Charbonneau, P.; Li, Z. Y.; Wiley, B. J. The Effect of Nanowire Length and Diameter on the Properties of Transparent, Conducting Nanowire Films. *Nanoscale* **2012**, 4, 1996–2004.
- (107) Lee, H. C. *Introduction to Color Imaging Science*; Lee, H.-C., Ed.; Cambridge University Press: Cambridge, 2005.
- (108) Kirby, B. J.; Hasselbrink, E. F. Zeta Potential of Microfluidic Substrates: 2. Data for Polymers. *Electrophoresis* **2004**, 25 (2), 203–226.
- (109) Niino, H.; Yabe, A. Positively Charged Surface Potential of Polymer Films after Excimer Laser Ablation: Application to Selective-Area Electroless Plating on the Ablated Films. *Appl. Phys. Lett.* **1992**, 60, 2697–2704.
- (110) Yip, J.; Chan, K.; Sin, K. M.; Lau, K. S. Study on the Surface Chemical Properties of UV Excimer Laser Irradiated Polyamide by XPS, ToF-SIMS and CFM. *Appl. Surf. Sci.* **2002**, 205, 151–159.

## NOTES

## NOTES

Vilniaus universiteto leidykla  
Universiteto g. 1, LT-01513 Vilnius  
El. p. [info@leidykla.vu.lt](mailto:info@leidykla.vu.lt),  
[www.leidykla.vu.lt](http://www.leidykla.vu.lt)  
Tiražas 25 egz.